Titre: Title:	Leveraging Artificial Intelligence to Improve EEG-fNIRS Data Analysis
Auteur: Author:	Parikshat Sirpal
Date:	2020
Type:	Mémoire ou thèse / Dissertation or Thesis
Référence: Citation:	Sirpal, P. (2020). Leveraging Artificial Intelligence to Improve EEG-fNIRS Data Analysis [Thèse de doctorat, Polytechnique Montréal]. PolyPublie. https://publications.polymtl.ca/5287/

POLYTECHNIQUE MONTRÉAL

affiliée à l'Université de Montréal

Leveraging Artificial Intelligence to Improve EEG-fNIRS Data Analysis

PARIKSHAT SIRPAL

Institut de génie biomédical

Thèse présentée en vue de l'obtention du diplôme de *Philosophiæ doctor*

Génie biomédical

Avril 2020

POLYTECHNIQUE MONTRÉAL

affiliée à l'Université de Montréal

Cette thèse intitulée :

Leveraging Artificial Intelligence to Improve EEG-fNIRS Data Analysis

présentée par **Parikshat SIRPAL**

en vue de l'obtention du diplôme de *Philosophiæ doctor*

a été dûment acceptée par le jury d'examen constitué de :

Frédéric LEBLOND, président
Frédéric LESAGE, membre et directeur de recherche
Dang Khoa NGUYEN, membre et codirecteur de recherche
Jean PROVOST, membre
Jean-Marc LINA, membre externe

DEDICATION

To my parents

ACKNOWLEDGEMENTS

First and foremost, I would like to thank my research supervisors: Drs. Frédéric Lesage and Dang K. Nguyen for the opportunity to study under their tutelage. The freedom to explore and formulate my ideas, as well as Dr. Lesage's mentorship, guidance and overall dedication to the scientific process has greatly shaped my approach to science and research. Dr. Lesage's unwavering support over the years has been instrumental to the success of this work. Dr. Nguyen's knowledge regarding epilepsy and his kind approach has also played a pivotal role in this research. Special thanks to Dr. Philippe Pouliot who offered his vast knowledge in statistics and mathematical modeling and to the scientific colleagues at École Polytechnique de Montréal and the laboratory of molecular and optical imaging: Mahnoush Amiri, Maxime Abran, Cong Zhang, Alexandre Castonguay, Hanieh Mohammadi, Joël Lefebvre, Yuankang Lv, Xuecong Lv, Sayed Mehran Sharafi, Xavier Beaule, Younes Zerouali, Rafat Damseh, Ali Kassab, Ke Peng, Srinil Saha, Alexandre Marcotte, and Patrick Delafontaine-Martel as well as my collaborators at CHUM. I would also like to acknowledge the financial help of the following institutions which have supported this research: The Natural Sciences and Engineering Research Council of Canada; Grant RGPIN-2017-06140; Canadian Institutes of Health Research Grant 396317; CIHR/NSERC Grants 387183, 239876-2011. Finally and most importantly, thank you to my family for the encouragement, support and kindness.

RÉSUMÉ

La spectroscopie proche infrarouge fonctionnelle (fNIRS) est apparue comme une technique de neuroimagerie qui permet une surveillance non invasive et à long terme de l'hémodynamique corticale. Les technologies de neuroimagerie multimodale en milieu clinique permettent d'étudier les maladies neurologiques aiguës et chroniques. Dans ce travail, nous nous concentrons sur l'épilepsie - un trouble chronique du système nerveux central affectant près de 50 millions de personnes dans le monde entier prédisposant les individus affectés à des crises récurrentes. Les crises sont des aberrations transitoires de l'activité électrique du cerveau qui conduisent à des symptômes physiques perturbateurs tels que des changements aigus ou chroniques des compétences cognitives, des hallucinations sensorielles ou des convulsions de tout le corps. Environ un tiers des patients épileptiques sont récalcitrants au traitement pharmacologique et ces crises intraitables présentent un risque grave de blessure et diminuent la qualité de vie globale. Dans ce travail, nous étudions 1. l'utilité des informations hémodynamiques dérivées des signaux fNIRS dans une tâche de détection des crises et les avantages qu'elles procurent dans un environnement multimodal par rapport aux signaux électroencéphalographiques (EEG) seuls, et 2. la capacité des signaux neuronaux, dérivé de l'EEG, pour prédire l'hémodynamique dans le cerveau afin de mieux comprendre le cerveau épileptique. Sur la base de données rétrospectives EEG-fNIRS recueillies auprès de 40 patients épileptiques et utilisant de nouveaux modèles d'apprentissage en profondeur, la première étude de cette thèse suggère que les signaux fNIRS offrent une sensibilité et une spécificité accrues pour la détection des crises par rapport à l'EEG seul. La validation du modèle a été effectuée à l'aide de l'ensemble de données CHBMIT open source documenté et bien référencé avant d'utiliser notre ensemble de données EEG-fNIRS multimodal interne. Les résultats de cette étude ont démontré que fNIRS améliore la détection des crises par rapport à l'EEG seul et ont motivé les expériences ultérieures qui ont déterminé la capacité prédictive d'un modèle d'apprentissage approfondi développé en interne pour décoder les signaux d'état de repos hémodynamique à partir du spectre complet et d'une bande de fréquences neuronale codée spécifique signaux d'état de repos (signaux sans crise). Ces résultats suggèrent qu'un autoencodeur multimodal peut apprendre des relations multimodales pour prédire les signaux d'état de repos. Les résultats suggèrent en outre que des gammes de fréquences EEG plus élevées prédisent l'hémodynamique avec une erreur de reconstruction plus faible par rapport aux gammes de fréquences EEG plus basses. De plus, les connexions fonctionnelles montrent des modèles

spatiaux similaires entre l'état de repos expérimental et les prédictions fNIRS du modèle. Cela démontre pour la première fois que l'auto-encodage intermodal à partir de signaux neuronaux peut prédire l'hémodynamique cérébrale dans une certaine mesure. Les résultats de cette thèse avancent le potentiel de l'utilisation d'EEG-fNIRS pour des tâches cliniques pratiques (détection des crises, prédiction hémodynamique) ainsi que l'examen des relations fondamentales présentes dans le cerveau à l'aide de modèles d'apprentissage profond. S'il y a une augmentation du nombre d'ensembles de données disponibles à l'avenir, ces modèles pourraient être en mesure de généraliser les prédictions qui pourraient éventuellement conduire à la technologie EEG-fNIRS à être utilisée régulièrement comme un outil clinique viable dans une grande variété de troubles neuropathologiques.

ABSTRACT

Functional near-infrared spectroscopy (fNIRS) has emerged as a neuroimaging technique that allows for non-invasive and long-term monitoring of cortical hemodynamics. Multimodal neuroimaging technologies in clinical settings allow for the investigation of acute and chronic neurological diseases. In this work, we focus on epilepsy—a chronic disorder of the central nervous system affecting almost 50 million people world-wide predisposing affected individuals to recurrent seizures. Seizures are transient aberrations in the brain's electrical activity that lead to disruptive physical symptoms such as acute or chronic changes in cognitive skills, sensory hallucinations, or whole-body convulsions. Approximately a third of epileptic patients are recalcitrant to pharmacological treatment and these intractable seizures pose a serious risk for injury and decrease overall quality of life. In this work, we study 1) the utility of hemodynamic information derived from fNIRS signals in a seizure detection task and the benefit they provide in a multimodal setting as compared to electroencephalographic (EEG) signals alone, and 2) the ability of neural signals, derived from EEG, to predict hemodynamics in the brain in an effort to better understand the epileptic brain. Based on retrospective EEG-fNIRS data collected from 40 epileptic patients and utilizing novel deep learning models, the first study in this thesis suggests that fNIRS signals offer increased sensitivity and specificity metrics for seizure detection when compared to EEG alone. Model validation was performed using the documented open source and well referenced CHBMIT dataset before using our in-house multimodal EEG-fNIRS dataset. The results from this study demonstrated that fNIRS improves seizure detection as compared to EEG alone and motivated the subsequent experiments which determined the predictive capacity of an in-house developed deep learning model to decode hemodynamic resting state signals from full spectrum and specific frequency band encoded neural resting state signals (seizure free signals). These results suggest that a multimodal autoencoder can learn multimodal relations to predict resting state signals. Findings further suggested that higher EEG frequency ranges predict hemodynamics with lower reconstruction error in comparison to lower EEG frequency ranges. Furthermore, functional connections show similar spatial patterns between experimental resting state and model fNIRS predictions. This demonstrates for the first time that intermodal autoencoding from neural signals can predict cerebral hemodynamics to a certain extent. The results of this thesis advance the potential of using EEG-fNIRS for practical clinical tasks (seizure detection, hemodynamic prediction) as well as examining fundamental relationships present in the

brain using deep learning models. If there is an increase in the number of datasets available in the future, these models may be able to generalize predictions which would possibly lead to EEG-fNIRS technology to be routinely used as a viable clinical tool in a wide variety of neuropathological disorders.

TABLE OF CONTENTS

LIST OF TABLES

LIST OF FIGURES

LIST OF SYMBOLS AND ABBREVIATIONS

AE	Autoencoder
18F-FDG	18Fluoro-2-deoxyglucose
AED	Anti-epileptic drugs
ANN	Artificial neural network
BBB	Blood brain barrier
BOLD	Blood level oxygen dependent
BoW	Bag-of-words
Ca^{2+}	Calcium
CBF	Cerebral blood flow
CEEG	Continuous electroencephalography
CNN	Convolutional neural network
CT	Computed tomography
CW-fNIRS	Continuous wave functional near infrared spectroscopy
Cyt aa3	Cytochrome aa3
DBN	Deep belief network
DMN	Default mode network
DPLF	Differential pathlength factor

ECD	Ethyl-cysteinate dimer
EEG	Electroencephalography
FFT	Fast Fourier transform
fMRI	Functional magnetic resonance imaging
fNIRS	Functional near infrared spectroscopy
GAN	Generative adversarial network
GBC	Global brain connectivity
GloVe	Global vectors for word representation
HbO	Oxygenated hemoglobin
HbR	Reduced or deoxygenated hemoglobin
HbT	Total hemoglobin
HFO	High frequency oscillations
HMPAO	Hexa-methyl-propylene-amine oximine
ICA	Independent component analysis
ICU	Intensive care unit
LFO	Low frequency oscillations
LFP	Local field potential
LSTM	Long short-term memory
MEG	Magnetoencephalography

MLP	Multilayer perceptron
MSI	Magnetic source imaging
MW	Mayer waves
MWA	Moving window analysis
NO	Nitric oxide
PCG	Precentral gyrus
PET	Positron emission tomography
RBM	Restricted Boltzmann machine
rCBF	Regional cerebral blood flow
rCMRG	Regional cerebral metabolic rate of glucose
RE	Reconstruction error
ReLU	Rectified linear units
REM	Rapid eye movement
RMSE	Root mean squared error
RNN	Recurrent neural network
RNS	Responsive neurostimulation devices
ROI	Region of interest
RSN	Resting state network
rSO_2	Regional cerebral oxygen saturation

SD	Spreading depolarization or source-detector pairing
Seq2seq	Sequence to sequence
SNR	Signal to noise ratio
SPECT	Single photon emission tomography imaging
SQUID	Superconducting quantum interference device
SVM	Support vector machine
TBI	Traumatic brain injury
VAE	Variational autoencoder
Word2vec	Word to vector

CHAPTER 1 INTRODUCTION

Following the quantitative derivation of axonal membrane currents by Hodgkin and Huxley in 1952, [1] dynamics between mathematical modeling and physiological systems has evolved to better understand the inner workings of the human brain. Advances in machine learning, particularly deep learning are well suited to address many questions in classical and applied neuroscience. One such central question is: “Can methods be developed to predict interactions between physiological parameters within networks of neurons?”. Key electrophysiological mechanisms, including how neurons and their synaptic connections operate have been discerned. The existing interplay and consequent prediction of the behavior of neuronal populations during an active and resting brain state is at the forefront of present computational neuroscience research. In this thesis, questions related to the application of the central question above with respect to epilepsy, a common neurological disease are explored. More precisely, this thesis focuses on exploring the utility multimodal neuroimaging technology offers for potential clinical use, as well as its ability to answer fundamental questions in human brain research.

Among the available multimodal neuroimaging techniques, scalp electroencephalography (EEG) and functional near infrared spectroscopy (fNIRS) signals are used in this thesis. EEG signals provide information related to cerebral electrical activity, whereas fNIRS signals help to elucidate cerebral hemodynamic information. Both are complementary and could be useful in clinical applications for example in: a) the long-term bedside monitoring of patients who are at risk for seizures (i.e., in critical care unit settings); and b) basic and/or clinical investigations of resting-state brain connectivity in normal and pathological populations. In this thesis, machine learning and in particular deep learning is used to bypass traditional forms of signal processing which may be too cumbersome and difficult to solve. This chapter provides: 1) a background on epilepsy and seizures, and rationale for long term brain monitoring, 2) the neurovascular coupling phenomenon and research in epilepsy, 3) a discussion on multimodal neuroimaging, and 4) a general overview of deep learning methods. The subsequent chapters give more background on the particular methods used in the thesis.

1.1 Epilepsy and seizures

Approximately sixty million people world-wide are diagnosed with epilepsy. In North America alone, epilepsy affects about 3 million people and is the third most common neurological disorder after Alzheimer's disease and stroke. Medically intractable seizures persist in almost 1.2 million epileptic patients, characterized by frequent and unpredictable seizures, despite pharmacological treatment by one or multiple anti-epileptic drugs [2]. Medically intractable seizures severely limit the independence and mobility of an individual and, as a consequence, can result in decreased quality of life parameters. Epilepsy's economic burden in terms of health care costs and the consequent loss in economic productivity nears 12.5 billion USD [3]. Thus, automated seizure onset detection systems allow for the engineering of novel therapeutic and alerting systems that can ease this burden. Eventually, a therapeutic system capable of detecting and reacting to seizure onset could mitigate frank seizure progression.

The following section briefly describes seizure monitoring using scalp EEG technology as well as unmet needs in seizure monitoring and detection. Although invasive monitoring methods can be useful for seizure monitoring, they are outside the scope of this thesis.

1.2 Seizure monitoring

Combined with a careful and thorough clinical examination of an epileptic patient, the scalp EEG has established itself as the clinical gold standard in seizure monitoring as it offers a continuous, non-invasive, safe, cost-effective, and reliable method for aiding diagnosis of epilepsy by determining electrical changes in the brain [4]. The scalp EEG method can be used in a variety of clinical settings ranging from the emergency room, epilepsy monitoring, critical care and neuro-intensive care units to name a few [5].

1.2.1 Long term monitoring

Long term monitoring allows for the early detection of electrical and physiological disturbances indicative of seizure events, so that timely medical intervention can salvage viable brain tissue and prevent secondary neurological injury [6]. Long term EEG recordings may be required in comatose patients, those with noted EEG abnormalities [7], and patients in intensive or neuro-intensive care units [5], [8] as prolonged EEG recordings offer a useful adjunct to other clinical interventions in these patients [9]. Long term continuous scalp EEG monitoring in comparison to routine EEG, has been noted to detect seizures in approximately 27% of critically

ill patients within the first 24 hours of admission, as compared to 11% detection in recordings performed with conventional EEG protocol in the same patient population [10].

While the continuous scalp EEG method offers many advantages, there exists limitations to its use and implementation. From a practical perspective, a primary limitation is related to the availability of clinical expertise for real-time interpretation of EEG patterns. Typically, only an experienced clinician (i.e., neurologist) can analyze the complexity of EEG patterns. Furthermore, from a technical standpoint, EEG monitoring does not provide information on cerebral hemodynamic status particularly oxygenation and related parameters. Changes in cerebral blood flow and oxygenation parameters can help in the assessment of the potential metabolic impact of seizures. As a result, other seizure monitoring techniques have been increasingly utilized in conjunction with scalp EEG recordings in vulnerable patient populations to offer increased insight into their underlying pathologies. Patients requiring such interventions typically have a past medical history of unexplained altered mental status and/or history of epileptic and non-epileptic seizures [8], [11], [12]. The following section discusses the neurovascular coupling phenomenon, which represents the fundamental relationship present between local neural activity and subsequent changes in cerebral blood flow. Section 1.3.3.1 specifically details the neurovascular coupling phenomenon in the context of epilepsy.

1.3 Neurovascular coupling

1.3.1 Basics of neurovascular coupling and its clinical significance

In the brain, neural activity is closely related to cerebral blood flow (CBF). When neural activity occurs within a localized brain region, perfusion follows to meet the increased cerebral metabolic demand. This phenomenon, known as neurovascular coupling [13], [14] (Figure 1.1) is controlled via metabolic and cellular signaling pathways. The relationship between neurovascular components forms the theoretical basis for hemodynamic based imaging of brain activity. This relationship can be altered in brain disorders, and the resulting homeostatic instability may further contribute to the primary cerebral pathology or lead to secondary disorders including ischemic stroke, Alzheimer's disease, and epilepsy [8], [13]. Basic and clinical research has focused on understanding the dynamism of the neurovascular coupling phenomenon in epilepsy and secondary brain pathologies [15]–[19].

Further investigations within the framework of the neurovascular coupling phenomenon offers the potential for advancement in drug development for epilepsy, increased precision in the diagnosis of epilepsy, and adding to the overall understanding of the mechanisms of the neurovascular system.

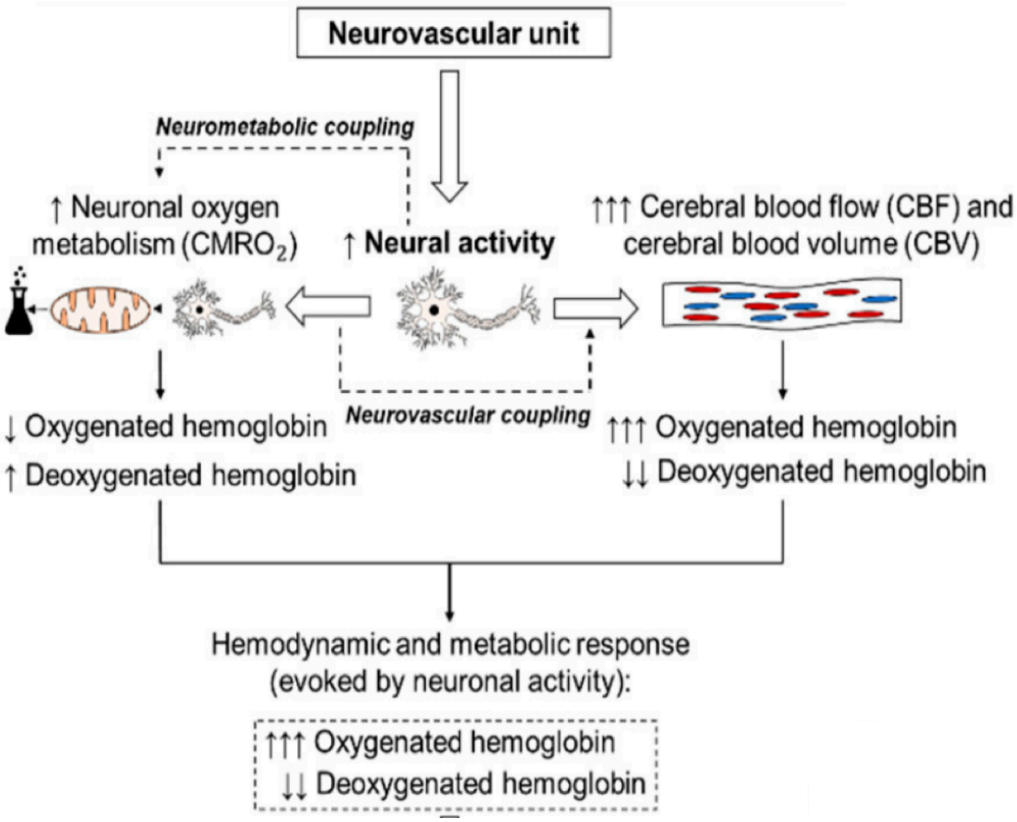

Figure 1.1: The hemodynamic response during increased activation of neurons in the context of neurovascular coupling.

1.3.2 Models explaining neurovascular coupling

At present there are two competing paradigms related to neurovascular coupling. The "positive neural feedback" model in which synaptic activity and the metabolic and clearance needs of brain tissue (including at resting state) [20]–[25] drives cerebral blood flow. This model further suggests that the metabolic byproducts of brain state (i.e., vasodilators) to a certain extent initiate the flow response [26]–[28]. However, support for an opposing hypothesis, a "feed forward model", also exists. This model suggests that an increase in cerebral blood flow is not particularly driven by the brain's resting metabolic state [13], [20], [29], [30]. Specifically, an excess delivery

of oxygen to brain tissues is tightly correlated with an increase in cerebral blood flow. The feed forward model suggests that cerebral blood flow changes via neural signaling pathways lead to a subsequent release of vasoactive products of synaptic activity (i.e. nitric oxide) [13], [20], [31], [32].

1.3.2.1 fNIRS may detect early vascular changes in epilepsy

Seizure dynamics are complex and the desynchronization of action potentials during seizure onset, followed by concomitant synchronization as the seizure progresses is occasionally seen [33], [34]. Desynchronization of action potentials, during seizure onset, has traditionally been seen in EEG beta and gamma frequency ranges [35], [36]. Provided the existence of strong coupling between vascular responses and electrical potentials, it has been theorized that pre-ictal activity may be dependent to some degree on non-synchronized neural action potentials, which are not always discernable on scalp EEG [13], [23], [37], [38]. This leads to a consumption of cerebral metabolic resources as described above. However, cerebral hemodynamic signals obtained by fNIRS recordings might offer insight in this regard. Specifically, cerebral hemodynamics (which may occur prior to changes seen on EEG), might help in understanding the relationship between desynchronized neural activity and pre-ictal and/or ictal activity [39], [40].

1.3.3 Neurovascular coupling studies in the human brain

The simultaneous recordings of electroencephalographic and functional magnetic resonance imaging (EEG-fMRI) or electroencephalographic and functional near infrared spectroscopy (EEG-fNIRS) provide high spatial and temporal resolution. Multimodal EEG-fMRI systems are more common as compared to multimodal EEG-fNIRS studies. Resting state studies mostly focused on the investigation of the relationship between the specific EEG frequency ranges and hemodynamics seen with fMRI. Research has examined the relationship between resting state alpha, beta, delta, gamma, and theta EEG frequencies and the hemodynamic response using simultaneous EEG-fMRI. Results from EEG-fMRI studies [41], [42], suggest that the amplitude of the EEG alpha rhythm is associated with increased levels of cortical activity. An increase in the power of the EEG signal over a specific frequency range generally indicates higher level of synchronized neural firing in those frequencies.

Simultaneous EEG-fNIRS recordings yield similar measurements as compared to EEG-

fMRI recordings [43]–[48]. Previous studies have demonstrated [49] that the EEG alpha power correlates with the fNIRS measure of HbR in the occipital cortex in EEG-fNIRS resting state experiments. Koch et al. [45] found that the blood oxygen level dependent (BOLD) signal to a visual stimulus is more pronounced when the amplitude of the resting EEG alpha frequency is low. Thus, these results suggested that cerebral hemodynamic changes are related to fluctuations in the intensity of recorded electrical signals. Utilizing a spatial navigation experimental setup, Eksrtom et. al., 2009 demonstrated correlation between the fMRI BOLD signal and EEG theta band activity in the hippocampal areas [50].

Results from experiments focused on the EEG gamma frequency range have suggested that the gamma band helps to influence communication between neuronal populations and phase coherence between two or more groups of neurons, thereby allowing for maximal inter-communication [51]–[53]. A third hypothesis, referred to as "binding by synchrony", suggests the EEG gamma band links differing neurons together in the representation of cerebral inputs, (i.e., visual sensory input). These notions strongly suggest the idea that the gamma EEG range strongly influences cerebral spike onset and timing, and thereby affects cortical computation and function.

1.3.3.1 Neurovascular coupling in epilepsy

The assessment of neurovascular coupling in vivo using simultaneous intrinsic optical signals and voltage-sensitive dye imaging of cerebral blood volume and membrane potential changes in small animals (e.g., rats), shows that seizures are the sum of multiple membrane potential changes and local blood volume changes evolves comparatively much slower than membrane potential changes [54]–[56]. Hence, the mechanism of neurovascular coupling in epileptic brains demonstrates dynamism since vascular response to electrical changes is secondary to an ictal event [54]–[57].

1.3.3.1.1 Onset of ictal events and neurovascular coupling

Although the exact mechanism of the cerebrovascular and metabolic changes preceding seizure onset is currently unknown, cerebral metabolism is thought to drive the cascade of electrical and vascular changes concomitant with seizure onset. Ictal events are preceded by blood vessel vasoconstriction in the proximity of the seizure onset zone approximately occurring $1-5$ seconds

prior to seizure onset [58]–[60], thus shunting oxygenated blood to serve the metabolic needs of the seizure focus [61], [62].

1.3.3.1.2 Propagation of ictal events and neurovascular coupling

During an ictal event, an increased metabolic demand is placed on the brain [63]. Histological studies have examined similarities between brain damage caused by cerebral ischemia and metabolic damage secondary to seizures. It has been determined that epilepsy leads to progressive damage of cerebral autoregulatory mechanisms in part by an increase in venous oxygenation [64] and not by cerebral anoxia as initially suggested by the so called "hypoxia–hypoperfusion hypothesis" [65]. Typically, cerebral hypoxic states partly mediated by arteriole vasoconstriction (via cycloxygenase-2) develop in brain regions post seizure events [56].

Studies by Ma et. al. suggest that in-vivo data (i.e., small animal studies) indicates that membrane potential change does not spread across the cortex from the seizure onset zone [57]. During seizure propagation, multiple propagating waves of electrical current spread at approximately $100\ \frac{mm}{s}$ across the cortex. Dynamic changes in cerebral hemodynamic activity, on the other hand, are characterized by a single slow steady wave.

1.3.3.1.3 Ictal termination and neurovascular coupling

The electrical, vascular, and metabolic etiologies of ictal termination is still not well understood, but it has been suggested cerebral hypoxia plays a defining role in the seizure termination process. Metabolic changes leading to changes in pH, the uptake of neurotransmitters, and electrical changes such as the closing of gap junctions are commonly observed [57], [62], [66]. In-vivo animal studies have suggested that cerebral hemodynamic changes continue on an average of 10 seconds post termination of dynamic changes in membrane potentials [57].

1.4 Imaging modalities used to measure brain activity

In this section, we focus on common modalities for measuring human brain function in the context of the epileptic brain. Frequently used methodologies in clinical settings include the scalp EEG, computed tomography (CT), anatomical magnetic resonance imaging (MRI), and single photon emission computed tomography (SPECT) methods. Modalities which are currently used in research settings include magnetoencephalography (MEG), functional magnetic resonance

imaging (fMRI), and the functional near infrared spectroscopy technique (fNIRS). We will begin with the scalp EEG, CT, MRI, and SPECT methods and then discuss the remaining modalities.

1.4.1 Electroencephalography

1.4.1.1 Introduction to electroencephalography

Electroencephalography (EEG) is the oldest non-invasive method for studying the brain and diagnosing brain related pathologies. EEG measures the electrical activity of cortical and subcortical neurons with temporal resolution in the millisecond range [4]. The scalp EEG signal is typically obtained using electrodes arranged on the scalp as shown in Figure 1.2 below [67]. Each EEG channel summarizes activity localized within a region of the brain and is obtained by taking the potential difference measured at two electrode sites. Generally, neurons that are closer to the scalp contribute more to the generated signal as opposed to neurons associated with deeper brain structures. EEG activity can be described in terms of spatial distribution on the scalp in addition to its associated frequency component. Experimentally, the presence of rhythmic activity oscillations with frequencies ranging from approximately $1-100\,\mathrm{Hz}$ during a resting state have been determined [68], [69]. Information regarding neuronal processing is obtainable from a cerebral region of interest via these rhythmic oscillations, which have been classified into characteristic frequency bands [70]–[73].

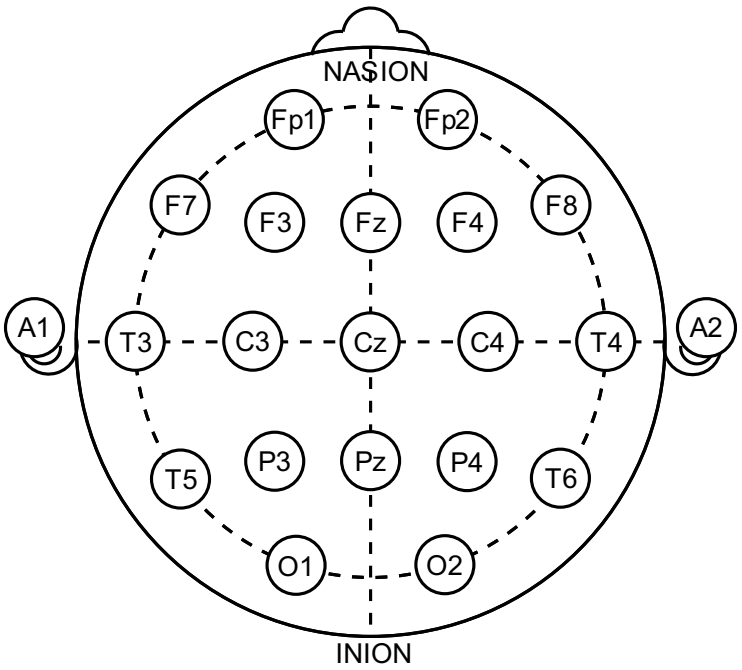

Figure 1.2: EEG scalp electrode array placed symmetrically. Pre-frontal (F_p), frontal (F), temporal (T), parietal (P), occipital (O), and central (C) electrodes correspond to their corresponding brain lobes, (A) auricular. Source: M. R. Nuwer et al. [67].

The following sections discuss the neurophysiological basis of EEG, including the cortical rhythms derived from electroencephalography, and finally EEG instrumentation.

1.4.1.2 Neurophysiological basis of electroencephalography

EEG activity reflects the summation of neural synchronous activity. Cortical pyramidal neurons typically are well aligned to produce the strongest fluctuations in voltage field gradients. EEG oscillations are generated in these neurons by both excitatory and inhibitory postsynaptic potentials [74]. Scalp EEG oscillatory activity is frequency dependent [75] and represent synchronized activity over a network of neurons. The constitution of these neuronal networks and their subcortical contributions to scalp EEG have been reported previously in the literature [73], [76], whereas cortical macro-columnar neurons are believed to be the major contributing force behind EEG signals. The amplitude of the electric field secondary to action potential propagation decreases faster than the amplitude of the fields produced by the postsynaptic potentials; the duration of action potentials is on the order of 1 millisecond. This is insufficient to obtain an adequate synchronization of large cortical neuronal populations as the generation of EEG signals

is largely based on ionic current flow generated by the neurons in the extracellular space [77]. The resulting net ionic current is subsequently recorded as the voltage existing through the resistance of the extracellular space and transmembrane voltage is equal to the product of membrane resistance. As a result, thousands of simultaneously activated neurons are necessary to generate an EEG signal strong enough to be detected from the electrodes on the scalp surface, since the electrical contribution of each cortical neuron is poor and signal must travel through several layers of non-neural tissues, including the meninges, skull and skin. Synchronous activation of over 100 cortical neurons in an area of at least 6 cm^2 is required to produce a discernable EEG signal from the scalp. Therefore, the amplitude of the EEG signal depends to a large extent on the synchronization of activated neurons.

1.4.1.2.1 Electroencephalography derived cortical rhythms

EEG signals can be classified into frequency bands as mentioned above. The figure below depicts the typical waveform of these bands and their frequency ranges [78].

Waves	Frequency bands (Hz)	Behavior Trait	Signal Waveform
Delta	**0.5-3 Hz**	Deep sleep	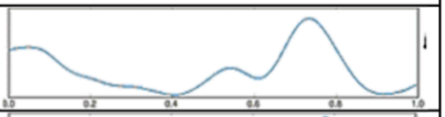
Theta	**4-7 Hz**	Deep Meditation	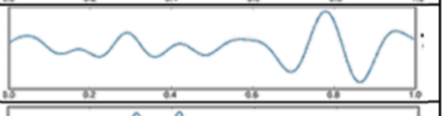
Alpha	**8-13 Hz**	Eyes closed, awake	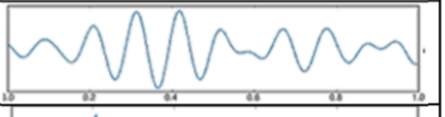
Beta	**14-30 Hz**	Eyes opened, thinking	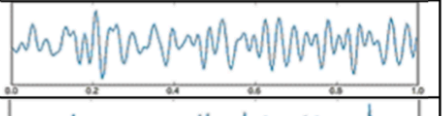
Gamma	**30-100 Hz**	Unifying consciousness	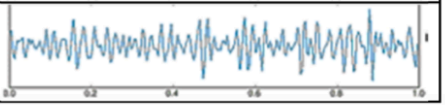

Figure 1.3: Typical EEG bands and their correlated traits.

Usually, for adult subjects EEG oscillations ranging between 0.1-100 microVolts in intensity and in the $0.5 - 100$ Hz frequency range are typically observed [73]. EEG temporal resolution (in milliseconds), allows for the discovery of not only changes in EEG activity as a result of demanding tasks but also differentiation between inhibitory functions and excitatory activity.

Generally, frequency oscillations in the delta and theta frequency bands display synchronized amplitudes, whereas higher frequency bands particularly in the beta and gamma ranges, have smaller desynchronized amplitudes. In order to examine specific EEG frequency ranges, the signal is decomposed into functionally distinct frequency bands, commonly achieved through Fast Fourier Transform (FFT) computations. Briefly, FFT computations return, for each frequency bin, a complex number from which the amplitude and phase of the signal at a specific frequency can be ascertained. Spectral analysis of the EEG signal commonly utilizes the magnitude-squared of the FFT to obtain an estimate of the power spectral density ($\frac{micro\ V^2}{Hz}$) of EEG signals.

The average band power derived from the spectral density is a scalar that summarizes the contribution of the given frequency band to the overall power of the signal. This is particularly useful in a machine learning and deep learning context, allowing for quick feature extraction from EEG signals. The average band power is also a relevant metric for neurological research as it allows differentiation between different seizure stages. For instance, the pre-ictal period is characterized by the predominance of slow waves with a frequency range comprising between $0 - 3\ Hz$, which reflects synchronized brain activity. Conversely, the ictal state is characterized in part by reduced delta activity [79]–[81]. In the following section, we briefly review the various EEG frequency oscillations.

1.4.1.2.1.1 Delta rhythm; $0.5 - 3$ Hz

Low-frequency activity in the normal human brain is characterized in part by the presence of delta oscillations in the $0.5 - 3$ Hz range. These oscillations are usually observed during periods of deep sleep and are prevalent during infancy. Delta band power is noted to be increased in brain lesions such as brain tumors as compared to normal brains, as well as during the onset of anesthesia and periods of deep sleep [82], [83]. The predominance of slow waves in the delta frequency range reflects synchronized brain activity. Conversely, wakefulness is characterized by increased higher frequency activity and decreased lower frequency activity in the delta frequency range. In pediatric brains, the delta frequency range dominates during the first two years of life. Aging leads to a decrease in delta activity and an increase in faster waves (alpha and beta waves) linearly.

1.4.1.2.1.2 Theta rhythm; $4 - 7$ Hz

Theta oscillatory activity observed within the $4 - 7$ Hz range is observed during drowsy,

hypnotic or sleeping states, but typically not during the deepest stages of sleep. Brain related pathology can give rise to abnormally strong or persistent cortical theta waves. EEG oscillations in the $4-7$ Hz frequency range are obtainable from the hippocampus and neocortex [84]. Hippocampal oscillations are typically short (less than one second) and associated with rapid eye movement (REM) sleep [85].

1.4.1.2.1.3 Alpha rhythm; $8-13$ Hz

Alpha oscillations, within the $8-13$ Hz range, dominate the EEG space during periods of relaxed wakefulness. Desynchronization in the alpha bands is closely related to processing of visual, auditory and sensory-motor signals. The alpha rhythm has been linked to a wide variety of cognitive tasks and is considered to be a multifunctional rhythm. Although the functional relevance of alpha rhythms is still not fully understood, it has been theorized that thalamocortical feedback loops as well as strengthened thalamic interconnections are prerequisites for cortically produced alpha rhythms [86], [87]. The amplitude of the alpha rhythm is proposed to be related to cortical activation. That is, an increase in alpha-power and the subsequent synchronization is linked to cortical and behavioral deactivation or inhibition [88]. Findings suggest that alpha rhythms not only reflect a resting or idle state in the human cortex but also may indicate the presence of several cognitive processes such as perceptual learning and memory [85], [89].

1.4.1.2.1.4 Beta rhythm; $14-30$ Hz

Beta frequency oscillations occur between the range of $14-30$ Hz. In adult brains, beta waves are characterized with amplitudes of 10-20 microvolts, and are typically observed bilaterally in the frontal lobes during cognitive tasks that require attention and/or cortical processing [74], [90].

1.4.1.2.1.5 Gamma rhythm; $30-100$ Hz

The gamma rhythm, between $30-100$ Hz, is characterized by relatively high frequency oscillations, and thought to be modulated by sensory input as well as cognitive processes such as working memory and attention. The contribution of gamma waves to brain function has been linked to neural encoding of sensory and cognitive information. The origins of these waves are under much debate. That is, whether they arise from intrinsic membrane properties or from neocortical excitatory and inhibitory circuits [91]. Gamma oscillations may also occur as a result of cerebral

network activity, since they can offer a signature of engaged networks, observable in cortical and subcortical structures. Not surprisingly, irregular gamma activity has been observed in neurological disorders, particularly Alzheimer's disease, Parkinson's disease, schizophrenia, and epilepsy [92].

1.4.1.3 Instrumentation

The typical electrodes used for scalp EEG recordings include bridge electrodes, cup electrodes and needle electrodes [93]. A bridge or pad electrode is a silver or silver chloride electrode mounted onto a plastic bridge to which connectors may be attached. These electrodes allow for reliable signal recordings, are flexible and easily positioned onto the subject's head. Signal acquisition from epileptic brains requires securing electrodes to the skin, to maintain contact during motion and violent spasms typical of seizure. For this purpose, collodion solution is typically used, followed by a stream of cold air to dry the collodion. Adhesive bentonite paste can be used in place of collodion solution. However, this lacks consistent adhesive properties and may cause skin sensitivity. Once all the electrodes are placed, a conductive gel is inserted into the concave side of the disc, before application onto the skin. Nineteen sensory electrodes are used in a clinical EEG, which are placed across the scalp surface in a standard formation defined by the 10-20 international placement system [94] as shown in Figure 1.2 above.

1.4.2 Computed tomography

Computed tomography (CT) is an imaging technique that utilizes differential levels of X-ray attenuation by tissues within the body to produce cross-sectional (i.e., tomographic) images of a region of interest. Computed tomography is widely available, relatively low cost, offers high spatial resolution, and strong penetration depth, thereby making it a commonly used brain imaging modality in clinical settings [95], [96]. The computed tomography method, however, does have some disadvantages. The high radiation dose is a limiting factor for scanning time and as compared to images derived from magnetic resonance (described in the next section), CT images offer relatively low-quality soft tissue contrast [97].

Despite these limitations, computed tomography is considered to be one of the modalities of choice in clinical neuroimaging. In epileptic patients, CT can accurately detect hemorrhage and infarcts, brain malformations, and large tumors [98]. However, with respect to epileptogenic

structural lesions (i.e., mesial temporal sclerosis), the CT scan may fail to detect abnormalities in up to 50% of these patients [37].

1.4.3 Single photon emission computed tomography

Single photon emission computed tomography (SPECT) is a minimally non-invasive method that utilizes radioisotopes (i.e., radiopharmaceuticals) to measure regional cerebral blood flow (rCBF) and indirectly evaluate metabolic activity [99]. Hexa-methyl-propylene-amine oximine (HMPAO) and ethyl-cysteinate dimer (ECD) are two commonly used radiopharmaceuticals in SPECT imaging. The SPECT method generates tomographic images of the three dimensional distribution of the radioisotopes [100].

SPECT system instrumentation often uses multiple detector-rings to achieve reasonably good spatial resolution and maximize recording brain activity [99]. The temporal resolution achieved via SPECT is relatively poor as the method is dependent on the hemodynamic response and sufficient detection of photon emissions. The spatial resolution of SPECT is fairly good, albeit not quite that of PET. A typical SPECT image will show symmetrical perfusion with the most intense perfusion in the cerebellum with HMPAO and in the occipital lobes with ECD [101]. Thus, SPECT image interpretation depends on accurately discerning areas of dynamic cerebral perfusion.

1.4.3.1 Ictal studies using single photon emission tomography

In ictal SPECT studies, the photon-emitting radiotracer is injected intravenously at seizure onset, allowing it to accumulate. These SPECT ictal studies allow for the localization of the epileptogenic zone via radiotracers and its subsequent cerebral metabolic and perfusion coupling. Epileptogenic zone localization using the SPECT method proves to be particularly useful in magnetic resonance negative partial epilepsy and focal cortical dysplasia [102], [103]. The SPECT method is similar in many respects to the positron emission tomography method (PET) detailed in Section 1.4.6. A comparison of these methods is presented in Section 1.4.6.4.

1.4.4 Magnetic resonance imaging

Anatomical magnetic resonance imaging (MRI) provides static anatomical information, as opposed to functional magnetic resonance imaging (fMRI) methods. Functional imaging can be regarded as providing dynamic physiological information [104], [105]. The fMRI technique is

discussed in Section 1.4.7. In MRI images, image quality is dependent upon on image resolution (i.e., field of view, slice thickness), signal to noise ratio (i.e., bandwidth, signal averaging) and lack of motion artifacts [104]. Briefly, in-plane resolution is related to the pixel number in the frequency and phase encoding directions, and through-plane resolution by the slice thickness. Signal to noise ratio is determined by pixel size, slice thickness, scan time (including the number of phase encoding steps) and the sequence used [106]. The following describes the use of anatomical MRI in the pre-surgical evaluation of epileptic patients. A discussion on advancements in the MRI technique is beyond the scope of this thesis.

1.4.4.1 Evaluating epilepsy using magnetic resonance imaging

Structural neuroimaging plays a central role in the presurgical evaluation of epileptic patients as it frequently allows detection of epileptogenic lesions and brain MRI scans are typically performed on newly diagnosed epileptic patients as well as those suffering from refractory epilepsy [107], [108]. An appropriate MRI investigation deems the use of specific protocols, selected based on identification of the region of onset by clinical and EEG findings. MRI based epilepsy protocols that offer increased image spatial resolution and multiplanar reformatting are often required since routine MRIs may miss subtle epileptic lesions [37], [109] and subsequent findings may be considered normal [110]. It is generally recommended that MRI epilepsy protocols include a T1-weighted acquisition to discern discrete structural brain lesions [37]. The table below compares the brain imaging modalities used in clinical settings.

Table 1.1: Comparison between EEG, MRI, CT, and SPECT modalities used in clinical settings.

Modality		**EEG**	**MRI**	**CT**	**SPECT**
Technical details	**Mechanism**	*Synchronized neural activity in the brain*	*Hydrogen atoms generate macroscopic polarization, measurable energy is emitted*	*X-ray measurements produces tomographic images*	*Radioisotopes measure regional cerebral blood flow*

			during relaxation		
	Measurement area	*Cortical surface and/or whole brain*	*Cortical surface and/or whole brain*	*Cortical surface and/or whole brain*	*Cortical surface and/or whole brain*
	Measurement property	*Postsynaptic potentials*	*Magnetic properties of tissue*	*High-energy electromagnetic radiation*	*Quantitatively measure physiological processes in vivo*
	Typical time resolution	*0.01 seconds*	*High*	*200 ms*	*High*
	Typical spatial resolution	*20 cm*	*High*	*0.5 mm*	*1 cm*
Instrumentation	**Size**	*Small*	*Large*	*Large*	*Large*
	Portability	*Yes*	*No*	*No*	*No*
	Cost	*30K-150K USD*	*1 Million + USD*	*1 Million + USD*	*1 Million + USD*
Other details	**Invasive**	*Non-invasive*	*Non-invasive*	*Minimally invasive*	*Minimally invasive*
	Clinical application potential	*Currently used in clinical settings*	*Currently used in clinical settings*	*Currently used in clinical settings*	*Currently used in clinical settings*

	Research application potential	*High*	*High*	*High*	*High*

1.4.5 Magnetoencephalography

Magnetoencephalography (MEG) is a non-invasive neurophysiological imaging technique that offers temporal resolution at approximately one millisecond and spatial resolution of approximately $3.5\,mm$ [111]. MEG has seen use primarily in human studies to study brain function. An advantage of the MEG method over other non-invasive neuroimaging methods is that it does not require the presence of a reference electrode, thus facilitating network modeling and functional connectivity analyses. However, MEG is not portable and is constrained by relatively large instrumentation as compared to EEG or fNIRS technologies. However, recent developments in portable magnetoencephalography might obviate this restriction [112], [113].

The MEG method is able to identify abnormal neural dynamics at the regional or network level and can monitor disease progression. Thereby, MEG can help to determine the efficacy of medical (i.e., pharmacological, medical, surgical, and/or behavioral) interventions. Furthermore, MEG records can be used to investigate neural markers of disease. As it relates to epilepsy and seizures, when MEG is combined with structural imaging, it is known as magnetic source imaging (MSI) [114].

1.4.5.1 Advantages of magnetoencephalography

Advantages of the MEG method over EEG include: the absence of magnetic field distortion and attenuation by highly variable conductivities between brain and sensor, and the ease of using high-density sampling [115]. Furthermore, MEG offers accuracy on the order of millimeters when mapping brain tumors as opposed to EEG methods [116]. MEG has increased sensitivity in detecting tangential currents to the scalp surface, whereas EEG is sensitive to tangential and radial neuronal activities. The cross sectional area of synchronized cortical brain activity is typically less using the MEG method as compared to synchronized cortical epileptic activity when using the EEG method ($3-4\ cm^2$ as opposed to $6-20\ cm^2$) [117].

Furthermore, magnetic fields as used in the MEG method are not distorted by the conductivity properties of the head and brain (scalp, skull, cerebrospinal fluid) as compared to electrical fields. Finally, the MEG method offers improved spatial resolution ($2-3\,mm$) as compared to EEG ($7-10\,mm$).

1.4.5.2 Limitations of magnetoencephalography

Equipment portability and instrumentation (specifically, the large array of sensors and the requirement of cooling the sensor array) cost are some limitations of the MEG technique. Separating brain signals from external environmental noise can pose a challenge as the superconducting quantum interference devices (SQUID), which are the highly sensitive magnetism detector arrays. Typically, SQUID arrays are situated as close as possible to the subject's head (approximately $2\,cm$) and require cooling to approximately $-270\,℃$ before they can provide a viable signal. Furthermore, the SQUID arrays need to be arranged close to each other in a helmet-like fashion to probe certain types of brain activity with a penetration depth of only a few centimeters into the brain. This placement ensures sensitivity to cerebral magnetic field changes as opposed to other magnetic field changes in the environment.

1.4.5.3 Magnetoencephalography and epilepsy

In some respects, the MEG method is similar to EEG, however, an important difference lies in the fact that the skull and the tissue surrounding the brain affect the magnetic fields measured by MEG much less than they affect the electrical impulses measured by EEG. This works to improve the accuracy of MEG recordings as compared to EEG [118]. Furthermore, epileptic focus localization is possible when MEG technology is combined with MRI methods.

1.4.5.3.1 Epileptic focus localization and magnetoencephalography

Since the development of multidetector array systems in the early 1990s, MEG has been studied for possible clinical applications [114]. Epilepsy localization and presurgical brain mapping using MSI has shown strong promise as it offers high spatial and temporal resolution to resolve networked areas of brain processing. Recordings with implanted dipoles placed in mesial, basal, and inferior lateral temporal regions showed that MEG predicted localizations of an epileptic focus are within $1-4\,mm$ of their actual locations [119].

Multiple studies have shown that localization of seizure focus is best seen in patients with intrinsically epileptogenic focal lesions [69], [120]–[122]. Results from simultaneous EEG–MEG studies suggest that MEG signals alone do not necessarily provide a clear advantage in comparison with EEG signals in detection sensitivity of deep epileptiform sources [118]. Furthermore, MEG is intrinsically better at focus localization from sources that are adjacent or a few centimeters away from a MRI-visible lesion [121], [123].

1.4.6 Positron emission tomography

Positron emitting radioisotopes of carbon, nitrogen, oxygen, and fluorine are commonly used as radioactively labelled molecules (i.e., tracer molecules), and injected intravenously (or inhaled) to measure regional cerebral blood flow and/or regional cerebral metabolic rate of glucose (rCMTG) via the positron emission tomography (PET) imaging technique [100], [124].

1.4.6.1 Instrumentation and image reconstruction

A cyclotron (i.e., positron accelerator) produces a large quantity of protons and accelerates them along a circular orbit inside a powerful alternating electromagnetic field chamber. The particles gain energy and are displaced toward a target at approximately the speed of light. This bombardment leads to radioactive unstable isotopes via a nuclear reaction. Due to the short half-life of radioisotopes, the cyclotron is typically placed in close proximity to the PET scanner [124], [125]. The unstable nucleus of these radioisotopes creates gamma rays by interacting with neighboring electrons and gamma ray energy is used to eventually form three-dimensional (3D) images of tracer concentrations within the body.

1.4.6.2 Positron emission tomography studies in epilepsy

PET studies focusing on metabolism measurement of cerebral glucose, serotonin and oxygen, in addition to cerebral blood flow changes are used in determining an epileptic focus [126]. In addition to localizing epileptogenic focus, PET studies provide additional important information pertaining to the functional status of the brain. PET studies aid in understanding the role neurotransmitters play in identifying epileptic foci [125]. Particularly, PET receptor imaging studies have shown reduced concentrations of 11C-flumazenil along with increased concentrations of mu opiate and delta opiate bindings in epileptic foci [125], [127].

1.4.6.3 Limitations of the positron emission tomography method

Instrumentation and its portability, cost-effectiveness, maintenance and safety are main limitations of the PET method. The cyclotron contributes significantly towards the higher acquisition cost of a PET system. Typically, access to the cyclotron is tightly controlled through a variety of safeguards. Lab work with radioisotopes takes place in sealed and shielded hot cells designed to contain spills. Specialized air and waste handling systems guard against accidental releases of radioisotopes.

1.4.6.4 Comparison of the PET and SPECT methods

In terms of cost comparison, SPECT systems are more affordable as compared to their PET counterparts since the SPECT method does not require a cyclotron. From a technical standpoint, the spatial resolution provided by the PET method is better compared to images obtained by the SPECT method [99], [100]. Furthermore, the radiation dose used in SPECT methods is considerably higher as compared to PET [103]. However, radioisotopes typically used in SPECT decay and directly emit gamma rays [127] as compared to the PET method.

1.4.7 Functional magnetic resonance imaging

Functional magnetic resonance imaging (fMRI) of the brain offers a non-invasive methodology to assess brain function using magnetic resonance signal changes [128]. Hemodynamic and metabolic changes drive neuronal responses resulting from the blood oxygenation level dependent (BOLD) method [128], [129].

1.4.7.1 Neurovascular coupling and fMRI BOLD signals

The BOLD signal is coupled to brain synaptic activity, thereby allowing for the probing of functional brain responses using the fMRI signal. The synaptic inputs and neuronal processes present at the site of activation form the basis of BOLD signal changes [38]. Brain hemodynamic coupling to synaptic and neuronal processes induce changes in the astrocytic Ca^{2+} concentration and consequently lead to an increase in blood vessel dilation and cerebral blood flow.

1.4.7.2 Advantages and disadvantages of the fMRI technique

The fMRI technique is a non-invasive, safe, radiation free, virtually risk-free method to evaluate brain function. It is relatively easy to use, and the images it produces have a resolution of approximately 1 millimeter. By utilizing the fMRI method, it is possible to record activation signals from all brain regions. Yet fMRI also has its disadvantages. It is not cost-effective, and while the method allows for understanding the blood flow in the brain, observing the activities of individual neurons is not entirely possible [130].

The fMRI method has relatively poor temporal resolution and the associated functional BOLD response peaks approximately 5 seconds after the start of neuronal firing [23], thus, making it difficult to distinguish BOLD responses occurring within a short time window. This can be mitigated by careful experimental design to a certain extent as well as utilizing multimodal approaches; specifically, combining the fMRI method (which offers a relatively high spatial resolution) with the EEG or MEG modalities (which have higher temporal resolution) [131].

1.4.8 Functional near-infrared spectroscopy

1.4.8.1 Introduction

Functional near infrared spectroscopy (fNIRS) is a non-invasive modality that uses optical measurements to measure blood oxygenation and hemodynamic parameters for both humans and animals. In a typical fNIRS setup, optodes corresponding to light sources and detectors are placed on the surface of the subject's head. Light sources emit near-infrared light into tissue, and light detectors act to collect the reflected light. Eventually, this detected light can be used to calculate the blood oxygenation changes associated with cerebral hemodynamic activity [132]. F.F. Jobsis published the first fNIRS study in humans and reported that near infrared spectroscopy is a feasible non-invasive method for monitoring the concentration of hemodynamic changes in the brain [133]. Blood level oxygen dependent based functional magnetic resonance measurements were introduced subsequently and building on these results, shortly after, the hemoglobin concentration changes during brain activation were first measured with fNIRS [134]–[137].

1.4.8.2 Fundamentals of near infrared spectroscopy

Near infrared spectroscopy technology utilizes light in the near-infrared (NIR) spectral

range with wavelengths between approximately $650-950\,nm$ within the so called "optical window" to penetrate several centimeters into biological tissue [138]. When NIR light is illuminated into tissue, photons can be absorbed or scattered by the tissue structures and molecules, primarily lipids, water or chromophores. Due to the fact that the human head is a highly scattering medium, the light path is longer than the source-detector separation. Experimental work and model based simulations confirm that approximately one out of every 10^9 photons eventually reach the brain [139]. Modeling photon propagation via Monte-Carlo simulations offers a flexible and approach to simulate photon transport through a biological medium [140], [141]. The Monte-Carlo method is essentially a statistical process that utilizes probability distributions to describe the step size of photon movement between interested sites of photon-tissue interaction and deflection angles in a photon's trajectory when a scattering event occurs. Monte Carlo simulations can keep track of multiple physical quantities simultaneously. To achieve precision, Monte-Carlo simulations require significant computation time. At the expense of computationally efficiency, Monte Carlo methods are often considered the standard for simulated measurements of photon transport [142]. This result is achieved in part by multiplying the source-detector separation by a differential pathlength factor which depends on several factors such as wavelength, age of the subject, and type of tissue. Of the photons that do eventually reach the target, light attenuation is used to calculate the hemoglobin concentration changes by using the Beer Lambert Law. Light attenuation is parametrized partly on the absorption and scattering properties of tissue structures and molecules, as mentioned earlier. Cerebral chromophores (HbO, HbR and cytochrome aa 3 (Cyt aa3)), have specific absorption characteristics in the NIR range, and the NIRS method has the capability to measure changes in these chromophores. The extinction coefficient associated with each chromophore dictates the absorption of light at a particular wavelength. The relationship between specific extinction coefficient (Ɛ) ($M^{-1}cm^{-1}$) and the associated absorption coefficient (α) (cm^{-1}) is related by the following:

$$\alpha = ln(10)\text{Ɛ} \qquad \textit{Equation 1}$$

Extinction coefficients corresponding to HbO, HbR and water are displayed in Figure 1.4 below. Oxygenated hemoglobin (HbO), reduced hemoglobin (HbR) and C. oxidase are the main types of chromophores and their concentration dynamically changes with time and oxygenation status. Cytochrome-c oxidase varies with oxygenation status, (driven by metabolism and blood

flow) but it does not significantly affect the measurement because the signal of Cytochrome c oxidase (due to high concentrations of Cytochrome-c oxidase) is approximately ten times smaller in magnitude as compared to hemoglobin.

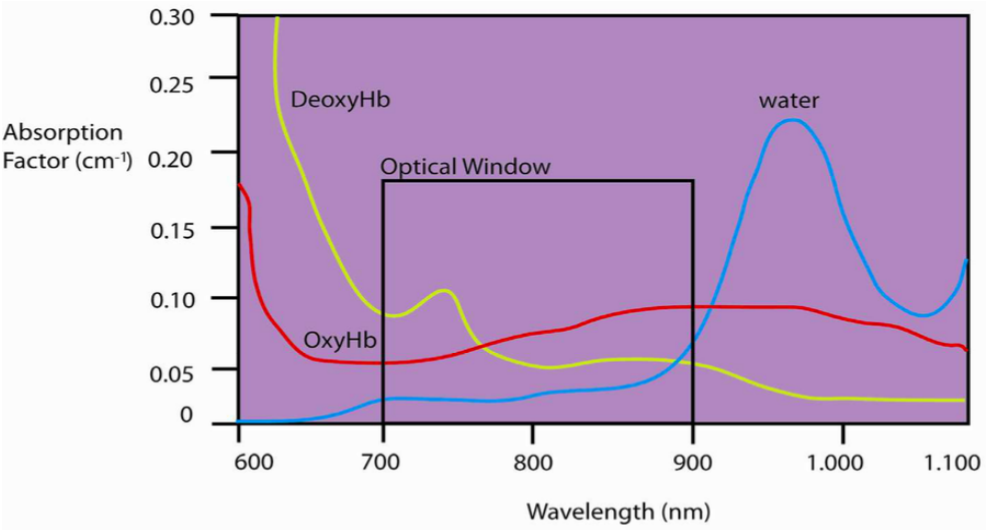

Figure 1.4: Specific extinction spectra of HbR, HbO and water. HbO is characterized by the presence of an oxygen molecule binding to the iron atom of the heme group in hemoglobin.

HbO and HbR have different absorption spectra in the NIR window which allow for the calculation of their respective concentration changes. The isosbestic point, where HbO and HbR have the same absorption coefficient, occurs around 800 nm. The skin absorbs near infrared light throughout the epidermal, dermal and hypo-dermal layers since melanin is a strong absorbing chromophore. Hair's melanin content absorbs NIR light, thus, to obtain a good signal to noise ratio, subjects with darker hair require their hair to be displaced [143].

1.4.8.3 The near infrared sampling region

Near infrared light is propagated into the head at one specific position and it subsequently diffuses in all directions, undergoing random scattering and absorption processes in the tissue which attenuate the original signal by orders of magnitude. A fraction of NIR light is able to propagate through tissue on a "banana shaped" path back to the surface where it is then detected by a photodetector. The banana shape is essentially the probabilistic density function of photons that were emitted by source "S" and detected by detector "D" as illustrated in Figures 1.5, 1.6 below. Each measurement channel is created by a source and its corresponding detector placed

over the surface of the head. NIRS signals are assumed to originate from the centered area between the sources and detectors [144]. The separation between sources and detectors is important since it defines the depth of penetration in the cortex. The NIRS method is sensitive to subject-motion induced noise and subsequent optode displacement leading to motion induced artifact. Thus, the distance between source and detector and subsequently the coupling between source-detector and scalp contributes to the fidelity of the NIRS signal [145].

If the distance is increased between sources and detectors, the arc of the banana shape will be larger which will obtain information from deeper structures in the cortex [146]–[148] (Figures 1.5, 1.6 below). While determining the distance between the source and detectors (typically, the distance between sources and detectors should be at least $2\,cm$), the spatial resolution of the measurement and sufficient signal quality, including the signal-to-noise ratio must be considered. Generally, a distance of 30-35 mm (distance between source and detector) is considered optimal, and the sensing depth into the adult human head is on the order of $15 - 25\,mm$ [40].

Typically, there are three types of noise in NIRS data: instrumental, physiological and experiment (i.e., subject induced head motion). A growing number of algorithms are being developed for NIRS noise reduction and signal improvement. Algorithms developed for noise reduction in the NIRS signal are generally organized into three categories: (1) reducing noise based on signal temporal characteristics, (2) reducing noise based on signal spatial characteristics, and (3) measuring noise independently and then subtracting it from the signal [139]. Reducing signal noise based on temporal qualities makes use of conventional methods such as band pass filtering and moving averaging techniques. This effectively eliminates high frequency instrument noise and low frequency drift. However, this typically does not remove abrupt changes in the signal [149]. Algorithms (i.e., eigenvector-based methods) in the second category rely on the assumption that the noise in the NIRS signal is spatially distributed. However, these methods often require subjective decisions regarding the number of components to retain. In the third category, noise can be measured independently by additional hardware (i.e., accelerometer to measure head motion) [150] as well as by using a close optode configuration. The resultant signal is deemed to be noise, which can be subtracted from the signal.

To counteract the typically weak fNIRS signal, signal amplification and signal extraction techniques can also be applied to increase the fNIRS signal via lock-in amplification methods

[151]. Additional information on lock-in amplification and subsequent signal recovery, can be found in Meade et. al., [152].

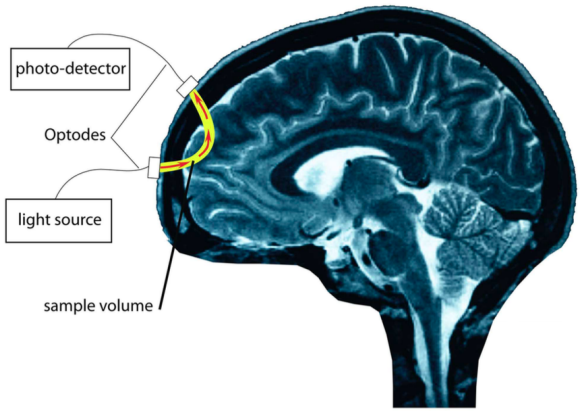

Figure 1.5: Schematic diagram of photons propagating in the curved “banana shape” (yellow curve).

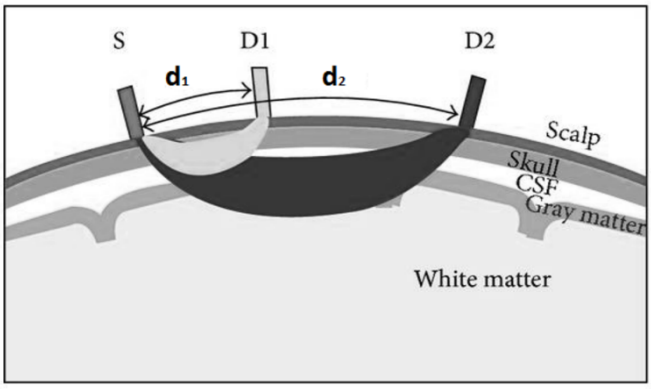

Figure 1.6: Schematic demonstration of the banana shape traveled by photons; S: Source, D1, D2: Detectors, d_1, d_2 are the distances between the sources and detectors.

1.4.8.4 The modified Beer-Lambert law

The Beer-Lambert Law relates the concentration of tissue chromophores to photon attenuation and considers the relationship to be linear. The Beer-Lambert law is defined as:

$$A = log\frac{I_O}{I} = \varepsilon C.d \qquad \textit{Equation 2}$$

where A is the light attenuation and the logarithmic ratio of two intensities; I_O is the intensity of the incident light, I is the intensity of the transmitted light, $C(M)$ is the concentration of a absorber, ε is the molar extinction coefficient ($mM^{-1}cm^{-1}$) and d (cm) is the distance that light travels (the inter-optode distance). If there is more than one absorber present in the medium, the law can be written as:

$$A = [\varepsilon_1.C_1 + \varepsilon_2.C_2 + \ldots + \varepsilon_n.C_n]d \qquad \textit{Equation 3}$$

with the explicit purpose to determine $C_{1\ldots,}C_n$ in the above equation. A is experimentally measured; d is the distance between source and detector, $\boldsymbol{\varepsilon}$ from the literature has been shown previously for HbO and HbR.

Scattering is considered to be zero in the Beer-Lambert Law. However, human tissue is inhomogeneous and by nature is a highly scattering medium, such that the Beer-Lambert law cannot be used for biological tissue. When a highly scattering medium is considered, the differential path length factor ($DPLF$) and the associated scattering losses (G) are important. The

modified Beer-Lambert Law [153], [154] can be written as:

$$A = log\frac{I}{I_O} = \varepsilon.c.d.DPLF + G \qquad \textit{Equation 4}$$

If we consider time (t) and wavelength (λ), this can be rewritten as:

$$A(t,\lambda) = \log(\frac{I(t,\lambda)}{I_O(t,\lambda)}) = \sum \boldsymbol{\varepsilon}(\lambda).C_i.(t).d.DPLF(\lambda) + \mathrm{G}(\lambda) \qquad \textit{Equation 5}$$

$DPLF$ defines the increase in optical path length due to scattering in the tissue and the light travels in a longer path due to the scattering phenomenon. During the calculation, it is assumed that G is not time-dependent and the change in scattering can be neglected when compared with changes in absorption [155]. As mentioned previously, photons are transported primarily by diffuse scattering, and their traveled mean pathlength can be expressed by a differential path length factor whose value is typically greater than the inter optode distance. Therefore, the concentration changes of hemoglobin can be shown as:

$$\Delta A(\Delta t,\lambda) = \log(\frac{I(t,\lambda)}{I_O(t,\lambda)}) = \sum_i \varepsilon(\lambda).\Delta C_i(t).d.DPLF(\lambda) \qquad \textit{Equation 6}$$

Experimentally, the $DPLF$ cannot be measured directly since the tissue properties cannot be determined absolutely with continuous wave NIRS systems. As a result, an absolute calculation of chromophore concentration cannot be obtained; only changes in concentration of chromophores can be measured with NIRS under several assumptions.

The hemodynamic response is typically slow in response to neural stimulation and the hemodynamic response begins approximately $2-3$ seconds after the onset of neural stimulation [146]. Figure 1.7 below shows the typical hemodynamic response measured by fNIRS; the time to peak is noted to be approximately 4 to 15 seconds after onset of activation [156]. Following neural activation, local blood flow and volume typically increase leading to an increase in HbO and a corresponding decrease in HbR albeit of smaller magnitude [147]. Parameters related to the task

type and its duration impact the magnitude of the hemodynamic response.

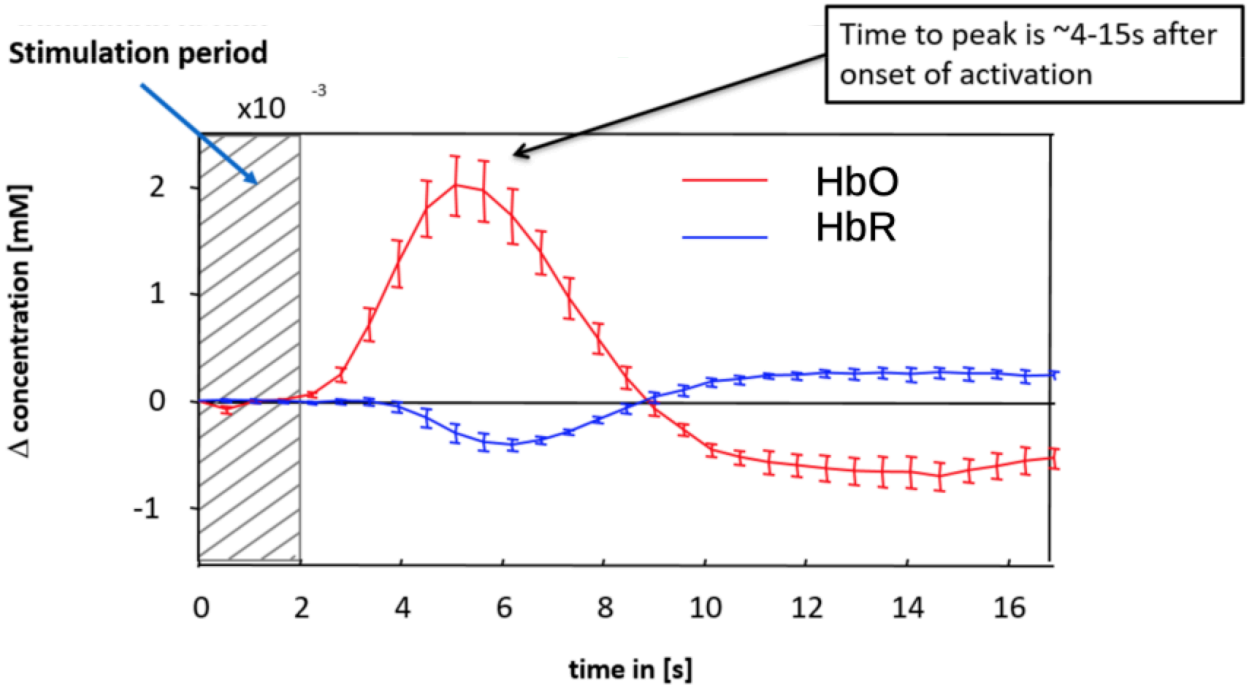

Figure 1.7: A typical NIRS activation in response to a stimulus with onset at 2 seconds.

1.4.8.5 Instrumentation used in NIRS systems

During the last twenty years, substantial improvements have been made to NIRS instrumentation [157]. Currently, the continuous wave (CW) mode of NIRS is extensively used in research and clinical settings due to its affordability and ease of use in natural settings [132]. NIRS systems emit laser light onto tissues at a constant intensity. Light detectors effectively measure the intensity of diffusely reflected light and for CW-NIRS, each source should have at least two distinct wavelengths to allow for discrimination of the HbO and HbR isoforms. Two wavelengths ($760 - 850\ nm$) will be emitted simultaneously and distinguished by modulation, each at different frequencies. The sources and detectors should be located a distance of a few centimeters over the tissue in order to make sure NIR light penetrates deep enough to reach the cortex and reflected light is collected by the detectors. Details regarding the NIRS instrumentation used in this thesis is presented in Section 4.4.3.2.

1.4.8.6 Advantages and limitations to the fNIRS method

Compared to fMRI, fNIRS offers advantages of improved temporal resolution, smaller size,

increased portability, less sensitivity to motion artifacts, cost effectiveness, and is able to obtain recordings in natural conditions. Furthermore, fNIRS provides information about both HbO and HbR isoform concentration changes, whereas fMRI measures the BOLD signal which is associated with the change in HbR concentration.

There are also several disadvantages to fNIRS imaging, namely being the limited penetration depth (which limits recordings from the cortex only), low signal-to-noise ratio, and the sensitivity of the superficial tissue impacting the signal-to-noise ratio to name a few [132].

The functional activity of the human brain can be measured with various imaging techniques including fMRI, fNIRS and EEG; each modality carrying its own advantages and disadvantages. The strengths and weaknesses of each method are shown in the table below.

Table 1.2: Comparison between fNIRS, fMRI, MEG, and PET modalities.

Modality		**fNIRS**	**fMRI**	**MEG**	**PET**
Technical details	**Mechanism**	*Measures brain activity via tissue optical absorption and scattering properties.*	*Measures brain activity by detecting magnetic changes associated with blood flow.*	*Magnetic fields produced by electrical activity within the brain*	*Injected or inhaled tracer molecules*
	Measurement area	*Cortical surface and/or whole brain*	*Cortical surface and/or whole brain*	*Cortical surface and/or whole brain*	*Cortical surface and/or whole brain*
	Measurement property	*HbO/HbR changes*	*HbR changes*	*Synchronized neural currents*	*Quantitatively measure biochemical and*

					physiological processes in vivo
	Typical time resolution	*1-2 seconds*	*2-3 seconds*	*10 milliseconds*	*1–2 min*
	Typical spatial resolution	*20 cm*	*5 cm*	*2-3 mm*	*4 mm*
Instrumentation	**Size**	*Small*	*Large*	*Large*	*Large*
	Portability	*Yes*	*No*	*No*	*No*
	Cost	*100-400K USD*	*1 Million + USD*	*1 Million + USD*	*8-10 Million + USD*
Other details	**Invasive**	*Non-invasive*	*Non-invasive*	*Non-invasive*	*Invasive*
	Clinical application potential	*Currently not used in clinical settings*	*Currently not used in clinical settings*	*Currently not used in clinical settings*	*Currently not used in clinical settings*
	Research application potential	*High*	*High*	*High*	*High*

1.4.9 Rationale for using EEG-fNIRS multimodal signals

However useful a scalp EEG recording maybe, it provides only the electrical parameter of brain function. The neuronal response to the hemodynamic changes associated with seizure events, initiates a series of events in which the end result is seizure propagation. As mentioned in previous sections, the continuous assessment of the EEG is useful in seizure monitoring, but it is not always clear to what extent recorded electrographic activity contributes to clinical impairment or ongoing neuronal injury [2-5,7,8].

Individual imaging techniques offer limited information about neurovascular coupling due to the complexity of the relationship between neural activity and the localized hemodynamic response. Multimodal approaches are needed which combine the advantages of individual imaging techniques (e.g., high temporal resolution of EEG) and mitigate their limitations (e.g., volume conduction). Recently, multimodal imaging has become increasingly important due to the complexity of neuroscience investigations. Multimodal measurements allow for examining the neurovascular coupling phenomenon, activity within a resting state brain network and specific clinical conditions such as epilepsy [158]. Measuring simultaneous electrical and hemodynamic information from the brain by way of EEG-fNIRS combined recordings offers a unique way to address in vivo the question of the integrity of the neurovascular coupling in the epileptic brain. Furthermore, in addition to studying brain mechanisms during the resting state in epileptic brains, multimodal measurements allow for the exploration of resting state functional connectivity in epilepsy patients [159]–[161].

fNIRS has powerful features that make it possible to perform functional investigations of the brain and EEG-fNIRS offer complementary imaging modalities and therefore an important resource for studying aspects of neurovascular coupling and its relationship with pathological brain physiology. The figure below shows multimodal resolution in both temporal and spatial domains [158].

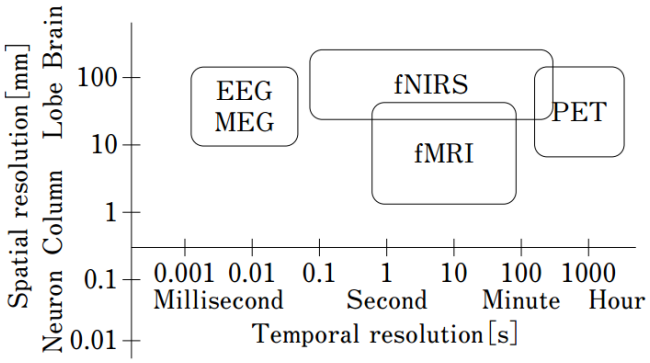

Figure 1.8: Temporal and spatial resolutions of the EEG, MEG, fNIRS, fMRI, and PET methods.

1.4.9.1 Confounding factors related to multimodal EEG-fNIRS recordings

Confounding factors intrinsic to EEG and fNIRS multimodal data technologies can potentially impact signal reliability. These confounding factors are generally divided into two groups (i.e., procedure dependent, and participant dependent) with occasional overlap. Procedural

factors are related to the experimental setup and data analysis techniques. Participant related factors are characteristic of the participants themselves; primarily their physical, mental or social state at the time of the experiment.

Confounding factors related to procedural aspects of data collection must be considered when making inferences from the collected data. These are inherent to the experimental design and should be consistent across all participants. With respect to data collection in clinical settings (i.e., the intensive care unit) experimental factors are taken into consideration when interstudy or interpatient comparisons are to be made. Furthermore, differences between individual participant data may exist in recording procedures devoid of specific instructions (i.e., typical of patient recordings in intensive care unit settings) owing to spontaneous physiologic and pathologic cerebral processes [162]. Typically, visual, auditory or other stimuli should be avoided if the goal of data collection is to obtain resting state brain data and to study resting state networks (RSNs) [163]. Furthermore, considerations whether the subject is to be instructed to remain at rest with their eyes open or closed is important as significant differences in RSNs have been reported between these two states [164].

Furthermore, the existence of instrument noise may become a source of confounding effects in measurements obtained during resting-state experiments and in the validity of comparisons obtained from these methods [165]. It has been determined that instrument noise can confound signals to produce differential activity in specific brain structures particularly the insula, cingulate gyrus and occipital cortex [166], [167]. The probable effect of noise on resting-state brain data highlights the possibility of noise attenuation instrumentation when using multimodal neuroimaging [168] technologies. Procedure based confounding effects can potentially be mitigated by using a standardized procedure for data collection [169], however this generally is not possible in the critical care patient population, due to the fact that these patients may be in compromised brain states (i.e., comatose or sedated statuses).

Participant dependent factors such as age, sex, motion, and sleep stage routinely can confound multimodal neuroimaging data [170]. The link between BOLD responses and neural activity may be altered due to age-related changes in the cerebral oxygen metabolic rate—thereby implying that changes in BOLD properties in older participants may be of physiologic rather than neuronal origin [171]. Age and specific characteristics of the EEG signal have been studied and

generally, the EEG spectral power has shown sensitivity to age differences in younger participants [172].

Sex has shown to be a possible confounding variable in multimodal measurements as anatomic differences are mirrored by differences in resting state functional connectivity by sex [173]. Men typically show greater connectivity than women within the right cuneus cortex and generally women display stronger functional connectivity metrics as compared to men in the left inferior temporal gyrus [174]. Furthermore, EEG resting-state sex based differences have also been reported [175], [176]. In the higher EEG frequency bands, particularly the gamma band, female brains have reported higher EEG spectral power differences as compared to male brains [176], [177].

Body motion, particularly head movement can confound measured signals and efforts are generally made to minimize movement. It has been determined that head motion leads to reduced inter-regional functional connectivity in the default mode network (DMN) and the frontoparietal control network [178]. Interestingly, it has been found that head movement introduced spurious correlation in resting-state results and long-range inter-regional correlations were reduced, while short-range correlations were increased [179]. Head motion can by itself induce neural activity, as EEG motion correlates with BOLD responses in the insula and thalamus [180]. Apparent differences in functional connectivity measures exist during periods of sleep and wakefulness [181]. Sämann et. al, determined that sleep pattern inconsistency reduces the functional connectivity in the DMN as compared with consistent sleep patterns [181] .

1.5 Deep learning techniques

Deep learning is fundamentally hierarchical or representation learning and is a subset of machine learning. Deep architectures are different from shallow models principally in their topology: deep models use several hidden layers to build more complex representations of input data. Traditionally, employing shallow networks consisting of one or two layers for a task was preferred mainly due to the absence of computational power to successfully train deeper models.

Recent advances have implemented novel algorithms to train deeper models: unsupervised pre-training [182] and new regularization functions [183]. These help to mitigate the vanishing gradient problem that kept deep models from learning proper data representations. Deep models

learn better representations as each layer specializes in creating an abstraction of the data based on the previous layers. Thus, low level layers will capture low level information of the data with which subsequent layers will build more abstract and useful representations. In summary, deep learning helps create complex and structured abstract representations of the data that embody the necessary features for solving the task that the model is being trained to solve. In this thesis, we specifically explore the long short-term memory variant, of recurrent neural networks, sequence to sequence autoencoders, convolutional neural networks, and finally a combination of these architectures.

1.6 Problem statement

Hemodynamic brain responses attributed to epileptic events are observed with a good degree of statistical significance and in concordance with clinical presentation. In the context of epileptic multimodal EEG-fNIRS recordings, the contribution of spectroscopic signals in real time seizure detection has not been explored. Furthermore, the intertwined relationship between the electrical and hemodynamic activity of the epileptic brain has not been thoroughly investigated. Resting state signals have the potential to offer insight into the functioning of the human brain in health and in disease. Although EEG resting state signals have been explored in tandem with fMRI in populations with healthy brains, there are limited studies of the resting epileptic brain using signals derived from EEG-fNIRS multimodal technology. Fundamental neuroscience relationships constituting the brain's interdependence on electrical and hemodynamic activity have not been explored.

The work in this thesis first studies the benefits of using multimodal signal in a seizure detection task based on deep learning. This first effort could impact monitoring of seizures in the context of long-term recordings where reading individual EEG recordings is not always practical. As a second investigation, we investigate how artificially intelligent models can be leveraged to predict the hemodynamic (fNIRS) correlates of spontaneous neural (EEG) activity in whole-head resting state EEG-fNIRS epileptic patients. These models could, in the future, be used to characterize the brain at rest and potentially develop biomarkers associated with silent seizures or dysfunctional brain networks. An extensive multimodal EEG-fNIRS dataset comprising signals from 40 epileptic brains was used to investigate these questions.

1.6.1 Objectives, hypotheses and research work overview

The objectives of this thesis are to: 1) utilize hemodynamic information from EEG-fNIRS signals obtained from epileptic patients for the task of detecting seizure events using deep learning models, and 2) develop a deep learning model to determine the underlying relationship between cerebral electrical and hemodynamic signals (within the context of neurovascular coupling) in the resting epileptic brain. The resting epileptic brain displays spontaneously occurring neural activity thought to reflect its functional organization. In addition, both neural (EEG) and hemodynamic (fNIRS) resting state signals affect local cerebral electrical and hemodynamic properties via neurovascular coupling. The interdependence of each component (neural and vascular) of this phenomenon is a topic of great interest to the wider neuroscience and clinical community due to its relationship with neuropathological conditions including epilepsy, stroke, subarachnoid hemorrhage, sleep, and traumatic brain injury to name a few.

The individual objectives and their corresponding objectives are stated below:

Objective 1: Based on EEG-fNIRS data collected from 40 epileptic patients, develop a deep learning model to detect seizure events with high sensitivity and specificity metrics.

Hypothesis 1-1: Hemodynamic information derived from fNIRS recordings provides additional benefit in seizure detection as compared EEG signals alone.

Hypothesis 1-2: Hyperparameter optimization of the long short-term memory unit variant of recurrent neural networks bypasses extensive feature extraction, selection, or signal preprocessing.

Article 1: **Sirpal, P.,** Kassab, A., Pouliot, P., Nguyen, D. K., & Lesage, F. (2019). "fNIRS improves seizure detection in multimodal EEG-fNIRS recordings." Journal of Biomedical Optics, 24(5)., https://doi.org/10.1117/1.JBO.24.5.051408.

Objective 2: Develop and implement deep learning methods that process EEG-fNIRS data to reconstruct resting state fNIRS waveforms from resting state EEG signals.

Hypothesis 2-1: Resting state EEG signals in epileptic patients contain relevant time and frequency domain information across patients and brain regions.

Hypothesis 2-2: As with full spectrum EEG signals, specific EEG frequency bands can drive prediction of resting state patient specific hemodynamic signals using sequence to sequence

learning.

Hypothesis 2-3: Using seed based functional connectivity methods, similar spatial patterns between experimental fNIRS and convolutional neural network long short-term memory autoencoder derived fNIRS reconstructions exist.

Article 2: **Sirpal, P.,** Damseh, R., Peng, K., Nguyen, D. K., & Lesage, F. (2020) "Multimodal autoencoder predicts resting state in EEG-fNIRS signals", submitted to *Neuroinformatics.*

This thesis is organized as follows: **Chapter 2** reviews the state of the art in terms of seizure detection in human epilepsy. **Chapter 3** describes the deep learning methodology with respect to data processing and model development, and details regarding the data used in this thesis. **Chapters 4 and 5** contain the manuscripts relevant to the research objectives and finally a discussion and conclusion are presented in **Chapters 6 and 7** respectively.

CHAPTER 2 LITERATURE REVIEW

2.1 Automated seizure detection

The unpredictable and sporadic nature of seizures imposes a high risk of injury or death. In recent years, there has been growing research interest regarding seizure detection and prediction using scalp and invasive EEG recordings [74], [184], particularly the extraction of characteristic features from EEG signals which correlate with seizure events. Prior to the ictal state, systemic and local acute physiological changes typically occur. These include an increase in oxygen availability, changes in cerebral blood flow, changes in regional blood concentrations of oxygenated and deoxygenated hemoglobin, and acute changes in heart and respiratory rate [185]–[188].

Automatic seizure detection is an important tool in the context of long-term epilepsy monitoring. Early seizure detection focuses on detecting seizure onset before clinical symptoms manifest, thereby allowing for timely clinical intervention. Many patients experience seizures sans aura or other warning signs [11] and it is impractical to have trained personnel continually examine patients and their respective EEG recordings for seizures. Thus, real-time automated seizure detection, can help to accurately diagnose and treat seizures. Practically, seizure detection denotes the automatic recognition of seizures shortly before or after actual onset in a short (few seconds) time window.

Seizure prediction represents the automatic recognition of seizures in advance of the actual seizure event where the prediction window can be several seconds to minutes long [189]. One common distinction between seizure detection and prediction is as follows: i) the target application of either seizure detection or prediction and its corresponding treatment strategy, and ii) detection metrics are generally higher than those reported for prediction. One other important distinction between seizure detection and prediction concerns the underlying methods utilized. There are two general approaches in seizure prediction studies with considerable overlap: statistical and algorithmic. Distinct characteristics of the EEG recording are evaluated in a retrospective manner, to discriminate between ictal and non-ictal states of the brain. These methods are mainly used for exploratory analysis of the recording and to mark seizure state [189], [190]. However, this approach can be impractical for a real-time application, where the goal is to identify live EEG data. Work by Viglione & Walsh 1975 helped to pioneer seizure prediction by determining seizure precursors in

absence epilepsy using a statistical approach [191]. Notably, Rogowski et al. 1981, Salant et al. 1998 used an autoregressive model of neuronal activity to find changes a few seconds prior to seizure onset [192], [193]. Siegel et al. 1982 determined changes in signal amplitude within one-minute epochs prior to the seizure and conducted further analysis on the spike occurrence rates in the EEG [194]. Thus, determining the inverse relationship between focal spike-rate and bilateral spikes prior to a seizure event. Le Van Quyen et al. 1999 compared pre-ictal dynamic variations to those of inter-ictal EEG and discovered the dynamical similarity index decreases in the pre-ictal state. Interestingly, Litt et al. 2001 conducted a controlled experiment on epileptic patients using multiple EEG recordings in an effort to show that an increase in the entropy of the EEG signal was present approximately 40 minutes prior to seizure onset [195], [196].

Other studies used an algorithmic approach on similar multiple EEG recordings. Iasemidis et al. 2005 reported 68% sensitivity and 0.15 false positive rate, for seizure state prediction approximately 78 minutes in advance using short-term maximum Lyapunov exponents as a single feature [197]. Chaovalitwongse et al. 2005 attempted to reproduce these results using a larger patient sample size ($(n = 10)$ as compared to $(n = 2)$) and reported a sensitivity of 68%, specificity of 85%, and an average prediction window of 72 minutes [198]. Table 2.1 below presents a brief summary of research in the field of seizure detection.

Table 2.1: Selected research work in seizure detection.

Authors	**Year**	**Features**	**Number of patients**	**Mean detection time (mins)**	**Sensitivity**	**Specificity**
Liu et al.	1992	Autocorrelation	13	-	42.9	90.2
Lehnertz et al.	1998	Correlation dimension	16	12	94	-
Martinerie et al.	1998	Correlation density	11	3	89	-
Le Van Quyen et al.	1999	Similarity index	13	6	83	-

Le Van Quyen et al.	2000	Similarity index	9	4	94	-
Mormann et al.	2000	Phase synchronization	2	-	100	100
Cerf et al.	2000	Lerner density	7	-	100	100
Iasemidis et al.	2001	Dynamical entrainment	5	49	91	-
Litt et al.	2001	Accumulated energy	5	19	90	88
Le Van Quyen et al.	2001	Phase synchronization	8	-	77	-
Lehnertz et al.	2001	Correlation dimension	59	19	47	100
Jerger et al.	2001	Multiple measures	4	2	100	-
Navarro et al.	2002	Similarity index	11	8	83	69
Celka & Colditz	2002	Signal complexity	13	-	66.1	56
Mormann et al.	2003	Synchronization and correlation	10	-	86	100
Khan et. al.	2003	Frequency spectrum	13	-	62.5	64
Mormann et al.	2003	Phase synchronization	18	4	81	100
Iasemidis et al.	2003	Dynamical entrainment	5	89	81	83

Shoeb et al.	2004	Multiple wavelet decomposition	36	6	-	85
Iasemidis et al.	2005	Dynamical entrainment	2	78	82	85
Le Van Quyen et al.	2005	Phase synchronization	5	7	69	-
Navarro et al.	2002	Similarity index	13	7.5	64	-
Chaovalitwongse et al.	2005	Dynamical entrainment	10	72	69	85
Schelter et al.	2006	Phase synchronization	4	-	70	95
Costa et al.	2008	Multiple features	2	5	98.5	99.5
Mirowski et al.	2009	Multiple features	21	Less than 1 minute	71	100
Santaniello et al.	2011	Multiple features	4	9.6	100	84
Park et al.	2011	Spectral band features	18	-	97.5	73

2.1.1 Traditional algorithms for seizure detection

In this section, we will discuss prominent algorithms used for seizure detection. Faul, Boylan, Connolly, Marnane, & Lightbody, 2005 sought to evaluate three common algorithms for automatic seizure detection in neonatal EEG recordings. Work by Celka & Colditz, 2002; Gotman et. al, 1997; Liu, Hahn, Heldt, & Coen, 1992 were included and all three approaches utilized one-minute EEG segments from a sample size of 13 neonates. The *Gotman approach* [200] uses Fast Fourier transformation (FFT) computations for determining rhythmic features of epileptic like

discharges. The rhythmic fluctuations present within a seizure consists of distinct changes in amplitude present at a specific main frequency, accompanied by possible minor frequencies. EEG classification via the *Gotman approach*, is dependent on differences in characteristics of the frequency domain. The frequency and bandwidth of the main peak in the frequency spectrum are measured, and these measures are cross checked against a group of threshold values to classify EEG signals. The power in the main frequency band is compared to the power in the same band of the frequency spectrum of a non-seizure segment, which typically have a lag of about 60 seconds from the seizure segment. Examination of the algorithm revealed that seizure detection rates were greatly influenced by the threshold values used in EEG classification. Using the *Gotman approach*, there exists an unintentional overlap of frequency spectrum characteristics of ictal and non-ictal EEG classes.

The *Liu approach* [201], aims to automatically detect seizures by searching for periodic, rhythmic data using autocorrelation, which is simply the cross-correlation of a signal with a delayed version of itself and can be used for finding repeating patterns within a signal. The approach is likely to detect seizures with high specificity and low sensitivity but fails to detect rapidly changing frequency and signal amplitude.

The *Celka approach* [202] examines the complexity of EEG data to detect seizures. This approach assumes that ictal EEG segments have differing complexity as compared to non-ictal EEG segments. The *Celka approach* detects seizures with high sensitivity and high specificity. The specificity produced by Celka et al., 2002; Khan et al., 2003; Liu et al., 1992) [201]–[203] are respectively $64.0\%, 90.2\%$ and 56.0%. The sensitivity metric was $62.5\%, 42.9\%$ and 66.1% respectively. In summary, Faul et al. 2005 concluded that based on the specificity and sensitivity rates of these methods, to detect seizures in real time, other techniques must be integrated to avoid overlap in the signal characteristics between seizure and non-seizure segments [199].

2.1.2 Current seizure detection techniques

In current practice, clinicians depend on a multitude of tools for early detection of seizure events ranging including primarily using scalp EEG monitoring and pathology specific monitoring devices [204], [205]. Continuous EEG (CEEG) monitoring refers to the prolonged (hours, days, or weeks) recording of the brain's electrical activity using scalp electrodes generally combined with simultaneous video recording [206], [207]. CEEG offers utility in differentiation of clinical events

frequently seen in critical ill patients which mimic seizures such as involuntary movements, whole-body rigidity, tremors/jerking, etc. from true seizure activity.

2.1.2.1 fNIRS for seizure detection

Technical advances in fNIRS technology and instrumentation over the last few decades have allowed for the continuous non-invasive monitoring of cerebral HbO, HbR and HbT for the explicit purpose of seizure detection [208], [209]. Over time, NIRS monitors have adapted technologies to become smaller, more mobile and more cost-effective. Furthermore, by improving user interfaces and minimizing calibration procedures, the overall ease of NIRS systems has improved [210]. Commercial NIRS systems are now available from a number of various companies, including Nonin Medical Inc. (Plymouth, MN, USA), Hutchinson Technology Inc. (BioMeasurement Division, Hutchinson, MN, USA), Covidien (Dublin, Ireland) and others [209].

In the adult head, the fNIRS signal mainly reflects the absorption at a depth of 1 to $2\ cm$ below the scalp when the inter-probe distance is set between 3 and $5\ cm$. Since fNIRS can provide estimates of brain activity, it can potentially be a worthwhile complement to neuromonitoring. In spite of its potential, the practical use of fNIRS technology in neurology in particular is limited [211]. Research indicates that the benefits of clinically using fNIRS to determine changes in cerebral perfusion are modest at best, and correlate with transcranial doppler and surface EEG [212]. Results from a prospective study on a cohort of 60 patients post cardiac arrest [213] provided preliminary indications of the possibility of determining neurological outcomes using NIRS based regional cerebral oxygen saturation (rSO2). To date, no feasibility studies definitively indicating benefit of using fNIRS in critical care situations has been demonstrated to recommend a change in clinical protocol or practice. Most clinical fNIRS systems consist of a patch containing a few fNIRS channels affixed to the patient's forehead to avoid hair contamination. Currently, this technique is mainly used in the perioperative setting [214] as an adjunct to well-established clinical diagnostic tools. At the moment, widespread use of NIRS technology for seizure detection is not in use.

2.1.2.2 Limitations of current methods

In spite of the recent technological and instrumentation advances, current methods for seizure detection have their limitations. The detection of seizures in clinical settings requires expert

interpretation which may not always be readily available. Furthermore, clinical staff generally encounter challenges in interpreting CEEG recordings primarily being: a) the presence of motion induced artifacts, and/or electrode displacement leading to a reduction in signal quality; b) a wide variety of less obvious ictal patterns seen in the critically ill; and c) a large quantity of data to analyze. For the latter problem, a number of quantitative EEG methods have been developed to simplify and analyze EEG data.

In fNIRS systems, low frontal cortical oxygenation (rSO2) levels often are mismatched between cerebral perfusion and regional oxygen requirements [215]. Absolute rSO_2 values of less than 50% and/or a relative 20% decrease from individual rSO2 baseline levels are commonly considered necessary for seizure onset and subsequent detection. However, these findings cannot be generalized [216], [217].

2.1.2.3 Multimodal monitoring as a potential tool for seizure detection

Multimodal long-term brain monitoring can overcome some of the limitations of the individual methods described above. Multimodal brain monitoring offers additional information that could be missed by each modality individually. Utilizing more than one monitoring technique, the observer in conjunction with algorithms for automated seizure detection, is more likely to determine whether a genuine change in cerebral physiology and subsequent epilepsy pathology has occurred and what the most appropriate clinical intervention should be. Multimodal brain monitoring combined with clinical standard of care has the potential to provide vital information about seizure activity to improve clinical diagnosis and prognostication [218], [219].

2.2 The resting state and functional connectivity as a biomarker of the pathological brain

Brain activity is spontaneous and constant, leading to constant fluctuations in cerebral blood flow and neural firing [220]. Resting state analyses offer insight into the functional organization of the brain and can help investigate changes in brain physiology in neurological disorders. Functional connectivity analyses in the resting state has revealed networks of sensorimotor, visual, auditory, and language systems in resting healthy brains [221]. One such network is the default mode network (DMN). The DMN is normally active during latent thought, memory, and future planning [222] and has been shown to exhibit highly correlated activity between interacting brain regions.

It has been noted that patients affected by neurological disorders (Alzheimer's disease and/or autism primarily) have disrupted connections in the DMN, mainly in the posterior cingulate cortex [223]. By extension, the resting state in epileptic patients might exhibit perturbations in functional connectivity.

Multimodal EEG-fMRI investigations by Gotman et al. sought to determine the mechanism of metabolic changes associated with epileptic burst discharges, and their subsequent effect on brain function [224]. Results suggest that regional blood oxygenation level-dependent signal changes are evident in response to epileptic discharges as seen in EEG signal fluctuations. Bilateral and symmetrical BOLD signal activations were observed in the thalamus, mesial midfrontal region, and insulae. The anterior frontal and parietal regions and the posterior cingulate gyri were sites of bilateral and symmetrical deactivations. Notably, thalamic and midfrontal regional activations have been known to be involved in the generation of generalized epileptic discharges.

Notably, the generation of epileptic like discharges is not believed to be exclusively dependent upon cerebellar activation. Negative blood oxygenation level-dependent responses (i.e., deactivations) in frontal and parietal regions are closely related to patterns seen in the default state of brain function (i.e., resting state brain activity). Thalamic activation and the subsequent changes in the brain's default activity may lead to a state of reduced responsiveness observed in spike-and-wave discharges; which is due to epileptic discharges and its related effects on normal brain function [224]. Mapping resting state networks offers great potential for basic and clinical research and can assist in greater understanding of neurological disorders.

2.2.1 Resting state in the epileptic brain

Epilepsy places large metabolic demands on the brain's autoregulatory mechanisms, particularly as a result of the acute and sudden change in cerebral blood volume and concomitant cerebral blood flow required to maintain brain function [225]. Secondary to spontaneous changes in cerebral hemodynamics at rest in epileptic brains, it is generally believed that cerebral anoxia initiates cell damage prior to, during, and after a seizure event [226]. Thereby, seizures induce acute increases in venous oxygenation [64] to maintain the brain's metabolic demand. At seizure onset, cerebral blood flow increases in comparison to baseline may be inadequate to meet the metabolic requirements of the brain during an ictal event. Investigations into the resting epileptic brain ushers in new insights into the complex networks organizing the brain.

Hemodynamic correlates of epileptic activity have been used to map epileptic foci with neuroimaging techniques (e.g., fMRI), however, there are limited studies of neurovascular coupling in epileptic brains. By examining the relationship (in the context of neurovascular coupling) between resting state EEG and the local hemodynamic response in the resting state of epileptic brains, we examine if the brain's electrical signals can be used as predictors of the brain's hemodynamic signals. This makes strides in gaining understanding of the relationships intrinsic to the epileptic brain (i.e., neural and vascular) as well as offers clinical relevance in understanding the fundamental organization of the epileptic brain.

2.2.2 EEG resting state analyses

Examining neural signals obtained by EEG recordings to study resting state networks is more difficult than examining the BOLD signal. EEG signals are typically of low amplitude and distinguishing underlying neural sources further complicates the task. Examining meta-stable brain states using electric field topographical analysis allows for estimation of resting state networks [227]. This method matches temporal patterns between sensors and sources to identify state specific networks. This sensor-source matching methodology only partly resembles networks determined by examining the BOLD signal.

2.2.3 fMRI resting state analyses

fMRI based functional connectivity analyses have become popular in resting state investigations, as the BOLD signal can be readily measured using fMRI technology. Methods used in studying fMRI resting state networks typically include independent component analysis (ICA), coherence, correlation, clustering, and graph theory to name a few. Regional correlation using the seed-based method is relevant to this thesis and is presented in more detail in Chapter 5. Briefly, correlations are computed using signals from specific voxels indicative of a region, with voxels from other brain regions [228]. The benefit of this method is that it is able to provide a precise examination of regional connectivity. Furthermore, connectivity between voxels from a region of interest (ROI) and all other brain regions can be averaged providing a measure of global brain connectivity (GBC) specific to the ROI in question [229].

2.2.4 fNIRS resting state analyses

Recently, interest has developed in determining if resting state functional connectivity studies can be successfully performed using fNIRS technology [40], [92], [157], [230]. It was determined that the low frequency fluctuations attributed to the resting state fNIRS signal was spontaneous and comparable to those of the low frequency fluctuations seen in fMRI [231]. Given fMRI's high spatial resolution and full head coverage, fNIRS is unlikely to replace fMRI for basic research. However, fNIRS offers certain advantages over fMRI in examining resting state functional networks, which can possibly lead to a more reliable resting state functional connectivity estimate. We will briefly discuss three such advantages.

First, fNIRS's practical qualities of being relatively low cost, portable, and allowing for long-term recordings, helps facilitate fNIRS-based resting state functional connectivity studies in a range of patient populations, including bed-ridden and comatose statuses; a common situation in critical care units [230], [232]. Second, fNIRS characterizes changes in both HbO and HbR, providing more information regarding cerebral metabolic changes as compared to BOLD-fMRI measurements. Third, fNIRS has a higher temporal sampling rate as compared to fMRI, thereby preventing aliasing of certain physiological activity (i.e., cardiac (approximately $0.8-2.5$ Hz) or respiratory (approximately $0.15-0.3$ Hz) activity) into low frequency fluctuations.

An investigation focusing on the relationship between brain electrical and hemodynamic signals and consequently mapping EEG and fNIRS signals has the potential to offer further insight into the coupling between neuronal and hemodynamic activity.

2.3 Summary

In this chapter, the current state of the art in clinical seizure detection was discussed and finally, a brief discussion on the resting state and functional connectivity was discussed. In the next chapter we will describe data processing and model development techniques particularly artificial intelligence and deep learning, used in this thesis.

CHAPTER 3 METHODOLOGY

In this chapter we present the methodology specifically the machine learning, deep learning and signal processing methods used in this thesis. In the first section, we introduce the terminology and mathematical notations that will be used throughout. In subsequent sections, we discuss deep learning strategies used in this work. The datasets used and data processing techniques performed is presented in detail in Chapters 4 and 5.

3.1 Machine learning terminology and notation

A subset of artificial intelligence, machine learning, is the scientific study of algorithms and statistical models that computer systems use to perform a specific task relying on inference and patterns intrinsic to the data without using explicit instructions. The input to a machine learning algorithm is a training dataset, with (supervised learning) or without (unsupervised learning) labels. In the case of supervised learning, the algorithm attempts to determine feature maps between training data and training labels. After this, the next step is to predict the label of the unseen testing set data and output the target vector. Each unseen data point has a specific target vector. Machine learning algorithms use a large collection of data points, namely training data to tune the parameters of a dynamic model. The algorithms used in machine learning are predominantly based on statistical methods; however, biologically inspired and graphical methods are also used in many cases. Generalization is the ability of the constructed model to correctly categorize unseen data. The training-set and test-set are typically pre-processed in order to simplify the pattern recognition or enhance the performance of the machine learning algorithm.

3.2 Deep learning

In this section, we formally introduce the deep learning models including concepts, architectures, and techniques used in this thesis. Deep learning, a subset of machine learning, hierarchically processes information for feature and/or representation learning [233], similar to the human brain. Typical networks are designed with multiple neuron layers including an input layer, a hidden layer, and an output layer. Learning algorithms are subcategorized into the following: 1) *Discriminative models*, 2) *Representative models*, 3) *Generative models*, and 4) *Hybrid models*.

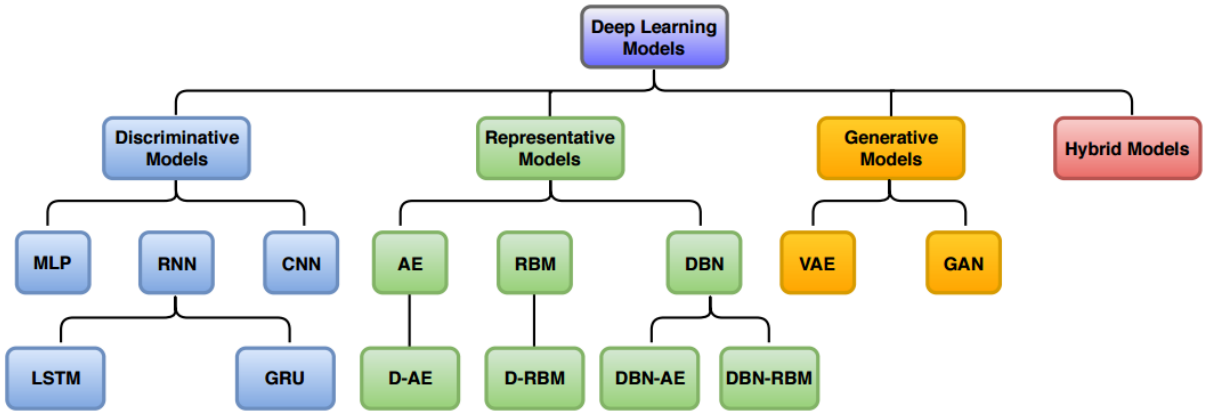

Figure 3.1: Deep learning models categorization. AE: Autoencoder, RBM: Restricted Boltzmann Machine, D-AE: Stacked-Autoencoder; Note that the Deep Belief Network (DBN) can be composed of an AE or RBM, therefore, DBNs can be divided into DBN-AE (stacked AE) and DBN-RBM (stacked RBM) [234].

We will briefly describe each category. Discriminative deep learning models classify input data to learn distinctive features by non-linear transformation, and probabilistic prediction. These models include the multi-layer perceptron (MLP), recurrent neural networks (RNN), convolutional neural networks (CNN), and their variants. RNN and CNN models used in this work fall under this category. Representative models learn representative features from input data. Autoencoders and the sequence-to-sequence variant are within this category and are used in this thesis. Generative deep learning models learn the joint probability distribution of input data target labels. Hybrid deep learning models combine two or more deep learning models: one for feature extraction (representation algorithm) and one for classification (discriminative algorithm). The table below summarizes the main characteristics of these deep learning models.

Table 3.1: Summary of deep learning model types.

Model	**Input**	**Output**	**Function**	**Training method**
Discriminative	Vector or tensor	Label	Feature extraction, classification	Supervised
Representative	Vector or tensor	Representation	Feature extraction	Unsupervised
Generative	Vector or tensor	New sample	Generation, signal reconstruction	Unsupervised
Hybrid	Vector or tensor	N/A	N/A	N/A

3.3 Discriminative deep learning models

In order to detect signals during different brain states, discriminative models receive input data and output the corresponding label. With respect to this thesis, the dataset of brain signal samples $\{\mathrm{X}, \mathcal{Y}\}$ where X denotes the set of brain signal observations and $\mathcal{Y}$ denotes the set of sample ground truth. From our multimodal dataset, we extract sample-label pairing such that $\{x \in \mathbb{R}\,\mathbb{N}, y \in \mathbb{R}\,\mathrm{M}\}$ where $\mathbb{N}$ and M correspond to the dimension of observations and the number of sample categories, respectively. Discriminative models learn a function with the mapping: $\mathcal{X} \longrightarrow \mathcal{Y}$. The discriminative models introduced in this section are supervised learning techniques which require the information of both experimental observations and the ground truth.

3.3.1 Multi-layer perceptron

The simplest deep learning model is the multilayer perceptron (MLP), with multiple hidden layers as compared to a shallow neural network [235]. In MLP, nodes are fully connected with the adjacent layer nodes but lack connection with other nodes in the same layer.

3.3.2 Recurrent neural networks

The recurrent neural network (RNN) is a type of discriminative deep learning model that is used to explore dependencies temporally. For each time point, t, a node receives a specific input, $\mathbf{I}$, and hidden state $\boldsymbol{c}$ from the previous time. Thus, for a given time point, the node receives input $\mathbf{I}_t$ and the hidden state (node memory) of the previous node $\boldsymbol{c_{t-1}}$. There are many variants to the RNN and for the purpose of this thesis we will focus on the "long short-term memory" (LSTM) variant.

3.3.3 Long short-term memory

Introduced by Hochreiter & Schmidhuber in 1997, the long short-term memory network (LSTM) is a variant of the recurrent neural network and is capable of learning long-term dependencies present within data [236]. LSTMs are scalable models with application in learning problems related to sequential data. Traditional methods have either been too specific (i.e., tailored to a specific problem) or were not able to scale to inherent time dependencies [236]–[238]. However, LSTMs are able to exploit long-term temporal dependencies and typically do not suffer from the optimization hurdles that are common to vanilla recurrent neural networks [239]. Thus, they have found application in and have been able to advance the state-of the-art in time series analysis, financial and weather forecasting, natural language processing, and medical image analysis [236], [240], [241].

3.3.3.1 Overview

LSTMs are essentially developed with repeating modules and multiple interacting layers, as opposed to a single layer in vanilla RNNs. The LSTM's memory cell maintains its state over time. As mentioned above, gating units control the flow of information into and out of the cell [183]. The following is a description of the "vanilla" variant of the LSTM network.

LSTM cells typically have three inputs $I_{t,}O_{t-1}, and\ c_{t-1}$ and two outputs $c_t\ and\ O_t$. Mathematically, I_t, denotes the input value at time t, and O_{t-1} denotes the output at the previous time, $t-1$ and c_{t-1}denotes the hidden state at the previous time. Outputs represent the hidden state and output. The output O_t is not only related to the input I_t but also related to information from the previous time step. Thus, the LSTM retains memory of important temporal information. The flow of memory in an LSTM occurs within the following gates: the *"input" gate, "forget" gate, "output" gate,* and *"input modulation"* gate. Each gate reports a weight value (determined by the neuron activation function) that controls information flow. For example, if forget gate's weight is "0", the LSTM cell would remember all the information passed from the previous time $t-1$. If the weight is unity, the LSTM remembers nothing.

3.3.3.1.1 The forget gate and peephole connections

The forget gate allows the LSTM to reset its own state, thereby allowing the LSTM to learn hierarchical information from sequential data [242]. In order to optimize learning and allow gates to exploit learning from the previous internal state, c_{t-1}, and the previous hidden state, s_{t-1}, peephole connections are integrated into the LSTM architecture [183], [242]. These connections are essentially connections from the cell state to the gates. This addition bypasses the requirement of an open output gate, and the integration of peephole connections allows the LSTM network to learn precise timings in the data [237], [242].

3.3.3.2 Data flow through the LSTM network

As data points enter the LSTM units, the LSTM cell state decides what data points will be sent through the LSTM and what information will be discarded from the cell state. This decision is essentially made by the "forget gate" which examine the input and hidden states $x_{t,}\ h_{t-1}$ respectively, and outputs a real value between $0, 1$, for each number in the cell state C_{t-1}. From here, the subsequent steps decide what information will be "stored" in the cell state. The "input gate layer" decides which data points to update and the consequently, the following layer creates a vector of new candidate values, to be added to the cell state. Following this, the LSTM's cell state will be updated, from C_{t-1} to a newer C_t state. Computations performed by the forget gate scales the new candidate values and decides update to each state value by adding and dropping values.

3.3.3.2.1 Notation

The hidden layer function, $\mathcal{H}$, is an element wise application of a given function. The hidden layer function, $\mathcal{H}$, is implemented by the following composite functions:

$$i_t = \sigma(W_{xi}x_t + W_{hi}h_{t-1} + W_{ci}c_{t-1} + b_i) \qquad \textit{Equation 7}$$

$$f_t = \sigma(W_{xf}x_t + W_{hf}h_{t-1} + W_{cf}c_{t-1} + b_f) \qquad \textit{Equation 8}$$

$$c_t = f_t c_{t-1} + i_t \tan h\,(W_{xc}x_t + W_{hc}h_{t-1} + b_c) \qquad \textit{Equation 9}$$

$$o_t = \sigma(W_{xo}x_t + W_{ho}h_{t-1} + W_{co}c_t + b_o) \qquad \textit{Equation 10}$$

$$h_t = o_t \tan h\,(c_t) \qquad \textit{Equation 11}$$

where σ is the logistic sigmoid function and $i, f, o, and\ c$ are respectively the *input gate, forget gate, output gate and cell* activation vectors; all of which are the same size as the hidden vector, h. Assuming the same hidden layer function is applied to all N layers in the network, the hidden vector sequence, h^n is computed iteratively from $n = 1$ to N and $t = 1$ to T and $h^0 = x$:

$$h_t^n = \mathcal{H}(W_{h^{n-1}h^n}h_t^{n-1} + W_{h^n h^n}h_{t-1}^n + b_h^n \qquad \textit{Equation 12}$$

Here we describe common weight notation (table below) used with respect to a vanilla LSTM. Assuming that $x_{t,}$ is the input vector at given time, t, N is the number of LSTM blocks, and M represents the number of inputs. the following weights are calculated:

Table 3.2: Weights for an LSTM layer

Input weights	$W_z, W_i, W_f, W_o \in \mathbb{R}^{N\times M}$
Recurrent weights	$R_z, R_i, R_f, R_o \in \mathbb{R}^{N\times N}$
Peephole weights (LSTM variant)	$p_i, p_f, p_o \in \mathbb{R}^N$
Bias weights	$b_z, b_i, b_f, b_o \in \mathbb{R}^N$

3.3.3.2.2 Data output

Data output from the LSTM is dependent on the cell state and is multiplied by the output of the forget gate and its associated activation function (e.g., sigmoid). The figure below shows the LSTM along with its input, forget and output gates. Input is denoted as x_t, C_t is the cell state, f_t is the forget gate, h_t is the hidden state, and O_t is the output gate. The input gate's activation vector is denoted as i_t. The network outputs, y_t, are computed as:

$$y_t = W_{h^N y} h_t^N + b_y \qquad \textit{Equation 13}$$

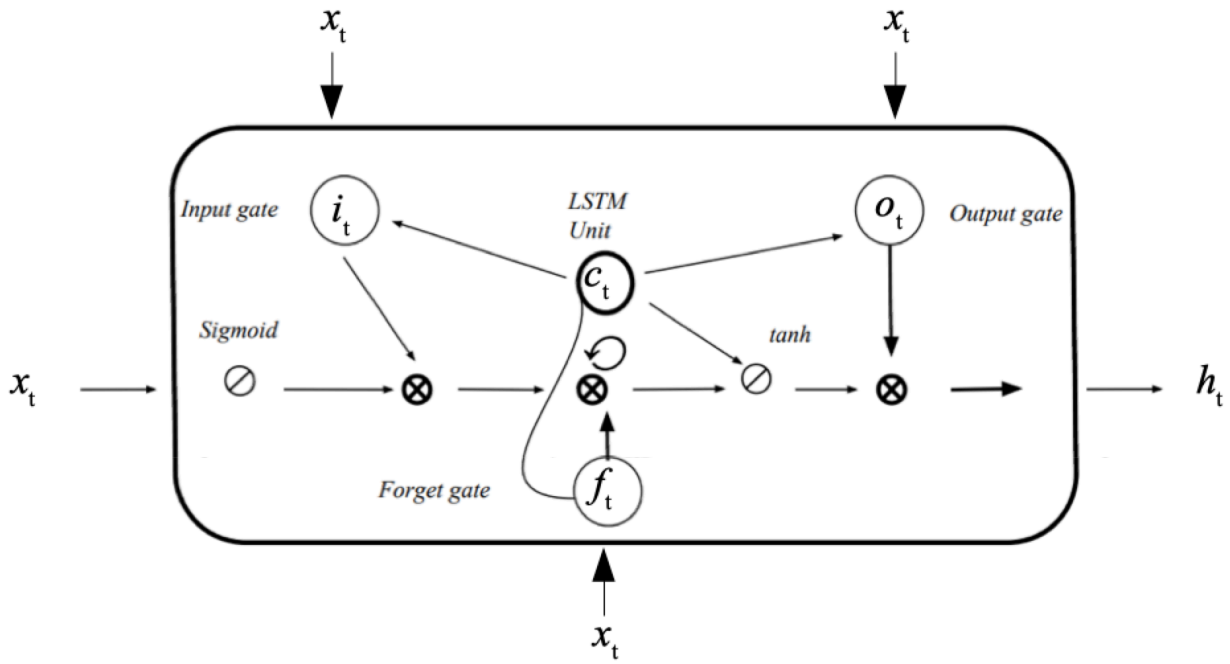

Figure 3.2: The long-short term memory variant of the recurrent neural network. Data input is denoted as x_t, C_t is the cell state, i_t is the input gate's activation vector, O_t is the output gate and the forget gate is denoted as f_t. Element wise multiplication between data input and flow throughout the LSTM module is denoted by the ⊗ symbol. The Ø symbol represents the application of a differentiable function ($sigmoid$ or $tanh$ function) to a weighted sum. Each of these gates are thought of as neurons which compute network activations.

LSTM configurations with peephole connections are similar to the vanilla LSTM network without these connections. These peephole LSTM configurations have control gates and output

activation functions [237] and the output of this LSTM network variant is recurrently connected back to the LSTM input and corresponding gates [183], [236], [237].

3.3.4 Convolutional neural networks

One of the most popular deep learning models for spatial information investigation is the convolutional neural network (CNN). In a neuroimaging context, CNNs are popular architectures which are able to exploit spatial dependencies. In the applications relevant to this thesis, the CNN attempts to determine such dependencies among EEG-fNIRS signals. The computational unit of the CNN is the convolutional layer with filters to convolve input data (EEG, fNIRS, or EEG-fNIRS signals) followed by non-linear transformation for feature extraction. The implementation of the CNN in this thesis can be found in more detail in Chapter 5 (Article 2).

3.3.5 Representative deep learning models

Representative models take input data and output dense representations. The building blocks of representative models are autoencoders, and restricted Boltzmann machines. We will discuss autoencoders and the sequence to sequence variant as it is pertinent to this thesis.

3.3.5.1 Autoencoders

An autoencoder typically has three layers: the input, latent (i.e., hidden) layer, and output layer as shown in the figure below.

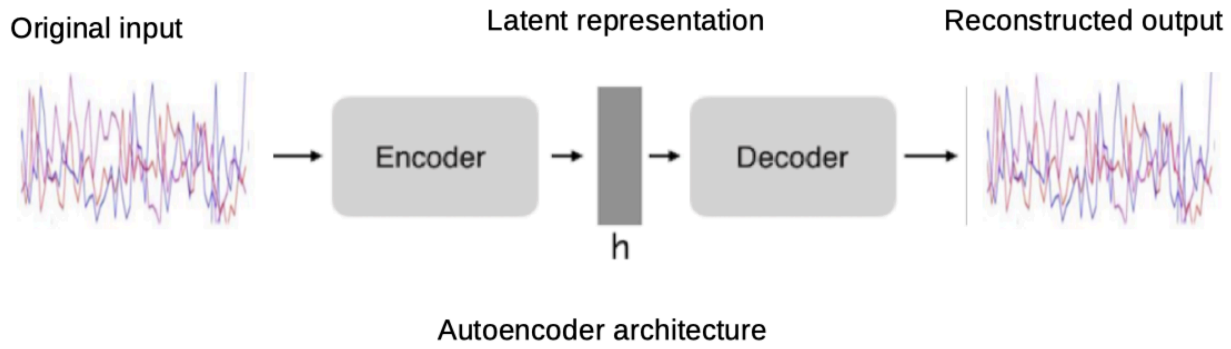

Figure 3.3: Autoencoders reconstruct input by flowing through encoder and decoder layers. The hidden layer (h) learns representations of the input.

The encoding layer embeds the observation to a latent representation. Mathematically,

$$x^h = \sigma(T(x)) \qquad \textit{Equation 14}$$

where x^h represents the hidden layer. The decoder (decoding unit) layer decodes the representation into the original space, $y' = \sigma(T(x^h))$ where y'represents the output. Autoencoders calculate reconstruction error based on the distance between $y'$and x and can compute the loss function only by using the input, x, sans the ground truth y:

$$error = \| y' - x \|_2 \qquad \textit{Equation 15}$$

Note, this equation uses the input x as the ground truth and therefore does not involve the variable y. Not surprisingly, Autoencoders can perform unsupervised learning. Naturally, one variant of autoencoders is the sequence to sequence model (seq-to-seq) as discussed below.

3.3.5.2 Sequence to sequence models

In continuation to the LSTM concepts introduced previously, we provide a foundational description of the sequence-to-sequence model used in this thesis. Section 5.4.3.3 provides a full description of the sequence to sequence model used in this thesis. To conclude this section, the tools used to build the sequences and neural network models are briefly discussed.

3.3.5.2.1 Sequence embeddings

In order to feed sequential data into machine learning models, there is a need for corresponding numeric representations. There has been multiple methods proposed in the literature to address this problem [243], such as bag-of-words (BoW) and one-hot representation. However, embeddings such as Global vectors for word representation (GloVe) [244] and word to vector (word2vec) [245] are most common. The notion of distributional similarity was introduced by [246], and stated that "words that occur in similar contexts would have similar meaning". For example, the words "sport" and "game" occur in similar contexts in documents and hence, share similarities in their meanings. This implies similarity in their numeric or vector representations. The cosine distance metric is typically used to measure similarity between two vectors as shown in the equation below.

$$cos\theta = \frac{\dot{a} \cdot \dot{b}}{|\dot{a}| \cdot |\dot{b}|} \qquad \textit{Equation 16}$$

where $|\cdot|$ refers to the $L2$ norm of the corresponding vector. A higher value of $\cos\theta$ implies that the angle between the two vectors is small, and hence they are more similar and vice-versa. This concept is extendable to EEG and fNIRS signals in that EEG and corresponding fNIRS signals also occur in a similar context and share similarities in their sequences.

3.3.5.3 Sequence to Sequence long short-term memory

Introduced by Sutskever et al., sequence-to-sequence (Seq2Seq) models have greatly benefited tasks requiring sequence generation such as question answering, dialog systems and machine translation. These models take an input sequence and generate an output sequence [247]. This is in contrast to vanilla classification models, which output only a single class label, and not an entire sequence. Seq2Seq models are typically implemented using two recurrent neural networks, one which is referred to as the "encoder" and the other is called the "decoder". The encoder creates a vector representation of the input sequence that is then fed into the decoder, which then generates tokens in a sequential manner. This study uses LSTM recurrent neural networks for encoding and decoding EEG and fNIRS sequences.

More concretely, let $x = (x_1, x_2, \ldots x_{|x|})$ be the tokens (i.e., the corresponding sequence embeddings) from the source sequence (EEG) and $y = (y_1, y_2, \ldots y_{|y|})$ be the tokens from the target sequence (fNIRS). At the end of the encoding process, we will have, the final hidden and cell states respectively from the source sequence. We can then set the initial states: $h_{|x|}^{(source)}$ and $c_{|x|}^{(source)}$, of the decoder LSTM to ($h_{|x|}^{(source)}$and $c_{|x|}^{(source)}$). This method known as hidden state initialization and transfers information from the source to the target sequence. Following which, at each subsequent time step of the decoding process, we are able to compute $h_j^{(target)}$ using an input sequence embedding, y_{j-1} (the ground truth during training and the prediction from the previous timestep during testing). This is given by:

$$\boldsymbol{h}_j^{(target)} = LSTM_\theta\left(\boldsymbol{h}_{j-1}^{(target)}, \boldsymbol{y}_{j-1}\right) \qquad \textit{Equation 17}$$

where θ refers to the weights of the LSTM network. The predicted sequence at timestep $\boldsymbol{j}$ is then given by a softmax layer as follows:

$$p(y_j) = softmax\left(W_{out}\boldsymbol{h}_j^{(target)}\right) \qquad \textit{Equation 18}$$

where $W_{out}$is a weight matrix and the softmax function is defined by the equation below:

$$softmax(y_{jk}) = \frac{exp\ y_{jk}}{\Sigma_{k=1}^{|V|} exp\ y_{jk}} \qquad \textit{Equation 19}$$

where y_{jk}refers to the value of the k^{th}dimension of the output vector at timestep j. In total the output vector at each timestep has $|V|$dimensions, where $|V|$ corresponds to the total sequence size. The softmax layer normalizes the output layer and computes a vector of probabilities. Among the $|V|$ dimensions of the output layer, the dimension with the highest calculated probability is chosen and generates the sequence corresponding to that index.

3.3.6 Deep learning in neurophysiology

In this section, we will discuss using deep learning methods used in neurophysiology particularly in seizures.

3.3.6.1 Seizures and deep learning

Recently, deep learning models have been developed for the task of seizure detection. CNNs have been used for the automatic detection of epileptic seizures in adult patients [248]. Ansari et al, 2018 used CNNs to extract spatial features extractor which were subsequently fed into a random forest classifier for neonatal seizure detection [249]. Supratak et al, 2014 used a deep autoencoder to extract seizure EEG features and a classifier (logistic regression) for seizure detection [250]. Hybrid deep learning models have also been used for seizure detection. Notably, Tsiouris et al., 2018 used a CNN-LSTM architecture to detect seizures on select EEG channels [251]. Deep learning using fNIRS signals is still in its nascent stages and with respect to using deep learning architectures for seizure detection using multimodal EEG-fNIRS signals. The

work presented in this thesis, for the first time showed that multimodal EEG-fNIRS signals increases metrics as compared to seizure detection with EEG signals alone.

3.3.6.2 Functional connectivity

Functional connectivity derived from resting-state fNIRS signals has recently gained attention as it is capable of providing valuable insight into the intrinsic networks present within the human epileptic brain [252]–[254]. Specifically, cerebral hemodynamic signals derived from fNIRS allow for greater understanding of the human brain. Furthermore, one of the principal motivations of functional connectivity computations is to better understand, detect and treat neurological diseases. Here, we employ seed-based correlation analysis to determine functional connectivity between the resting epileptic brain compare band-specific EEG (gamma band) connectivity with connectivity in fNIRS. Specifically, we will consider ground truth and reconstructed fNIRS signals to discover resting-state functional connectivity patterns derived from the developed LSTM-CNN autoencoder model. The main contribution of the present work is to emphasize that reconstructed fNIRS signals derived from specific EEG bands compares with the estimate of the temporal relation among brain networks during resting state. Full details are found in Article 2 in Chapter 5.

3.3.7 Summary

This chapter presented an introduction to some of the machine learning and signal processing concepts and algorithms used throughout this thesis. Some of the topics were presented at a high level of abstraction. There are primarily two reasons for this: 1) the topics presented here constitute a research domain and a full examination of their details is outside of the scope of this thesis. 2) Details of specific methods will be presented in future chapters. In this chapter, we discussed deep learning models as they relate to seizure detection and prediction. The studies using scalp EEG signals are significantly more than the sum of all the other paradigms including fNIRS. The next chapter will describe the datasets used in this thesis in detail: 1) The CHBMIT public EEG data set and 2) An in-house EEG-fNIRS data set; as well as the data processing performed (Sections 4.4.3.1 and 4.4.3.4 respectively).

CHAPTER 4 ARTICLE 1: FNIRS IMPROVES SEIZURE DETECTION IN MULTIMODAL EEG-FNIRS RECORDINGS

4.1 Article details

Sirpal, P., Kassab, A., Pouliot, P., Nguyen, D. K., & Lesage, F. (2019). fNIRS improves seizure detection in multimodal EEG-fNIRS recordings. *Journal of Biomedical Optics*, *24*(5), 051408 (2019). https://doi.org/10.1117/1.JBO.24.5.051408.

This article addresses the first objective of the thesis, namely the development of a deep learning model to detect seizures with high sensitivity and specificity based on EEG-fNIRS data. This work was presented at the Britton Chance Symposium, Perelman School of Medicine, University of Pennsylvania and subsequently published in the *Journal of Biomedical Optics* Special Section on Metabolic Imaging and Spectroscopy.

4.2 Context and rationale

At the time of writing, the state-of-the-art approach for seizure detection was to use traditional machine learning approaches such as an SVM as a final classifier on scalp and/or invasive EEG datasets. The preceding steps included extensive data processing, filtering, and feature extraction followed by tedious training. This motivated the use of deep learning architectures to automatically learn relevant features so that time consuming and sporadic feature selection can be avoided while maintaining or exceeding performance metrics.

4.3 Contributions

This work uses fNIRS data from epileptic patients for seizure detection using the LSTM variant of the RNN. The use of the open source and well referenced CHBMIT dataset provided validation to our methods. Our architecture performed better than other deep learning methods evidenced in the literature. The addition of fNIRS was shown to improve detection metrics as compared to EEG alone. This work was novel in that it was the first-time multimodal EEG-fNIRS signals were used for seizure detection.

4.4 Article 1

fNIRS improves seizure detection in multimodal EEG-fNIRS recordings

Parikshat Sirpal[a,b,*], Ali Kassab[b], Philippe Pouliot[a,c], Dang Khoa Nguyen[b], Frédéric Lesage[a,c]
[a] École Polytechnique de Montréal, Université de Montréal, C.P. 6079, succ. Centre-Ville, Montréal, H3C 3A7, Canada
[b] Neurology Division, Centre Hospitalier de l'Université de Montréal (CHUM), 1000 Saint-Denis, Montréal, H2X 0C1, Canada
[c] Research Centre, Montreal Heart Institute, Montreal, Canada
[*]parikshat.sirpal@polymtl.ca

4.4.1 Abstract

In the context of epilepsy monitoring, electroencephalography (EEG) remains the modality of choice. Functional near-infrared spectroscopy (fNIRS) is a relatively novel modality that cannot only characterize hemodynamic profiles of seizures but also allow for long-term recordings. Here, we employ deep learning methods to investigate the benefits of integrating fNIRS measures for seizure detection. We designed a deep recurrent neural network with long short-term memory units (RNN-LSTM) and subsequently validated it using the CHBMIT scalp EEG database - a compendium of 896 hours of surface EEG seizure recordings. After validation using EEG data, fNIRS, and multimodal data comprising a corpus of 89 seizures from 40 refractory epileptic patients was used as model input to evaluate the integration of fNIRS measures. Following heuristic hyperparameter optimization, multimodal EEG-fNIRS data provided superior performance metrics (sensitivity and specificity of 89.7% and 95.5% respectively) in a seizure detection task, with low generalization errors and loss. False detection rates were generally low, with 11.8% and 5.6% for EEG and multimodal data respectively. Employing multimodal neuroimaging, particularly EEG-fNIRS, in epileptic patients, can enhance seizure detection performance. Furthermore, the neural network model proposed and characterized herein offers a promising framework for future multimodal investigations in seizure detection and prediction.

Keywords: EEG-fNIRS, functional brain imaging, deep neural networks, epilepsy, seizure detection

4.4.2 Introduction

Continuous video-EEG surveillance is often used in hospitals to monitor patients at high-risk of epileptic seizures[1] particularly patients with drug-resistant chronic epilepsy admitted in epilepsy monitoring units or critically ill patients admitted to the intensive care unit after an acute brain injury such as stroke, head trauma, brain hemorrhage, or brain infection. While some seizures are clinically evident, such as generalized tonic-clonic seizures, others are subtle in terms of clinical manifestations (ex. subtle facial or limb twitches) for which recognition by EEG is particularly well suited. Moreover, some seizure events are purely electrical being only detectable on EEG or even completely asymptomatic (from isolated electrical seizures to non-convulsive status). Non-convulsive status epilepticus (defined as a continuous state of seizures without convulsions, or multiple nonconvulsive seizures for more than 30 minutes without interictal full recovery) has been found to account for up to 20% of all cases of status epilepticus in general hospitals, and up to 47% in the intensive care unit[2]. Functional near infrared spectroscopy (fNIRS) has emerged as a safe, non-invasive optical technique that exploits neurovascular coupling to indirectly measure brain activity. Measured relative changes in both oxygenated and deoxygenated hemoglobin can be used to assess cortical activation during overt and subtle seizures[3]. Continual fNIRS cerebral monitoring provides the ability to track regional oxygenation changes before, during and after these ictal events[4-7]. In recent years, multimodal approaches have emerged integrating EEG with fNIRS to offer dual hemodynamic and electro-potential characterization of a seizure event[8-10]. Whereas EEG data records the macroscopic temporal change in brain electrical activity, fNIRS approximates brain hemodynamic changes via spectroscopic measurements of oxy-and deoxy-hemoglobin. fNIRS depends on the slow dynamics of the hemodynamic response, thereby yielding lower temporal resolution. According to literature and with the optode spacing used in this work, NIRS yields a spatial resolution of approximately 1 cm [11]. Given the different characteristics and physiological information provided by each modality, multimodal EEG-fNIRS data provides complementary electrical and hemodynamic information, which may be exploited to implement appropriate diagnostic and treatment strategies.

Seizure detection has traditionally been approached using EEG with quantitative feature signal processing techniques such as the application of Fourier transform analysis (FFT), wavelet transforms, and spectral decompositions[12, 13]. Briefly, EEG FFT analysis allows for the convenient processing of lengthy and noisy recordings in the frequency domain, allowing hidden features within the time series to become apparent. Wavelet analysis can be thought as an extension of the Fourier transform that works on a multi-scale basis instead of on a single scale either in time or frequency. This multi-scale feature of the wavelet transform allows coarse to fine time-frequency signal resolution analysis of the signal. Using the above features as input, artificial neural networks (ANN), have been used and emerged as better models than traditional

techniques for seizure detection if appropriate processing of data occurs a-priori[14]. Traditionally, researchers have used ANNs as a final step to classify hand engineered features[15-17]. In contrast to the process of hand engineering features, deep learning (DL) methodologies learn intrinsic data features to obtain relevant data abstractions[18]. DL models have been used for seizure detection using EEG data streams[19-22] in which impressive metric scores were achieved. This work aims to investigate for the first time the additional benefit that hemodynamic information derived from fNIRS recordings provides in a seizure detection task in the context of multimodal EEG-fNIRS recordings. Our work exploits artificial intelligence models, particularly the long short-term memory unit, on human epilepsy data without performing extensive feature extraction, selection, or signal preprocessing.

4.4.3 Methods

4.4.3.1 Patient recruitment, characterization and seizure types

Forty patients between the ages of 11-62 years with refractory focal epilepsy admitted to the epilepsy-monitoring unit to record their seizures (and determine if they could be good candidates for epilepsy surgery) were recruited for this study. The Ethics Committees of Sainte-Justine and CHUM Notre-Dame Hospitals approved the study and informed consent was obtained from all subjects. Patient inclusion criteria primarily consisted of the following: patient (or parental) consent and focal epilepsy confirmed by clinical history, electroencephalographic and/or imaging findings. Exclusion criteria included the following: subjects with significant progressive disorders or unstable medical conditions. Patients underwent a full physical exam, an anatomical magnetic resonance brain image (MRI), positron emission tomography (PET), ictal single photon computed tomography (SPECT), and a magnetoencephalography study. Subsequently, continuous EEG-fNIRS recordings were performed at the Optical Imaging Laboratory of Sainte-Justine Hospital in Montreal, Canada. An epileptologist was available at all times to ensure patient safety and inspected data for congruency with clinical semiology analysis, the location of scalp EEG findings, and location of the epileptogenic lesion on MRI if present. The data corpus collected included 266 epileptiform abnormalities in total. Of these, 89 were seizures, the majority of which were temporal lobe seizures followed by frontal lobe seizures. The remainder of the data set included interictal epileptiform discharges and periodic epileptiform discharges. Seizure duration ranged from 5.1-62 seconds with an average of 21.7 seconds. Details concerning patients, seizure types, MRI findings, and foci seen using EEG and fNIRS modalities used in this study are detailed in Table 1 below.

Table 4.1: Clinical profiles of refractory epilepsy patients. F: female; M: male; FLE: frontal lobe epilepsy; FPLE: fronto-parietal lobe epilepsy; OLE: occipital lobe epilepsy; NTLE: neocortical temporal lobe epilepsy; MTLE: mesial temporal lobe epilepsy; RF: right frontal, LF: left frontal, Bi: bilateral, P: parietal. F: frontal, P: parietal, N: normal, L:

left, R: right; HA: hippocampal atrophy, CD: cortical dysplasia, RHA: right hippocampal atrophy, LHA: left hippocampal atrophy.

Patient	Age, Sex	Total recordings	Epilepsy classification	MRI findings	EEG focus	fNIRS focus
1	11, M	9	R FLE	N	RF	RF
2	21, M	11	L FLE	N	LF	Bi-F (L > R)
3	13, F	2	R FPLE	N	LP	LP
4	35, F	4	R FLE	N	RF	RF
5	25, F	5	R FLE	N	LF	LF
6	16, M	7	L FLE	RF encephalomalacia	LF	PF
7	63, M	5	L TLE	N	LT	LT
8	47, F	3	R LNTLE	N	Bi-T	LT
9	23, M	5	R FLE	N	RF	RF
10	43, M	8	R FLE	RF encephalomalacia	RF	RF
11	19, F	4	L MBTLE	N	RT	RT
12	45, M	7	R FLE	N	Bi-F (R > L)	Bi-F
13	38, F	1	L LNTLE	N	LF	LFT
14	53, F	11	L LFPLE	N	LFP	Bi-F (L > R)
15	24, M	6	L LNTLE	N	RT	RT
16	31, M	3	Bi-MBTLE	R HA	Bi-T (R > L)	RT
17	31, M	11	R LNTLE	N	RT	RT
18	23, M	6	R FPLE	RF CD	RF	RF

19	27, M	3	R FLE	N	RF	RF
20	21, M	11	R FLE	RHA	RT	RF
21	50, M	6	L MBTLE	LHA	Bi-F	RF
22	38, F	5	R LNTLE	N	RT	RT
23	34, M	10	L LNTLE	N	LT	LT
24	56, M	7	R FLE	N	RF	RF
25	11, M	4	R LNTLE	N	RT	RT
26	43, M	5	L LPTLE	N	LT	LP
27	24, M	3	R FLE	N	RF	RF
28	46, M	7	L FLE	N	LF	LF
29	30, F	5	L LNTLE	N	LT	LT
30	62, F	6	L FLE	N	LF	LF
31	43, M	8	L FLE	N	LF	LF
32	13, M	6	Bi-LNTLE	N	Bi-T	Bi-T
33	22, M	5	R FLE	N	RF	RF
34	25, M	7	R FLE	N	RF	RF
35	28, M	9	L FLE	N	LF	LF
36	44, F	7	R FLE	N	RF	RF
37	49, M	3	R FLE	N	RF	RF
38	32, M	2	R FLE	N	RF	RF
39	19, F	4	R FLE	N	RF	RF

40	19, F	3	R FLE	N	RF	Bi-F (R > L)

4.4.3.2 EEG-fNIRS instrumentation and data acquisition

The EEG-fNIRS instrumentation included the use of custom helmets designed to mount a total of 80 optical fibers (64 light sources in pairs for both wavelengths, 16 detectors) and 19 carbon EEG electrodes. First, the EEG data recording system was installed according to the traditional 10-20 system. Following this, we installed a custom made helmet holding optical fibers. The installation time including hair removal, patient positioning, adjustment of signal intensity and optode repositioning typically was between 1-2 hours. A description of our setup, and its near full-head coverage, is provided in previous publications [8,9]. Optode and electrode positions were co-registered onto 3-D high-resolution anatomical MRI images using neuro-navigation (Brainsight, Rogue-Research Inc.). The EEG data stream was recorded at 500 Hz with a Neuroscan Synamps 2TM system (Compumedics, USA). In order to remove instrumental noise, bandpass filtering between 0.1 Hz and 100 Hz was applied. Simultaneously, the fNIRS data stream was acquired using a multi-channel frequency domain system at 19.5 Hz (Imagent Tissue Oximeter, ISS Inc., Champaign, IL, USA) with wavelengths of 690 nm and 830 nm for sensitivity to deoxyhemoglobin (HbR) and oxyhemoglobin (HbO) respectively. The channel positions were cross-referenced with the MRI and were adapted to ensure coverage of the epileptic focus, the contralateral homologous region, and as much area as possible of the other lobes. Data was acquired for two to twelve consecutive sessions of 15 minutes while the patient was in a resting state. Multiple sessions of data acquisition were performed since during a single acquisition, seizure events are not sure to occur. Sensitivity of near-infrared light to cortical tissue was maintained by positioning the optical channels approximately 3-4 cm apart. During installation, we verified channel quality using signal intensity.

4.4.3.3 Seizure identification

The EEG tracing was analyzed using Analyzer 2.0 (Brain Products GmbH, Germany) by a certified clinical neurophysiologist and reviewed by an epileptologist to identify interictal epileptiform discharges and seizures. Seizures were marked in the presence of a transient electrographic rhythmic discharge evolving in amplitude, frequency and spatial distribution changes associated with stereotypical seizure semiology on video.

4.4.3.4 Data processing and analysis

As mentioned in 2.1, recordings obtained from known epileptic patients were evaluated for seizure occurrence, leading to a compendium of 200 recordings totaling 50 hours of recording time and 89 seizure

events lasting in duration from a few seconds to approximately one minute. An average time offset of 4.5 seconds was used between modalities to feed the neural network corresponding to the average time delay between neural activity and the hemodynamic response [23]. Prior to analysis, each channel was further verified for signal quality (intensity and presence of physiology, e.g. heart beat). Channels that did not have good signal were eliminated from the analysis. For each recording, distinct seizure and non-seizure classes were partitioned from the data. Entire seizure segments were extracted and non-seizure segments were subsequently defined as those data points that do not overlap with seizure segments. Post-acquisition, raw data were processed using the HomER package[24] (Photon Migration Imaging Lab; Massachusetts General Hospital, Boston, USA) in order to convert raw fNIRS data into hemodynamic parameters, namely oxygenated and deoxygenated hemoglobin[25]. In our analyses, the modified Beer-Lambert law (MBLL) was used to relate light attenuation to changes in absorption and enable the estimation of changes in oxygenated and deoxygenated hemoglobin as they vary in space and time.

4.4.3.5 Deep neural networks

To a large extent, human seizure activity is highly unpredictable. Longitudinal analyses suggest temporal and spatial irregularities to be intrinsic to seizure activity. Recurrent neural networks (RNNs) have become state of the art for sequence modeling and generation[26]. The "Long short-term memory (LSTM) unit" is a popular variant of RNNs with proven ability to generate sequences in various applications, particularly text and sequence processing [27,28]. LSTM models learn important past behaviors due to their innate ability to learn from and remember previous time steps and their important features. LSTM units hold an advantage over other methods in modeling long-term dependencies due to automatically learned "input", "output" and "forget" gates. The success of RNNs in these domains motivated our work of applying LSTM-RNNs for human seizure activity detection in multimodal EEG-fNIRS recordings.

4.4.3.6 Model architecture

In this section, we describe the vanilla LSTM model architecture that was used to perform the seizure detection task. The architecture consists of: (1) input layer, (2) LSTM units, and (3) a dense layer. Figure 1, illustrates the LSTM unit structure, featuring input, forget, and output gates. We designed our architecture to use the following activation functions: (1) hyperbolic tangent for the LSTM units and (2) logistic sigmoid for the gates. Softmax, categorical cross-entropy was used as the loss function, with alpha=0.95, since it is well suited for categorization problems[18]. The hyperparameters, shown in Table 2 below, used to train our model were heuristically tuned to achieve sufficient performance and we validated our results by comparing performance with other techniques developed in the literature (Table 3). The hidden state, h_t is an element

wise application of the sigmoid function[27, 28]. The output of each block is recurrently connected back to the input and the gates. Our model generates subsequent data sequences according to the following two steps:

(1) At every time step, the LSTM layer receives input, x_t**.** Inputs to the LSTM cell include the previous hidden state and the previous memory state.

(2) The LSTM layers then produce output, which is used to sample a new set of input variables x_{t+1}. The outputs from the LSTM cell are the current hidden state and the current memory state.

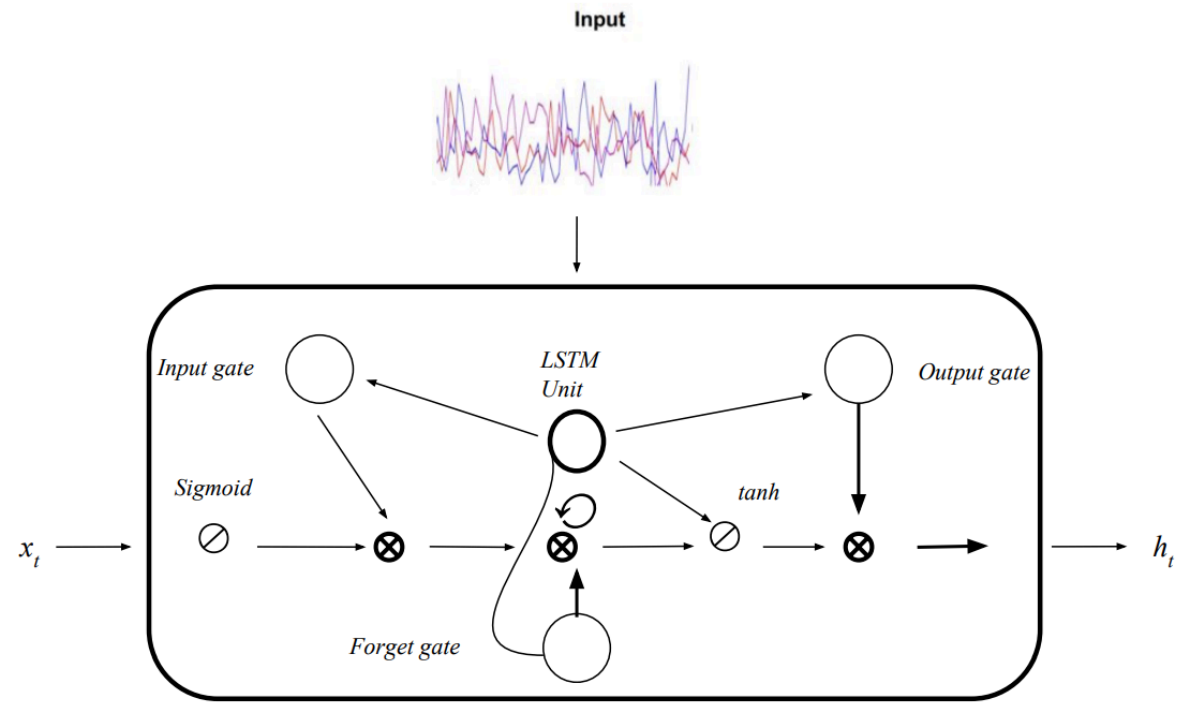

Figure 4.1: LSTM unit structure. The input is fed into LSTM units with 64 hidden units followed by a final dense layer. The input gate decides which values will be updated and creates a vector of new values to be added and updated to the state. After data input, the LSTM's forget gate decides which information to discard. This gate examines the prior hidden state (*h*) and current input, yielding a binary output. Subsequently, the LSTM decides what new information to store in the cell state. Finally, the LSTM unit decides sequential output, which is based on the current cell state. The sigmoid and hyperbolic activation functions determine which parts of the cell state to output.

Input data is transformed into a three-dimensional tensor with standard dimensions of an LSTM-RNN[18]. The final gradients are back propagated at each time step with adaptive moment estimation as an optimizer for stochastic gradient descent. The prediction is a binary output derived from the softmax function[18].

Table 4.2: LSTM-RNN heuristic hyperparameters.

Hyperparameters	**Value**	**Method**

Learning rate	$1x10^{-3}$	Adam
Epochs	100	Experimental
Batch size	784	Experimental
LSTM units	10	Experimental

Adaptive moment estimation and dropout on non-recurrent connections[29,30,31]was utilized to regularize our model to avoid over-fitting.

4.4.3.7 Network training and model validation

A feed dictionary was generated, and for each step, mini-batches of training examples were presented to the network. Input data was binary partitioned into appropriate seizures and non-seizures segments. Using these newly segmented classes as input, our network was trained to compute scores for seizure and non-seizure segments. Truncated back propagation through time (TBPTT), a modified form of the conventional back propagation through time (BPTT) training algorithm for RNNs[32] was used for training. Briefly, BPTT works to unroll the recurrent neural network and backward propagate the error between the expected output and the seen output for a given input. The weights are then updated with the accumulated gradients. We first validated our model using k-fold cross-validation *(k=10)*, on the standard CHBMIT scalp EEG dataset[16, 33] as this dataset is vast, and the seizures contained within are of long duration. Following this, we aimed to test our hypothesis regarding the relevance of adding fNIRS data for improving the task of seizure detection using our database. Standalone in-house EEG data, followed by standalone fNIRS data, and finally multimodal data was used as input for the network. Our models were implemented on two NVIDIA TITAN X GPUs with 12 GB memory using the Keras platform with Tensorflow backend for a total training time of 10 hours.

4.4.4 Experimental Results

This section describes the model validation results using the standard CHBMIT database and finally statistical analyses of the model using our in-house datasets are described.

4.4.4.1 Model validation on the CHBMIT database

The CHBMIT dataset includes 198 seizures from 22 patients. To evaluate performance, we defined the following metrics: Accuracy:

$$Accuracy = \frac{True\ positives + True\ negatives}{Total\ number\ of\ examples} \quad (1)$$

Sensitivity, also known as recall, measures the proportion of actual positives that are correctly identified. Specificity, also called the true negative rate, measures the model's performance at classifying negative observations. False positive rate is defined as:

$$False\ positive\ rate = \frac{False\ positives}{Total\ number\ of\ negative\ examples} \quad (2)$$

Precision is also known as the positive predictive value, and is defined as:

$$Precision = \frac{True\ positives}{Total\ number\ of\ positive\ examples} \quad (3)$$

Using this dataset, our model derived performance metrics of accuracy, sensitivity, specificity, and false positive rate of 98.2%, 95.9%, 92.1%, 2.9% respectively. The validation results of our network using the CHBMIT corpus are shown in Tables 3,4. Table 4 details our model's performance on both the CHBMIT standard data set and our in-house EEG data. It should be noted that accuracy is the most intuitive performance measure and works best when there is symmetry in the available data. In our experiments, we assumed the seizure state to be a rare state[34] and used more representative parameters to evaluate performance.

Table 4.3: A comparison of selected studies in the automated detection of seizure using EEG signals from the Bonn and CHBMIT databases. AAN: artificial neural network; CNN: convolutional neural network; SVM: support vector machine; LSTM-RNN: long-short term memory recurrent neural networks.

Author	Year	Database	Research novelty	Neural Network Architecture	Performance
Ghosh-Dastidar et al.[35]	2007	Bonn	Wavelet-chaos	ANN	**Accuracy = 96.7 %**
Shoeb et al.[15]	2004	CHBMIT	SVM	ANN	**Accuracy = 96 %**
Chua et al.[36]	2009	Bonn	Entropy feature determination	Gaussian mixture models	**Accuracy = 93.1 %, Sensitivity = 89.7 %, Specificity = 94.8 %**
Acharya et al.[37]	2017	Bonn	Ten-fold cross validation	Convolutional neural network	**Accuracy = 88.7 %, Sensitivity = 95.0 %, Specificity = 90 %**

Shoeb et al.[16]	2009	CHBMIT	Patient specific detection	ANN, SVM	**Accuracy =96 %**
Martis et al.[38]	2012	Bonn	Empirical mode decomposition (Hilbert-Huang transformation)	Decision trees	**Accuracy = 95.3 %** **Sensitivity = 98.0 %** **Specificity = 97.0 %**
Guo et al.[39]	2011	Bonn	Genetic programming	ANN with k-nearest neighbors	**Accuracy = 93.5 %**
Bhattacharyaa et al.[40]	2017	Bonn	Tunable Q-Factor wavelet transform	ANN, SVM	**Accuracy = 99.4 %** **Sensitivity = 97.9 %** **Specificity = 99.5 %**
This work	2018	CHBMIT	Validation of LSTM-RNN model	LSTM-RNN	**Accuracy = 98.2 %** **Sensitivity = 95.9 %** **Specificity = 92.1 %**

The algorithms were further validated with in-house data. Focusing first on stand-alone EEG data we observed no significant difference in learning rate when comparing to the CHBMIT dataset. Studying the integration of measurement type, performance scores steadily increased for each data type: EEG, fNIRS, and EEG-fNIRS. The performance of the proposed model with respect to each data type is summarized in Table 4.4 Monitoring cross-entropy loss ensured network generalization.

Table 4.4: Performance results for EEG data derived from the CHBMIT dataset and our in-house EEG data**.**

Data	Epochs	Mean Accuracy (%)	ROC
CHBMIT EEG	100	98.20	0.94
In-house EEG	100	97.60	0.90

4.4.4.2 Model Evaluation

This section presents the classification results for seizure and non-seizure classes using our in-house datasets. Our evaluation uses all of the seizure and non-seizure blocks from all subjects and all recordings. To estimate performance of our model on unseen data, we utilized statistical methods derived from *k*-fold

cross-validation. The dataset was randomly shuffled and subsequently split it into *"k"* groups. The model was fit on the training set and evaluated on the test set, yielding an evaluation score. Each fold has data points from a subset of patients, chosen randomly from *"k=10"* folds. The data was pre-shuffled to allow for randomization and we sequentially instantiated *"k"* identical models, and trained each one on *"k-1"* partitions while evaluating on the remaining data.

Table 4.5: The overall classification result across all ten folds for each data type. Multimodal data consistently provided superior results compared to stand-alone EEG or fNIRS data alone. SD: standard deviation

Accuracy	**Mean value post cross-validation, *k=10***
EEG	97.6 ± 0.4 SD
fNIRS	97.0 ± 0.7 SD
EEG-fNIRS	98.3 ± 0.8 SD
Precision	**Mean value post cross-validation, *k=10***
EEG	82.8 ± 0.5 SD
fNIRS	80.7 ± 0.6 SD
EEG-fNIRS	87.3 ± 0.8 SD
Recall	**Mean value post cross-validation, *k=10***
EEG	85.2 ± 0.8 SD
fNIRS	81.3 ± 0.6 SD
EEG-fNIRS	89.7 ± 0.5 SD

Performance metrics on all measures improved in EEG-fNIRS data as compared to either EEG or fNIRS alone. From our cross validation results, we notice that multimodal data consistently performs better as compared to either stand-alone EEG or fNIRS data. Mean squared error between EEG and fNIRS recordings was determined to be 0.61 and between EEG and multimodal recordings 0.79. Likewise, the mean absolute error between EEG and fNIRS recordings was reported as 0.58 and between EEG and multimodal recordings as 0.76. Between EEG and multimodal data types, one-way ANOVA testing yielded p=3.2 X 10^{-3}. Tukey post-hoc comparisons indicated that EEG and multimodal data had significant differences, $p < 0.05$. Multimodal recordings achieved sensitivity and specificity of 89.7% and 95.5% respectively. The precision-recall curve confirmed this finding with multimodal EEG-fNIRS recordings having the highest values for both precision and recall.

4.4.4.3 Seizure detection and spatial foci localization

We further investigated our algorithm's ability to classify signals correctly into seizure and non-seizure segments and localize classifications corresponding to the epileptogenic zone and relevant ictal processes. To this end, we performed analyses to determine if our algorithm's outputs yielded similar cerebral

localization results as traditional methods, primarily the general linear model (GLM)[9]. We first analyze the data on marked events and then performed GLM analysis on positive outputs from the network. In Figure 2, green and orange bars denote true positive and false negative segments respectively. The red and blue curves correspond to oxygenated and deoxygenated hemoglobin respectively and the hemodynamic curves from the right (solid lines) and left sides (dashed lines) of the epileptic foci are shown.

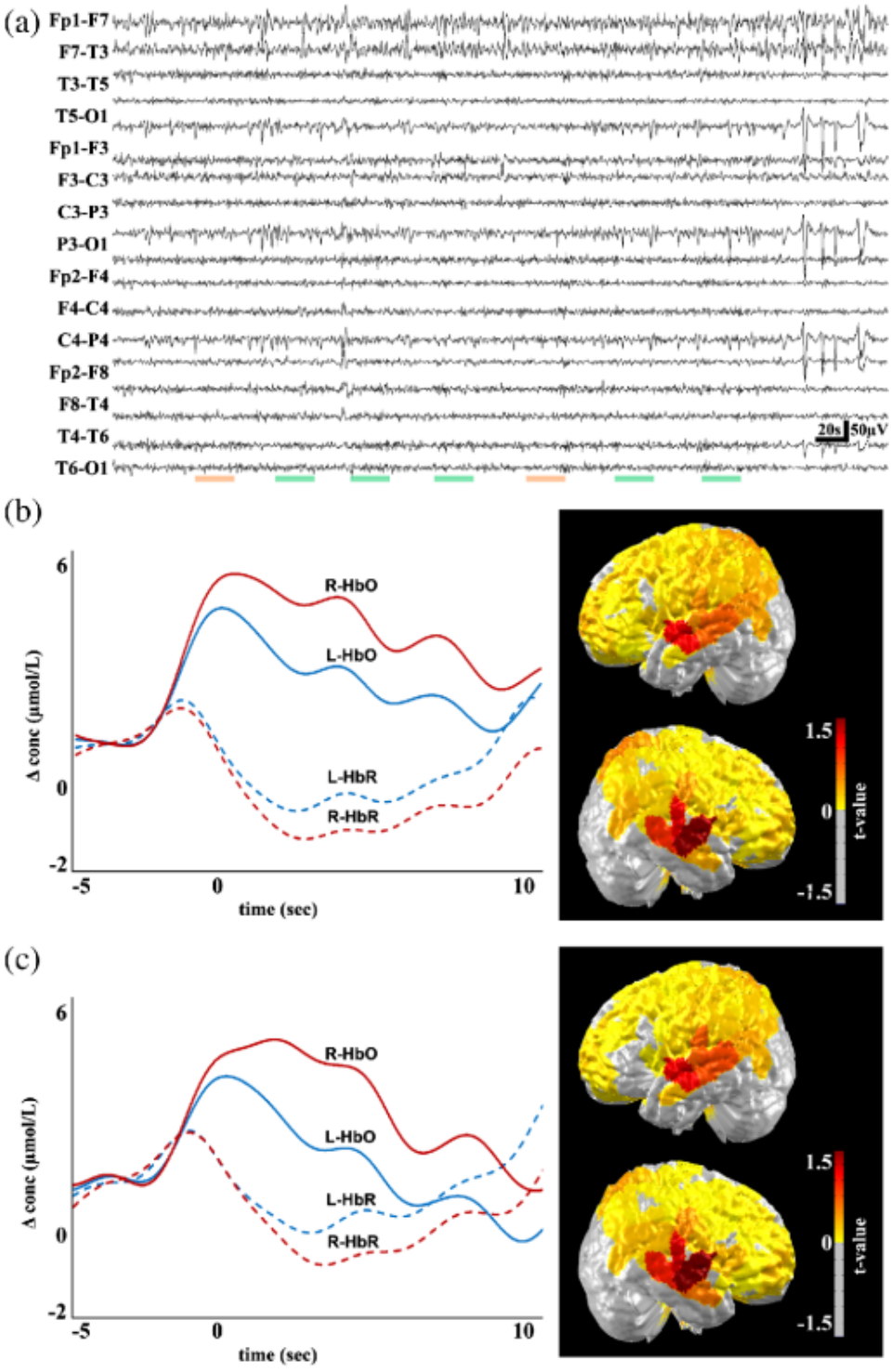

Figure 4.2: Multimodal recordings from patient 10, a 43-year-old male. On the day of the recording, the patient experienced multiple seizure events ranging from duration of 3 to 10 s, with an average duration of 7 s. The analyzed EEG recording is shown in (a), with the colored green bars representing seizure events and false positives denoted by orange horizontal lines. The hemodynamic response to marked events and network events (with false detections) and

the corresponding cerebral topographic analysis are shown in (b) and (c). Red and blue curves represent oxygenated (HbO) and deoxygenated (HbR) hemoglobin, respectively. Solid red and blue and dashed red and blue lines correspond to the right (R-) and left (L-) side of the brain, respectively.

4.4.5 Discussion

The recent rapid technical advances in machine learning and particularly deep learning algorithms, have allowed for automated detection and prediction of anomalies in time series data. Similarly, these approaches hold promise for automated seizure detection with minimal processing of input data. In particular, input streams such as EEG, fNIRS, and multimodal EEG-fNIRS are well suited to be used in these algorithms. The LSTM model developed in this work was proven to be efficient in the task of seizure detection. Our architecture bypasses laborious hand feature selection, and delivers good performance based on multimodal data input. LSTM-RNN architectures, like neural networks generally, can be a powerful tool, but they require long periods for training time, often require more data to train than other models, and can contain a large number of parameters to tune. The gradient vanishing problem and subsequent gradient exploration makes training LSTMs difficult. Adaptive learning methods, particularly, adaptive moment estimation (Adam), root mean square propagation (RMSProp), and adaptive gradient algorithms (AdaGrad), offer solutions to these gradient problems. Adam, which was used in this work, is an extension of and an optimization algorithm for stochastic gradient descent. Adam provides an optimization algorithm that can handle sparse gradients on noisy datasets, which is well suited for our purpose. Another technique used to handle noisy gradient estimates is to utilize mini-batches, as was done in our model. Smaller batches provide reduced computation time per update and offer faster model convergence.

Validation of our architecture on the standardized CHBMIT dataset yielded superior accuracy metrics (98.2%) compared to other studies using convolutional neural networks, support vector machines, and artificial neural networks on the same dataset [15,16]. Compared to other model architectures and related work in the literature, LSTMs offer a powerful framework for seizure detection. Particularly, the LSTM is well suited for time series data because it is well designed to extract patterns where the input data spans over long sequences; a characteristic unique to seizure data. Once our model was validated on the CHBMIT standard dataset, we extended our model to multimodal data. Our implementation of a multilayered LSTM-RNN model for automated classification of multimodal EEG-fNIRS signals displays convergence and good performance metrics. Heuristic parameter tuning, and the requirement of large datasets remain limitations of our model. We in part solved this problem by collecting data points from multiple recordings allowing for a relatively large data corpus. This provides enough data variability to increase the power of the detection algorithm. Our experiments demonstrate that the hemodynamic profiles derived from fNIRS recordings provide discriminatory power in differentiating between seizure and non-seizure states. Furthermore,

multimodal EEG-fNIRS data produced globally superior performance metrics when compared to stand-alone EEG or fNIRS data (Table 5). We obtained an improvement in performance when fNIRS recordings were stacked with the EEG data stream as compared to EEG data only. Our statistical analyses note significant differences in precision and recall metrics between EEG and multimodal data. The mean precision of EEG compared to multimodal data was 82.8, 87.3 respectively. Likewise, the recall values between these data types was 85.2, 89.7 respectively. Figure 2, suggests that our observations are consistent with our algorithm's detections and those from analysis using the GLM. These findings suggest that deep neural models may eventually be a useful clinical tool in the demarcation of seizure zones for tailored medical therapy. Our analyses may also be useful in identifying the side of greater seizure susceptibility and the localization derived from the network may potentially help guide epilepsy surgery and predict outcome post-surgery. Further, prospective studies with longer follow-up periods are needed to properly assess the utility of the model in this capacity. These changes might be indicative of pre-ictal changes in the states of activity in localized neuronal networks and possibly beyond the ictal onset zone. Most patients suffering from epilepsy experience spikes, pre-and post-seizure. This phenomenon was present in our dataset as well. Our algorithm has the potential to be extended to utilize interictal spikes as an additional feature (Tanaka et al. 2010), thereby, producing more comprehensive detection capabilities and providing a more complete clinical picture. This model can be particularly useful in situations in which a trained epileptologist is not readily available in which paroxysmal cerebral electrical and hemodynamic changes may signal epileptic events. Our experimental findings have shown that combining fNIRS with EEG allows for improved seizure detection ability as compared to EEG alone, which could provide additional information in critically ill patients admitted in the ICU, thus improving detection of seizure (in addition to the other advantages of fNIRS in the ICU such as monitoring of brain hypoxia).

4.4.6 Conclusion

This study focused on determining the potential of fNIRS, a cost effective, portable neuroimaging technique in the detection of seizure events in multimodal EEG-fNIRS recordings. Our primary objective was to examine the enhanced capabilities that fNIRS signals provide for a seizure detection task, in particular when combined with EEG data in a multimodal framework, and our secondary objective was to utilize the power of neural networks for this task. For the present study, we aimed to obtain strong and robust hemodynamic response signals. Towards this aim, we collected long-term continuous multimodal EEG-fNIRS data from 40 known epileptic patients comprising a total of 50 hours of recordings. We proposed an LSTM-RNN model that is capable of learning explicit classes from human seizure data. Hyperparameter optimization and monitoring model validation loss (cross-entropy) to ensure network learning and reduce over-fitting was a priority. Eventually, a multi layered RNN-LSTM neural network was designed to encode the

sequential order of features using the rectified linear unit objective function. To examine the generative power of the LSTM-RNN model, we validated our model on a standard dataset followed by in-house data. Post validation, our recordings were scored and subsequent classes were formed from which a multi layered RNN-LSTM neural network was fed standalone EEG, standalone fNIRS data and finally multimodal data. Our methodological approach proves its ability to automatically learn robust features from information contained in multimodal signals while conserving intrinsic waveform properties of seizure and non-seizure activity. Utilizing appropriate model hyperparameters, we performed model training, testing, and validation on a benchmarked scalp EEG data set, which was followed by in-house EEG, fNIRS, and multimodal data from 40 epileptic patients. We explored the benefit that cerebral hemodynamic data provides for a seizure detection task in EEG-fNIRS neuroimaging data and we show that the addition of cerebral hemodynamics improves model performance when compared to EEG alone. Our model's ability to learn the general representation of a seizure is showcased by cross-patient performance indicators as multimodal data reaches performance metrics detailed in Table 5. Increased data collection including different seizure types can enhance our model's performance and lend itself to increase generalizability. Furthermore, the neural network models proposed and characterized herein offer a promising framework for future investigations in early seizure detection. Since our proposed model correctly classifies sequences, this suggests automation of this process can enhance the diagnostic decision-making and treatment planning for epileptic patients. Our model has the potential to be extended to a real time clinical monitoring system in which trained clinical personnel are not readily accessible.

Disclosures

The authors have no relevant financial interests in this article and no potential conflicts of interest to disclose.

Acknowledgments

This project was supported by The Natural Sciences and Engineering Research Council of Canada grant RGPIN-2017-06140 and Canadian Institutes of Health Research grant 396317.

4.4.7 References

1. Bateman, David E. "Neurological assessment of coma." *Journal of Neurology, Neurosurgery & Psychiatry* 71. suppl 1 (2001): i13-i17.
2. Kantanen, Anne-Mari, et al. "Predictors of hospital and one-year mortality in intensive care patients with refractory status epilepticus: a population-based study." *Critical Care* 21.1 (2017): 71.

3. Chiarelli, Antonio MM, et al. "Simultaneous functional near-infrared spectroscopy and electroencephalography for monitoring of human brain activity and oxygenation: a review." *Neurophotonics* 4.4 (2017): 041411.
4. Villringer, Arno, et al. "Near infrared spectroscopy (NIRS): a new tool to study hemodynamic changes during activation of brain function in human adults." *Neuroscience letters* 154.1-2 (1993): 101-104.
5. Watanabe, Eiju, Yukihiro Nagahori, and Yoshiaki Mayanagi. “Focus diagnosis of epilepsy using near-infrared spectroscopy.” *Epilepsia* 43 , 2002: 50-55.
6. Hawco, Colin S., et al. "BOLD changes occur prior to epileptic spikes seen on scalp EEG." *Neuroimage* 35.4 (2007): 1450-1458.
7. Wallois, F., et al. "Haemodynamic changes during seizure-like activity in a neonate: a simultaneous AC EEG-SPIR and high-resolution DC EEG recording." *Neurophysiologie Clinique/Clinical Neurophysiology* 39.4-5 (2009): 217-227.
8. Nguyen, Dang Khoa, et al. "Non-invasive continuous EEG-fNIRS recording of temporal lobe seizures." *Epilepsy research* 99.1-2 (2012): 112-126.
9. Peng, Ke, et al. "fNIRS-EEG study of focal interictal epileptiform discharges." *Epilepsy research* 108.3 (2014): 491-505.
10. Kassab, Ali, et al. "Multichannel wearable fNIRS-EEG system for long-term clinical monitoring." *Human brain mapping* 39.1 (2018): 7-23.
11. Firbank, Michael, Eiji Okada, and David T. Delpy. "A theoretical study of the signal contribution of regions of the adult head to near-infrared spectroscopy studies of visual evoked responses." *Neuroimage* 8.1 (1998): 69-78.
12. Mohseni, Hamid R., et al. "Automatc Detection of Epileptic Seizure using Time-Frequency Distributions." *Advances in Medical, Signal and Information Processing, 2006. MEDSIP 2006. IET 3rd International Conference On*. IET, 2006.
13. Osorio, Ivan, and M. Frei. "Feasibility of automated warning in subjects with localization-related epilepsies." *Epilepsy & Behavior* 19.4 (2010): 602-607.

14. Nigam, Vivek Prakash, and Daniel Graupe. "A neural-network-based detection of epilepsy." *Neurological Research* 26.1 (2004): 55-60.
15. Shoeb, Ali, et al. “Patient-specific seizure onset detection.” *Epilepsy & Behavior*, 5.4 (2004): 483-498.
16. Shoeb, Ali Hossam. Application of machine learning to epileptic seizure onset detection and treatment. Diss. Massachusetts Institute of Technology, 2009.
17. Yuan, Qi, et al. "Epileptic EEG classification based on extreme learning machine and nonlinear features." Epilepsy research 96.1-2 (2011): 29-38.
18. LeCun, Yann, Yoshua Bengio, and Geoffrey Hinton. “Deep learning.” *Nature*, 2015: 436-444.
19. Acharya, U. Rajendra, et al. "Deep convolutional neural network for the automated detection and diagnosis of seizure using EEG signals." *Computers in biology and medicine* 100 (2018): 270-278.
20. Luca, Stijn, et al. "Detecting rare events using extreme value statistics applied to epileptic convulsions in children." *Artificial intelligence in medicine* 60.2 (2014): 89-96.
21. Pisani, Francesco, and Elena Pavlidis. "The role of electroencephalogram in neonatal seizure detection." *Expert review of neurotherapeutics* 18.2 (2018): 95-100.
22. Supratak, Akara, Ling Li, and Yike Guo. “Feature extraction with stacked autoencoders for epileptic seizure detection.” *Engineering in Medicine and Biology Society (EMBC)*, *2014 36th Annual International Conference of the IEEE*. IEEE, 2014.
23. Lindquist, Martin A., et al. “Modeling the hemodynamic response function in fMRI: efficiency, bias and mis-modeling.” *Neuroimage* 45.1 (2009): S187-S198.
24. Huppert, Theodore J., et al. "HomER: a review of time-series analysis methods for near-infrared spectroscopy of the brain." *Applied optics* 48.10 (2009): D280-D298.
25. Kocsis, L., P. Herman, and A. Eke. "The modified Beer–Lambert law revisited." *Physics in Medicine & Biology* 51.5 (2006): N91.
26. Sutskever, Ilya, Oriol Vinyals, and Quoc V. Le. "Sequence to sequence learning with neural networks." *Advances in neural information processing systems*. 2014.

27. Graves, Alex. "Generating sequences with recurrent neural networks. " *arXiv preprint arXiv:1308.0850,* (2013).
28. Gregor, Karol, et al. "Draw: A recurrent neural network for image generation." *arXiv preprint arXiv:1502.04623* (2015).
29. Cooijmans, Tim, et al. "Recurrent batch normalization." *arXiv preprint arXiv:1603.09025* (2016).
30. Schmidhuber, Jürgen. "Deep learning in neural networks: An overview." *Neural networks* 61 (2015): 85-117.
31. Zaremba, Wojciech, Ilya Sutskever, and Oriol Vinyals. "Recurrent neural network regularization." *arXiv preprint arXiv:1409.2329* (2014).
32. Wang, Lin, Zhigang Wang, and Shan Liu. "An effective multivariate time series classification approach using echo state network and adaptive differential evolution algorithm." *Expert Systems with Applications* 43 (2016): 237-249.
33. Goldberger, Ary L., et al. "PhysioBank, PhysioToolkit, and PhysioNet: components of a new research resource for complex physiologic signals." *Circulation* 101.23 (2000): e215-e220.
34. Shorvon, Simon, et al., eds. *Oxford textbook of epilepsy and epileptic seizures*. OUP Oxford, 2012.
35. Ghosh-Dastidar, Samanwoy, Hojjat Adeli, and Nahid Dadmehr. "Mixed-band wavelet-chaos-neural network methodology for epilepsy and epileptic seizure detection." *IEEE transactions on biomedical engineering* 54.9 (2007): 1545-1551.
36. Chua, K. C., et al. "Automatic identification of epileptic electroencephalography signals using higher-order spectra." *Proceedings of the Institution of Mechanical Engineers, Part H: Journal of Engineering in Medicine* 223.4 (2009): 485-495.
37. Acharya, U. Rajendra, et al. "Deep convolutional neural network for the automated detection and diagnosis of seizure using EEG signals." *Computers in biology and medicine* 100 (2018): 270-278.
38. Martis, Roshan Joy, et al. "Application of empirical mode decomposition (EMD) for automated detection of epilepsy using EEG signals." *International journal of neural systems*22.06 (2012): 1250027.

39. Guo, Ling, et al. "Automatic feature extraction using genetic programming: An application to epileptic EEG classification." *Expert Systems with Applications* 38.8 (2011): 10425-10436.

40. Bhattacharyya, Abhijit, et al. "Tunable-Q wavelet transform based multiscale entropy measure for automated classification of epileptic EEG signals." *Applied Sciences* 7.4 (2017): 385.

CHAPTER 5 ARTICLE 2: MULTIMODAL AUTOENCODER PREDICTS FNIRS RESTING STATE FROM EEG SIGNALS

5.1 Article details

Sirpal, P., Damseh, R., Peng, K., Nguyen, D. K., & Lesage, F. (2020) "Multimodal autoencoder predicts fNIRS resting state from EEG signals", Submitted to *Neuroinformatics*

This article addresses the second objective of the thesis—using a deep learning sequence to sequence autoencoder to predict fNIRS signals given full spectrum and specific frequency resting state EEG signals.

5.2 Context and rationale

The hemodynamic response obtained from the resting state in the context of epileptic recordings is of significance as neuronal resting membrane potential allows for low frequency oscillations to cause rapid electrical and cerebral hemodynamic changes. Furthermore, the resting state networks in the epileptic brain have differences as compared to resting state networks in healthy brains [255]. In an effort to further understanding the fundamental relationships at play in epileptic human brains, it is hypothesized here that hemodynamic brain signals (fNIRS) can be predicted from resting state scalp EEG signals derived from epileptic patients within the framework of a sequence to sequence autoencoder.

5.3 Contributions

This article uses full spectrum and frequency filtered EEG (seizure free intervals) signals to predict resting state fNIRS waveforms using a sequence to sequence convolutional neural network long short-term memory autoencoder. The second part of this work included a functional connectivity study to measure temporal correlations between experimental fNIRS and model fNIRS predictions. Network connectivity was computed by calculating the Pearson correlation coefficients of the hemodynamic responses between fNIRS channels belonging to experimental fNIRS and model fNIRS predictions.

The results from this work suggest that the gamma (30-100 Hz) EEG band is most predictive of resting state fNIRS waveforms. This is corroborated by a functional connectivity study between experimental fNIRS and our model fNIRS reconstructions. This work demonstrates for the first time that intermodal autoencoding from cerebro-electropotential (EEG) signals can predict cerebral hemodynamics (fNIRS) to a certain extent. Findings from this work suggest that higher frequency EEG components offer hemodynamic (fNIRS) predictive capacity.

5.4 Article 2

Multimodal autoencoder predicts fNIRS resting state from EEG signals

Parikshat Sirpal[a,b,*], Rafat Damseh[a], Ke Peng[a,b], Dang Khoa Nguyen[b], Frédéric Lesage[a,c]
[a] École Polytechnique de Montréal, Université de Montréal, C.P. 6079, succ. Centre-Ville, Montréal, H3C 3A7, Canada
[b] Neurology Division, Centre Hospitalier de l'Université de Montréal (CHUM), 1000 Saint-Denis, Montréal, H2X0C1, Canada
[c] Research Centre, Montreal Heart Institute, Montreal, Canada
[*]parikshat.sirpal@polymtl.ca

5.4.1 Abstract

In this work, we introduce a deep learning model for evaluation on multimodal electroencephalographic (EEG) and functional near infrared spectroscopy (fNIRS) recordings from 40 epileptic patients. We exploit a deep learning framework where long-short term memory (LSTM) units and convolutional neural networks (CNN) are integrated within an intermodal sequence-to-sequence autoencoder. The trained model predicts resting state fNIRS waveforms from EEG, sans a priori, by hierarchically extracting deep features from EEG full spectra and specific EEG frequency bands. Results show that higher frequency EEG ranges are predictive of low frequency fNIRS waveforms with the gamma band inputs dominating fNIRS prediction. Seed based functional connectivity demonstrates similar spatial patterns between experimental fNIRS and our model fNIRS reconstructions. This work demonstrates for the first time that intermodal autoencoding from cerebro-electropotential (EEG) signals can predict cerebral hemodynamics (fNIRS).

Keywords: *EEG-fNIRS, functional brain imaging, deep neural networks, epilepsy, resting state*

5.4.2 Introduction

The multimodal integration of electro-potential measures via scalp electroencephalography (EEG) and cerebral hemodynamic information by means of functional near infrared spectroscopy (fNIRS) has established itself as a non-invasive, portable, and cost-effective tool in characterizing and localizing brain activation responses (Goldman et al., 2002; Laufs et al., 2003; Martinez-Montes et al., 2004; Salek-Haddadi et al., 2003). While scalp EEG measures cerebro-electropotential activity, hemodynamic fNIRS signals result from the dynamic variations in oxy- and deoxyhemoglobin (Chiarelli et al., 2017; Ogawa et al., 1992), with a spatially dependent delay of approximately 3 seconds following neural activity. Although both

modalities measure brain activity, they reflect distinct processes linked by neurovascular coupling. Simultaneous experimental setups recording cerebral electrical activity and fNIRS hemodynamics have established causality between neuronal firing and changes in oxy-hemoglobin (HbO), deoxy-hemoglobin (HbR), and total hemoglobin (HbT) (Logothetis et al., 2001; Mukamel et al., 2005; Singh, 2012). Recent interest has focused on determining spatial hemodynamic correlates from EEG recorded activity, particularly, from signal modulations in ongoing oscillatory activity measured by EEG, and the blood level oxygen dependent hemodynamic signal (BOLD) from fMRI (Czisch et al., 2004; Lemieux et al., 2001; Lövblad et al., 1999). These studies have successfully demonstrated that modulations in certain low frequency EEG bands, are negatively correlated with modulations in the BOLD signal. Particularly, infra-low gamma EEG band envelopes have been shown to modulate resting state signals (Jia & Kohn, 2011).

Scalp EEG recordings can be classified within five main ranges of frequencies: alpha, beta, delta, gamma, and theta (Cho et al., 2014; Freeman et al., 2003; Pedregosa et al., 2011; Zhao et al., 2018). The delta frequency range encompasses low frequencies near 0.25 Hz up to 3 Hz. Frequencies in this range tend to have higher amplitude and slower waveforms. Physiological delta frequencies are common as a dominant rhythm in certain sleep stages and in infants up to one year. Pathological delta activity may appear focally with focal lesions and more widespread with diffuse lesions, metabolic encephalopathy, hydrocephalus or deep midline lesions. Theta frequency ranges include frequencies between 4 and 7 Hz. While normal in children up to 13 years old, they are interpreted as slow activity in awake adults (F. et al., 2015; Mantini et al., 2007; Sitnikova et al., 2016). As with delta waves, they may be seen regionally in focal lesions or in a more generalized distribution in diffuse disorders such as metabolic encephalopathy. Alpha frequencies are between 8 and 13 Hz, representing the posterior-dominant rhythm in awake adults. Beta activity ranges in frequency between 14-30 Hz and are usually observed in a bilaterally frontal symmetrical distribution, especially in anxious patients or those taking benzodiazepines (Gross & Gotman, 1999). Gamma wave oscillations contain frequencies between 30-100 Hz. Gross and Gotman demonstrated that gamma activity spiked during cognitive tasks (Gross & Gotman, 1999). Research has also demonstrated that gamma frequency activity is enhanced in rapid eye movement during sleep (Gross & Gotman, 1999).

The characterization of the relationship between the electrophysiology of neuronal systems and their slower hemodynamics is relevant from a number of perspectives particularly in cerebrovascular clinical situations (e.g., stroke, subarachnoid hemorrhage). In this study, we develop a sequence-to-sequence autoencoder model with long short-term memory units and convolutional neural network modules. This deep learning architecture aims to learn the predictive correlations between EEG (full spectrum and frequency bands) and fNIRS activity. A full description of the model developed is detailed in section 2.2. For this purpose, we make use of multimodal EEG-fNIRS recordings collected from a cohort of 40 epileptic

patients focusing on resting periods (no seizures). We investigate predicted fNIRS hemodynamics from EEG frequency ranges in the resting state. Subsequently, predictions from our model are used for a functional connectivity study to determine the connectivity patterns in the resting epileptic brain. Seizures alter normal functioning of the brain, producing dysfunctional resting state networks within the brain, making functional connectivity an ideal technique for understanding these complex effects (Tracy & Doucet, 2015). These results suggest that a multimodal autoencoder can learn multimodal relations to predict resting state signals.

5.4.3 Methods

5.4.3.1 Subjects and protocol

Forty patients with refractory focal epilepsy were recruited for prolonged EEG-fNIRS recordings. Epilepsy diagnosis and localization of the epileptic focus for each patient was based on a comprehensive evaluation which included clinical history, video-EEG recording of interictal spikes and seizures, brain magnetic resonance imaging (MRI), positron emission computed tomography (PET) and for some patients ictal single photon emission computed tomography (SPECT) and magnetoencephalography (MEG). Full details regarding patient profiles including age, gender, EEG and MRI findings are found in table 1 of Peng et al., 2014 and Sirpal et al., 2019 (Peng et al., 2014; Sirpal et al., 2019). A subset of patients had MRI evidence of encephalomalacia, cortical dysplasia, and/or hippocampal atrophy, a common finding in epilepsy, but this was neither an inclusion nor exclusion criterion. Additionally, some of the patients displayed bilateral pathological changes. The institutional review boards of Sainte-Justine Hospital and CHUM approved the study. changes.

5.4.3.2 EEG-fNIRS data acquisition and pre-processing

Continuous EEG-fNIRS recordings were performed at the Optical Imaging Laboratory of Sainte-Justine Hospital in Montreal, Canada. Functional imaging data was collected using the Imagent Tissue Oximeter system (ISS Inc.), a multi-channel frequency domain system recording at 19.5 Hz with wavelengths of 690 nm and 830 nm for sensitivity to HbR and HbO respectively. EEG data was recorded according to the standard 10–20 system using 21 electrodes (in positions Fp1, Fp2, F7, F3, Fz, F4, F8, T7, C3, Cz, C4, T8, P7, P3, Pz, P4, P8, O1, O2) at 500 Hz (Neuroscan Synamps 2TM system). Custom-made helmets with a total of 64 light sources, 16 light detectors and 19 EEG electrodes were used allowing for stable optical coupling between cortical regions and the scalp, preventing optode shifts and resulting direct movement artifacts to a large extent. Sensitivity of near-infrared light to cortical tissue was maintained by positioning the optical channels approximately 3-4 cm apart.

Signal fidelity was examined prior to analysis by channel-wise verification of signal intensity. EEG data was band pass filtered between 0.1-100 Hz to remove instrumental noise and to remove drift related to physiological activity, particularly, higher frequencies. For fNIRS, channels deemed to have subpar SNR (less than 30% of the mean SNR of all channels) were eliminated and not included due to poor quality. This analysis led to an average of 138 channels per patient. Changes in HbO and HbR were calculated via the MNE software package (Gramfort et al., 2014). The unprocessed raw time series of the HbO and HbR signals was band-pass filtered to remove specific frequency components attributed to cardiac (~1 Hz) and/or respiratory activity (~0.2-0.3 Hz) (Gramfort et al., 2014; Lu et al., 2010; Peng et al., 2014). Anatomical MRI registration of optode and electrode position was done using neuro-navigation (Brainsight, Rogue-Research Inc.), channel positions being cross-referenced with the MRI and adapted to ensure coverage of the epileptic focus, the contralateral homologous region, and as much area as possible of other brain regions. Multiple consecutive sessions for a total of approximately 15 minutes per recording session led to a compendium of 200 recordings totaling 50 hours of recording time. The resting state is devoid of frank epileptic activity and is band pass filtered in the 0.01 to 0.1 Hz frequency range.

5.4.3.3 Neural network architecture

To investigate how EEG can predict fNIRS signals, we built a multimodal autoencoder. Autoencoders are powerful machine learning models trained in self-supervised fashion to reconstruct inputs by learning their abstract representations (Kocsis et al., 2006; Lindauer et al., 2010; Socher et al., 2011; Vincent et al., 2010) . Here, we used a deep autoencoder for embedding signals in a low dimensional latent space, where both the encoder and decoder are formulated as deep neural networks. Our architecture accepts data sequence that accounted for hemodynamic delays to perform sequence-to-sequence encoding (Luong et al., 2016; Truong et al., 2018; Vincent et al., 2008; Zhang, 2018). EEG data samples are projected in the latent space with fixed length vectors that provide more compressed representations, which are then used to decode and reconstruct the output fNIRS data.

Recurrent neural networks (RNN) have been widely used in time series modeling since they account for the temporal state within data (Baytas et al., 2017; Chung et al., 2016; Merity et al., 2018; Mikolov et al., 2010). RNN's output depends on hidden states and feedback connections present within the hidden units and allow for previous states to be used as inputs, thereby allowing RNNs to hold historical information in memory. In our model, we used backpropagation through time, a common gradient descent type training technique (Sutskever et al., 2014a). The innate problem of RNN gradient based training is that derivatives propagated via recurrent connections either become exceedingly small or large (Goodfellow et al., 2016; Luong et al., 2016), causing a vanishing or exploding gradient respectively. LSTM, a special variant of the vanilla RNN architecture overcomes the vanishing gradient problem (Greff et al., 2017; Gregor et al., 2015;

Lecun et al., 2015). LSTM units receive external inputs and generate hidden outputs via input, output, and forget gates and a memory cell. The gates and memory cell are internally connected with weighted links, and the gates are also connected with external sources, which are current sequential inputs and previous hidden states. This prevents the LSTM from storing useless or noisy input information (Greff et al., 2017; Gregor et al., 2015; Lecun et al., 2015).

Multiple LSTM layers were used in building our sequence-to-sequence multimodal autoencoder to learn sequential inputs and temporal representations. The LSTM autoencoder model (LSTM-AE) as proposed by Srivastava et al. consists of encoder LSTM units and decoder LSTM units (Srivastava et al., 2015). The encoder LSTM receives input sequences and encodes them into a feature vector as the LSTM generates hidden outputs (Lipton et al., 2016; Wang et al., 2016). Likewise, the decoder LSTM receives the feature vector and decodes it into the original input sequences. LSTM-AEs learn a compressed representation of sequence data and have been used in the context of video, text, audio, and time series sequence data (Lipton et al., 2016; Srivastava et al., 2015; Wang et al., 2016). Here, multiple LSTM layers were integrated to build a sequence-to-sequence multimodal autoencoder to exploit temporal representations. Our model also encompasses convolutional layers to extract high level spatial percepts from channel combinations. In summary, our neural network receives EEG time-series sequences, represented as a single matrix, of resting state (time series devoid of frank epileptic activity) free cerebral fluctuations during multimodal EEG-fNIRS recordings and is trained to reconstruct the corresponding fNIRS resting state output.

After testing multiple architectures with exhaustive hyper-parameter optimization, we designed our model as follows: The encoder is comprised of LSTM layers preceded by convolutional blocks. Convolutions in each block has a kernel size of (1, 7) and stride size of (1, 2). The decoder is comprised of LSTM layers which manipulate the vectors in the latent space to provide a final output dimension equal to that of an fNIRS sample. We evaluated our model in terms of cross-modal reconstruction error (Zhao et al., 2018), denoted RE. Once trained, the RE was calculated on an independent testing subset (see below) by computing the sum of the Euclidean distance between the output x_t and its corresponding reconstruction, $\hat{x}$, over all L dimensions, as expressed in Equation 1 below:

$$\in_t = \sum_{l=1}^{L} |\hat{x}_{t,l} - x_{t,l}|, t\epsilon\, T \qquad (1)$$

Model output is denoted as $|\widehat{x_t}|$. EEG data is processed as follows. First, matching EEG and fNIRS data are found from our data directory, following which the respective data (EEG or fNIRS) is labeled according to the resting state periods. Feature scaling is performed using the MinMaxScaler class (Pedregosa et al.,

2011) on EEG input data and sets the range of values between 0 and 1. Input signals are mean centered prior to being fed into the model. Then, data is fed into the convolutional layers and travels to the LSTM and deconvolution modules. A detailed schematic view of our model is shown in Fig. 1 below.

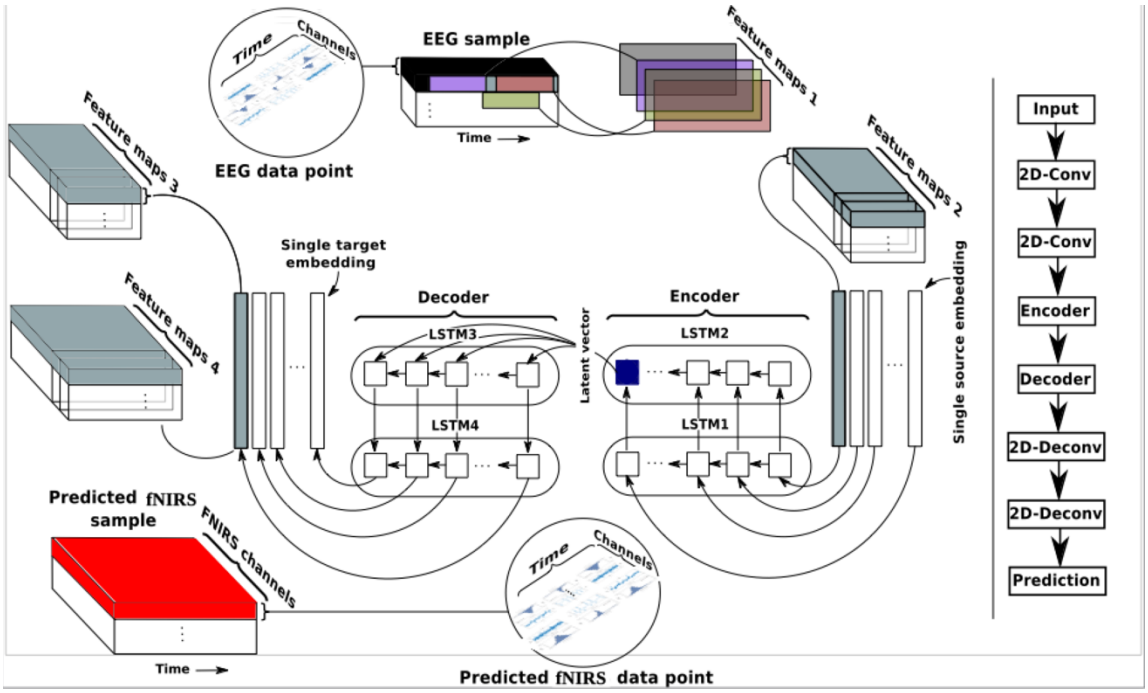

Figure 5.1: Multimodal EEG to fNIRS reconstruction using our patient specific sequence to sequence LSTM autoencoder model. Given EEG input data into the encoder, the model decodes and reconstructs fNIRS output. After data collection and resting state segment annotation, data processing and model development, the data is finalized as a 4-D tensor with shape: *(samples per batch, sequence length, time points, and channels)*. The model has encoder and decoder compartments, each with 2 LSTM layers, determined heuristically. Table 1 below provides details of the model.

Table 5.1: Detailed overview of the proposed convolutional neural network long-short term autoencoder (CNN-LSTM AE) model. Model specifications and hyperparameters were heuristically determined. Convolutions and deconvolutions have kernels of size (1,2), and thus their effect is along the time dimension. Convolutions help in generating embeddings with higher level abstraction of the input EEG sequence. Deconvolutions reconstruct the fNIRS sequence at full resolution based on output embeddings. The decoder and encoder LSTM units have ReLU (Rectified linear units) activations.

Layer	**Description**	**Output size**
Input	EEG sample sequence	(EEG sequence length, number of time points is 500, number of EEG channels is 21)
EEG Sequence Embedding		
2D conv+AveragePooling+ Dropout	2D convolution: stride=(1,2); $Kernel\ size = (1,7)$; ReLU activation. Dropout: 20%. Average Pooling kernel: (1,2).	(EEG sequence length, 125, number of Features Maps)
2Dconv+AveragePooling+ Dropout	2D convolution: stride=(1,2); kernel size=(1,7); ReLU activation. Dropout: 20%. Average Pooling kernel: (1,2).	(EEG sequence length, 62, number of Features Maps)
Reshape	Reshape into an elongated tensor.	(EEG sequence length, 62 * number of Features Maps)
Encoder		
LSTM1 + Dropout	An LSTM layer with number of cells equal to the number of EEG sequence length. ReLU activation. Dropout: 20%.	(EEG sequence length, 512)
LSTM2 + Dropout	An LSTM layer with number of cells equal to the number of EEG sequence length. ReLU activation. Dropout: 20%.	(1, 256)
Decoder		
Repeat	Create repeated version of the latent vector.	(fNIRS sequence length, 256)
LSTM3 + Dropout	An LSTM layer with number of cells equal to the number of EEG sequence length. ReLU activation. Dropout: 20%.	(fNIRS sequence length, 312)

LSTM4 + Dropout	An LSTM layer with number of cells equal to the number of EEG sequence length. ReLU activation. Dropout: 20%.	(fNIRS sequence length, 695)
fNIRS Sequence Reconstruction		
Reshape	Reshape into a 2D tensor.	(fNIRS sequence length, 5, number of Feature Maps 3)
Deconv1+Dropout	2D deconvolution: $stride = (1,2)$; ReLU activation; $Kernel\ size = (1,2)$. Dropout: 20%.	(fNIRS sequence length, 10, number of Feature Maps 4)
Deconv2+Dropout	2D deconvolution: $stride = (1,2)$; ReLU activation; $Kernel\ size = (1,2)$. Dropout: 20%.	(fNIRS sequence length, 20, number of fNIRS channels)

5.4.3.4 Training details

The model was designed to use patient specific EEG signals as input to output fNIRS waveforms. For each patient, data was divided into three subsets: a training set, validation set, and testing set, with a proportion of 70% training, 20% testing and 10% validation. We experimented with various model depths and determined deep LSTMs to outperform shallow LSTMs. This is likely due to the larger hidden state which occurs as a result of increasing layers. Complete training details are given below:

• We initialized the LSTM's parameters with the uniform distribution between 0 and 1.0. This was done to counteract the exploding gradients problem intrinsic to LSTMs, thereby enforcing a hard constraint on the norm of the gradient by scaling it between 0 and 1. Simultaneously, we specified starting node values for the LSTM computations by preparing a feed dictionary which has input data (EEG) and a target label. It is important to note that the LSTM is able to learn how to map input sequences (model training is patient specific) into a fixed dimensional vector representation and can learn temporal dependencies.

• Backpropagation through time was used with a learning rate of 0.05, batch size of 60 and 50 epochs, all of which were heuristically determined.

• Each fNIRS waveform generated corresponds to an EEG sequence input. An element in the EEG sequence corresponds to 1 second of recording with 500 time points (sampling frequency is 500 Hz) for each EEG channel. Data batches were generated for sequence processing by using the utility class for batch generation in the Keras framework. Briefly, this class uses as input a sequence of data points to produce batches for training and validation. Data points outside of the start and end indices of resting state periods (as marked in our ground truth) are not used in the output sequences. This is useful in that it reserves part of the data for testing and validation. The final EEG (full spectrum and frequency band) data used as input is two dimensional, i.e., [***data points, channels***].

To summarize, the model was trained as follows: **(a)** we designed LSTM layers with corresponding LSTM cells **(b)** model parameters were uniformly initialized in the range between [0,1], **(c)** dropout was applied with value of 0.2, and average pooling was applied to reduce the probability of model overfitting, **(d)** we used backpropagation through time with a learning rate of 0.05, **e)** we used a batch size of 60 and 50 training epochs for each patient.

5.4.3.5 Model validation

After training and saving our model's weights, we validated the model's intra-patient predictive capacity by using as input individual EEG recordings to predict fNIRS signals. This was possible since our dataset contains multiple recordings from each patient. To diagnose performance, we plotted learning curves to ensure we did not overfit during training. As an illustrative example, the figure below shows the learning curves for patients 1,4, and 23.

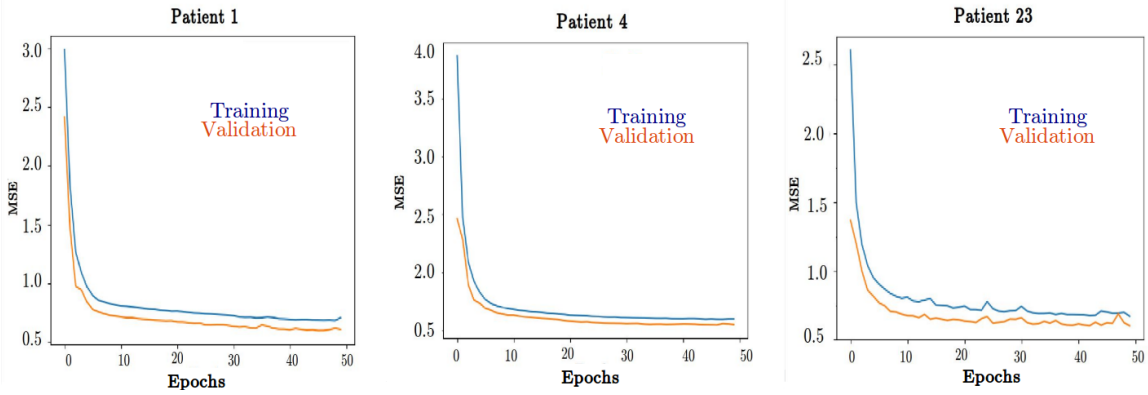

Figure 5.2: Learning curves are generated for the training and validation sets. The training and validation loss decrease to a point of stability with a minimal gap between the two final loss values. We note that the validation loss decreases to a point of stability and has a small gap with the training loss (mean squared error (MSE)).

5.4.3.6 Model predictions

The model predicts waveforms by appending 'output state', and 'output prediction' matrices. Decoder inputs are two-dimensional matrices which are passed into decoder LSTM layers. fNIRS data is shifted one sequence ahead to hold data in LSTM memory and finally decoder outputs are returned as a result of the data passing through the deconvolution layers. LSTM cells are connected recurrently to each other.

5.4.3.7 Functional connectivity analysis

Neural rhythms can be classified by slow cortical oscillation in complex wave sequences. Cortical areas may be associated by responses to specific neurophysiological conditions including cognition, motor activity, and resting state (Steriade, 2001), as most tasks recruit large networks of coactivated areas. Identifying these patterns between functionally coactivated areas is difficult during a particular neurological state. Resting-state functional connectivity (RSFC), albeit traditionally a functional magnetic resonance imaging (fMRI) technique claims that absent of any task or specific event, spatially distant cortical regions experience correlated patterns of blood oxygenation level-dependent (BOLD) activity (Varela et al., 2001). This activity can be both spatially dependent (Brilla, 2019; Dressler et al., 2004; Tyvaert et al., 2008) and seen across individuals (Biswal et al., 1995; Fox & Greicius, 2010). Evidence suggests that brain regions with RSFC correlations are also functionally active (Greicius et al., 2003; Shulman et al., 2004; Steinbrink et al., 2006) and these correlations are dependent upon structural connections, though indirectly.

Research using fNIRS for exploring functional connectivity has increased recently and provides similar results obtained using fMRI (Tyvaert et al., 2008) --revealing networks of sensorimotor, visual, auditory, and language systems in the resting state. Here, our experiments centered on investigating which EEG frequency band best predicts resting state networks in fNIRS. We defined the seed channel from a functional region of interest (a region which we were able to have adequate optode coverage confirmed by our source/detector montage) and had an acceptable level of signal fidelity (high SNR). Subsequently, we first computed the Pearson product-moment correlation coefficients between the experimental fNIRS timeseries of the seed channel and the experimental fNIRS timeseries of all other channels, and then between the experimental seed channel timeseries and our model's predicted timeseries for all the other channels. The two sets of correlation coefficients were respectively projected to an MRI head template based on the 3-dimensional coordinates of the corresponding channels with the MATLAB based Atlasviewer (Aasted et al., 2015). The connectivity value at each voxel of the cortex was obtained from the correlation coefficients of all channels with a weighted-average method using the reciprocal of the cube of the distance from the voxel to each fNIRS channel as the weight.

In order to quantitively evaluate and compare the results of our functional connectivity studies, we computed the root mean square error (Equation 2) i.e., the standard deviation of the residuals between functional connectivity values in experimental fNIRS and reconstructed fNIRS time courses derived from full spectrum EEG and gamma band signals for all patients in our cohort.

$$RMSE_{FC_C} = \sqrt{\frac{\sum_{i=C}(fc_i - \hat{f}_C)^2}{C}} \quad (2)$$

Where *"C"* is the number of channels per functional connectivity analysis, fc_i is the connectivity value of experimental fNIRS and $\hat{f}_C$ is the connectivity value of model fNIRS reconstructions.

5.4.4 Results

This section describes the reconstruction results obtained using: 1.) full spectrum EEG and subsequently 2.) EEG frequency ranges as model input. Intra-patient reconstructions are also presented; we explore spatial reconstruction, resting state predictions, and functional connectivity.

5.4.4.1 Full spectrum EEG performance and feature analysis

Resting state scalp full spectrum EEG signals from all channels were input in the model. To decode fNIRS channels from encoded EEG channels, the model's decoder layers used the encoder's latent state as input as data traveled through LSTM units. Figure 3 below quantifies performance on selected individual patients with full spectrum EEG signals as input. Figure 4 provides the group estimate of reconstruction error for all patients given scalp full spectrum EEG recordings.

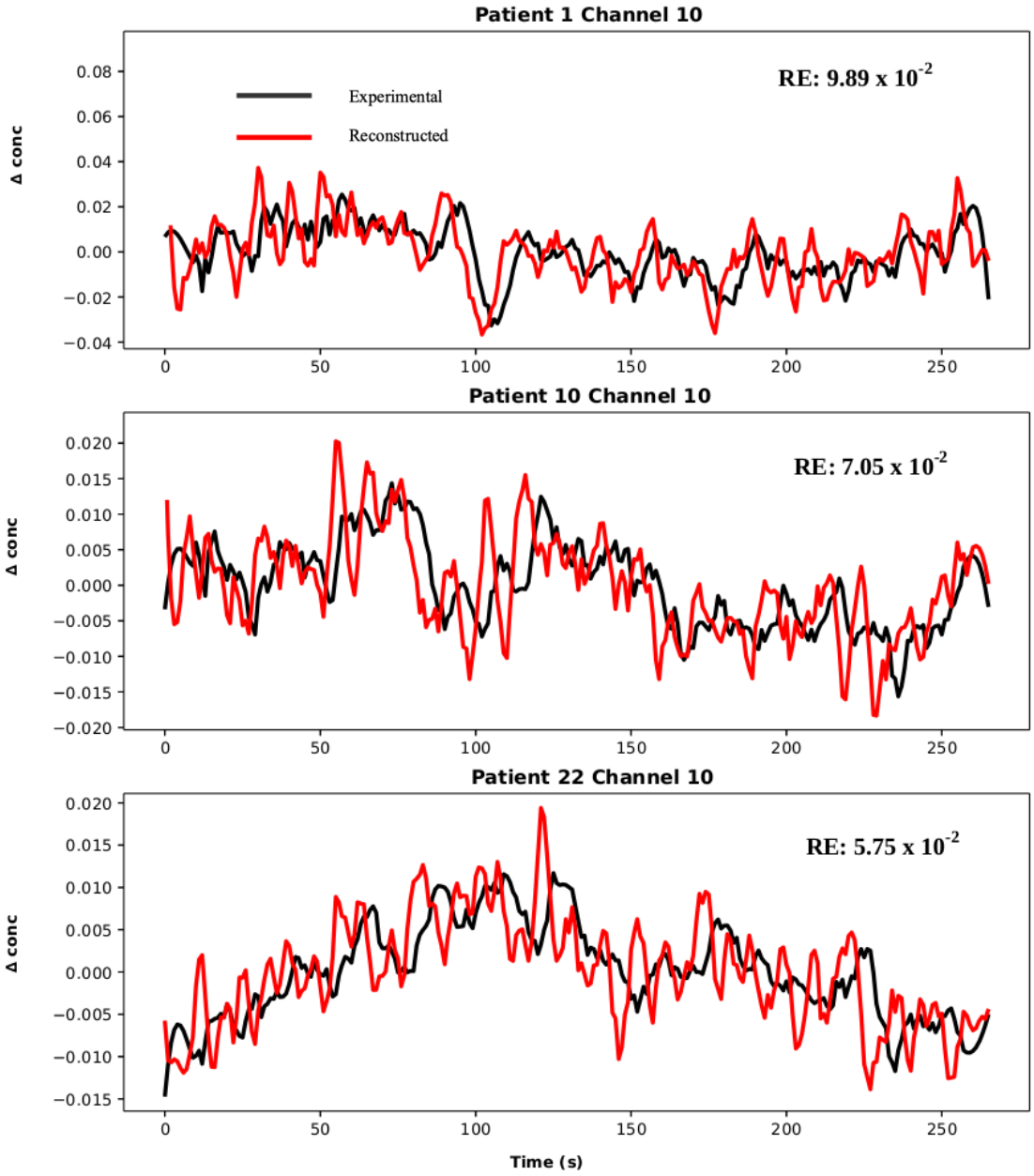

Figure 5.3: Decoded predictions of hemodynamic waveforms from cerebral electrical activity. Full spectrum EEG signals from all channels were used as input. fNIRS HbO reconstructions are shown from 3 patients in channel 10 (Channel 10's SNR was adequate, located on the left temporal lobe). Black and red curves correspond to experimental and reconstructed fNIRS waveforms respectively. Data from patient 1 reconstructed with the lowest reconstruction error, RE, while patient 22 had the highest. The data has been mean centered and baseline is near zero, 250 seconds is shown here to illustrate seizure free, resting state periods of fNIRS signals that are devoid of seizure and spikes. Note that the model accounts for the delay between EEG and fNIRS (~few seconds) and the model fNIRS predictions are indicative of this delay.

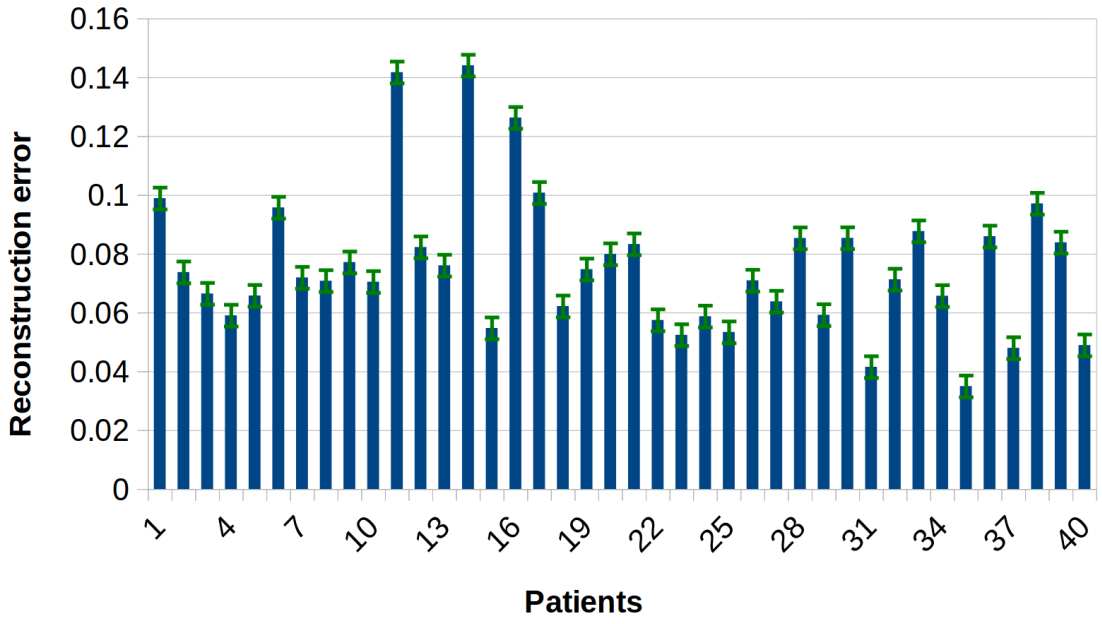

Figure 5.4: Full spectrum EEG to fNIRS reconstructions. The group estimate of full spectrum EEG signals from all channels were used as input in our network architecture, to reconstruct full fNIRS waveforms from all fNIRS channels.

5.4.4.2 Intra-patient reconstructions on separate recording sessions

Here, we report results on intra-patient fNIRS reconstructions provided EEG resting state as input. Specifically, we hypothesized that our model when trained with a patient's single recording was able to reconstruct fNIRS signals from a subsequent recording. To examine our model's predictive capacity, we first trained our network on a patient's single recording. Next, we used our newly trained network and aimed to reconstruct fNIRS signals from a subsequent recording from the same patient. This can be considered as cross-validation of our model. Figure 5 displays the reconstructions.

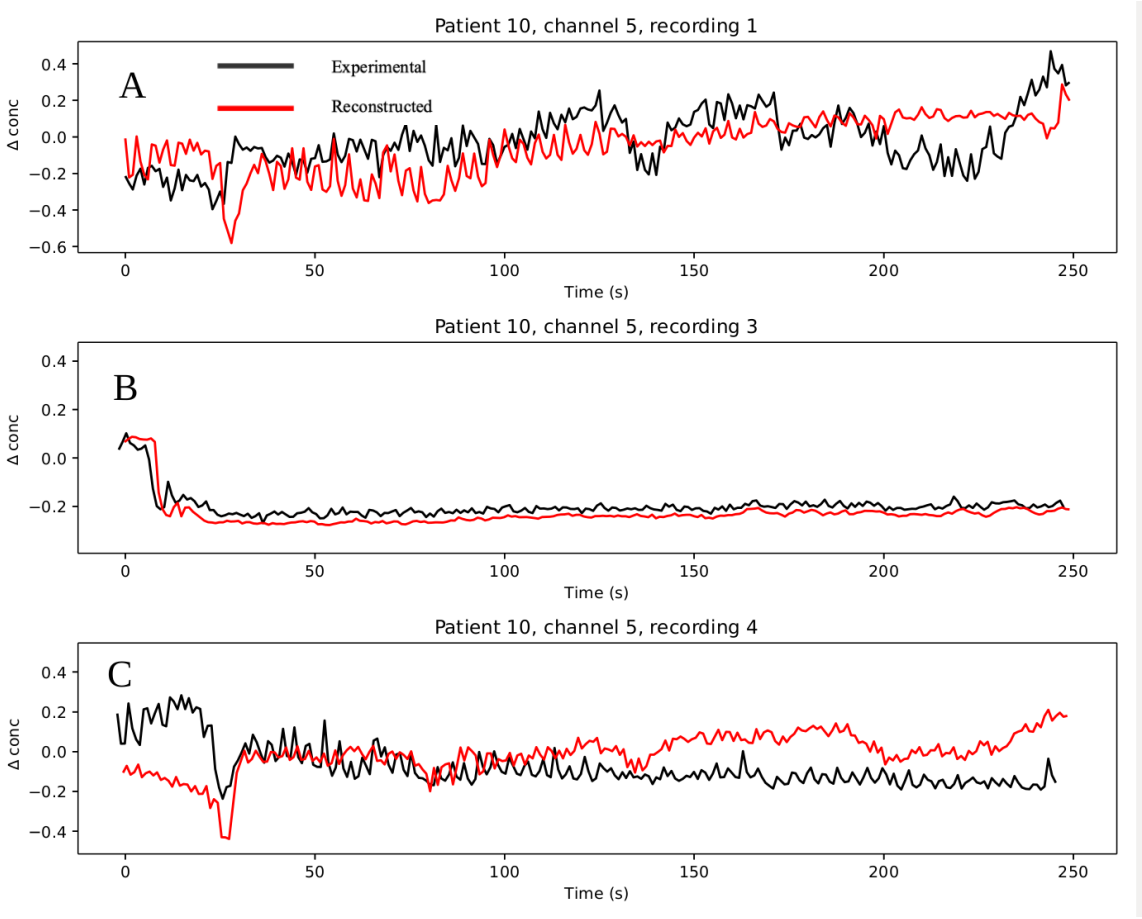

Figure 5.5: Intra-patient predictions of hemodynamic waveforms from cerebral electrical activity. A full spectrum resting state EEG single recording (patient 10 all channels) was used to train the model. After training, we saved the model weights and used as input a subsequent recording from the same patient. fNIRS reconstructions are shown here from 3 such recordings. Panels A, B, C show the respective reconstruction of channel 5 from recordings 1,3,4. Black and red curves correspond to experimental and reconstructed fNIRS waveforms respectively.

5.4.4.3 Spatial variability of reconstructions

We then explored the model's predictions sensitivity to channel location on the head. Figure 6 below depicts the network's spatial predictions. The topographic robustness of the model suggests the predictions are reasonably invariant across the brain. Channel locations were chosen if they: 1. offered coverage of most of the brain within the constraints of the source/detector montage and 2. had an acceptable level of signal fidelity as indicated in section 2.1.1. As an illustrative example, Figure 6 below shows the model's spatial predictions for patient 10.

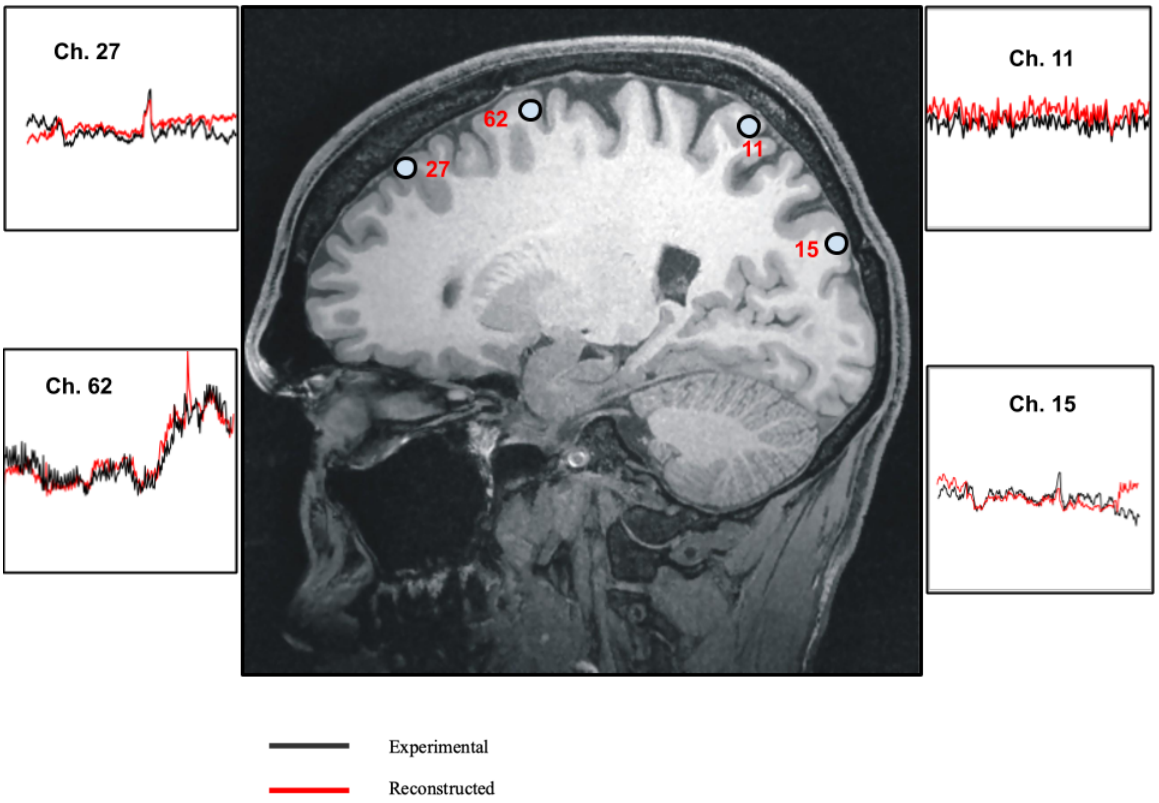

Figure 5.6: fNIRS spatial reconstructions, patient 10. To illustrate our network's fNIRS reconstructions spatially, signals from multiple EEG channels are used as input, for which the locations are shown on the brain (blue circles). Reconstruction error ranges from 6.41 x 10^{-1}(channel 11) to 7.83 x 10^{-3} (channel 62), with the mean RE being 6.52 x 10^{-2} for all reconstructions. Black and red curves correspond to experimental and reconstructed fNIRS waveforms respectively.

5.4.4.4 EEG frequency decomposition and resting state predictions

After model training and validation, we computed EEG frequency bands, namely: Delta [0.5–3 Hz], Theta [4–7 Hz], Alpha [8–13 Hz], Beta [14–30 Hz], and Gamma [30-100 Hz]. As mentioned earlier, these frequencies are present within the resting state of scalp EEG recordings [256]–[259] and are obtainable via Fourier decomposition. Spectral power of raw EEG signals was obtained using the Welch's power spectral density function. Restricting model input to these frequency ranges and using experimental resting state fNIRS signals (seizure and spike free intervals filtered in a "resting state band" ~ 0.01-0.1 Hz) (Tong et al., 2012) as the ground truth, the model was used for cerebral hemodynamic signal prediction provided a specific EEG frequency range. All computations (Fourier decomposition, Welch's power spectral density)

were performed using the MNE software package (Gramfort et al., 2014). Figure 7 below shows the model's predictions from EEG frequency ranges input using patient 10 (fNIRS channel 10).

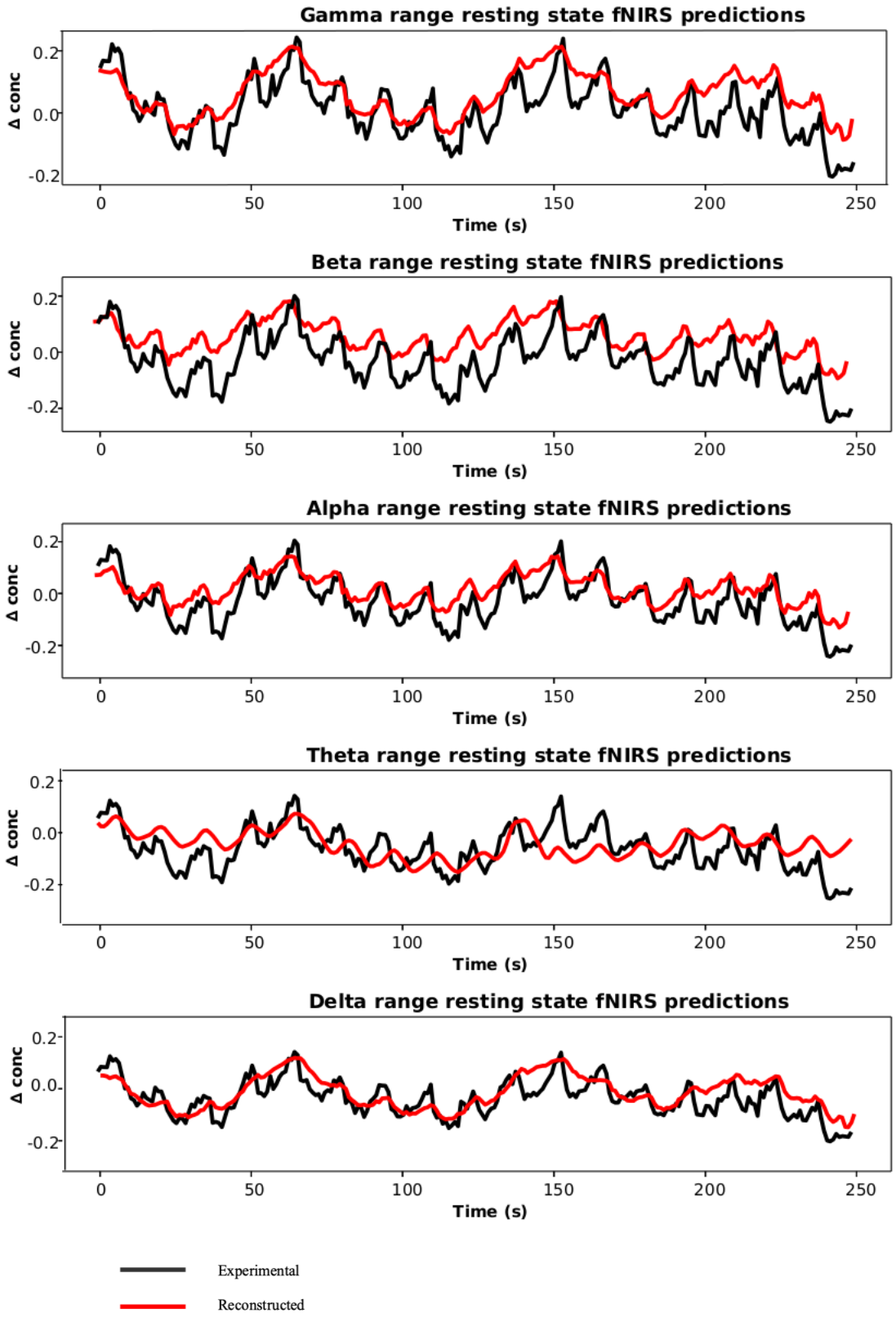

Figure 5.7: Resting state fNIRS oscillatory predictions given EEG frequency range input, patient 10, channel 10. We obtained predicted fNIRS reconstructions given filtered EEG input for the following frequency bands: Delta: 0-3 Hz; Theta: 4-7 Hz; Alpha: 8-13 Hz; Beta: 14-30 Hz; Gamma: 30-100 Hz. Black and red curves correspond to experimental and reconstructed fNIRS waveforms respectively. We used a constant experimental fNIRS waveform for comparison. The gamma range, which contains the greatest number of EEG frequencies reconstructs with more fidelity compared to ranges with less frequency components.

We calculated decoded fNIRS reconstruction error metrics, as shown in figure 8 below, for each EEG frequency range and calculated patient wise reconstruction error. The gamma and beta frequency bands demonstrated the lowest error rates and in the lower EEG frequency ranges, we noticed increased fNIRS reconstruction error, possibly owing to the fact that our model was possibly not able to learn appropriate features to reconstruct fNIRS signals.

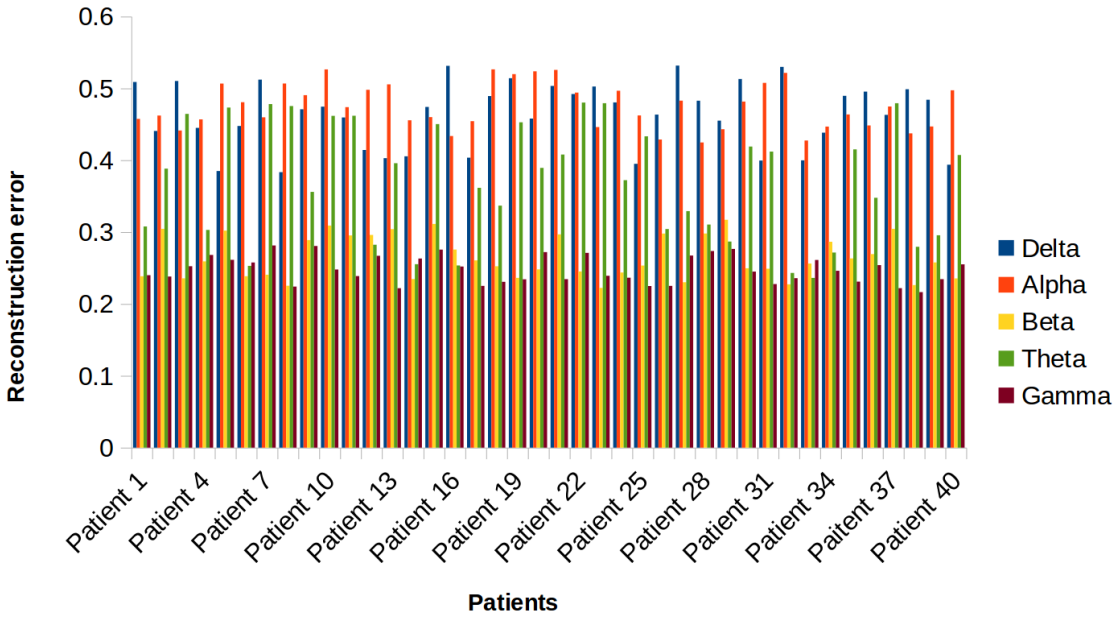

Figure 5.8: fNIRS reconstruction error given specific EEG frequency ranges for all patients, all channels. We obtained predicted reconstructions given filtered EEG input for the following frequency ranges: Delta: 0-3 Hz; Theta: 4-7 Hz; Alpha: 8-13 Hz; Beta: 14-30 Hz; Gamma: 30-100 Hz. The gamma range, which contains the greatest number of EEG frequencies, reconstructs with more fidelity and lowest reconstruction error metrics compared to ranges with less frequency components.

To further determine which EEG frequency band is able to reconstruct fNIRS waveforms with the lowest reconstruction error on average, we calculated band-wise reconstruction error for all patients, as shown in figure 9 below. Following, we conducted one-tailed paired t-tests to test whether there is a statistical difference in reconstruction error between any two of the five bands when compared to gamma in the following combinations: [delta, gamma], [theta, gamma], [alpha, gamma], and [beta, gamma]. Bonferroni correction was then applied to control the family-wise error rate to be less than 0.05. The gamma frequency band reconstructs fNIRS waveforms with increased fidelity on average as compared to other frequency bands.

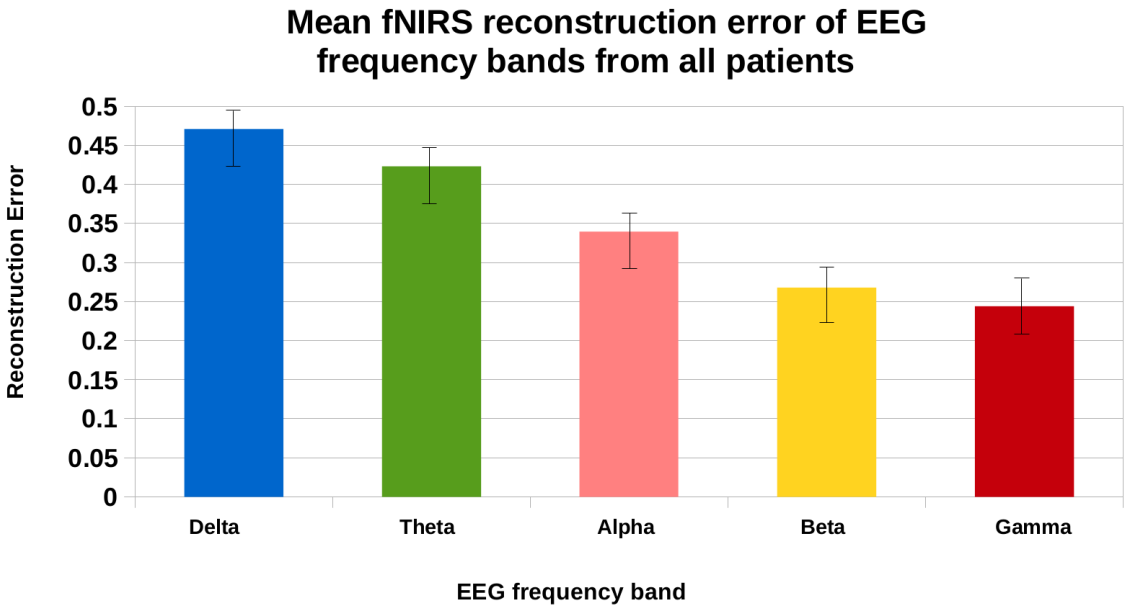

Figure 5.9: Mean fNIRS reconstruction error given specific EEG frequency ranges for all patients. The gamma range, which contains the greatest number of EEG frequencies, reconstructs with more fidelity and lowest reconstruction error metrics compared to other ranges with less frequency components.

5.4.4.5 Functional connectivity results

We computed functional connectivity mappings for experimental fNIRS and our model's fNIRS reconstructions. We compared experimental fNIRS and fNIRS reconstructions derived from both full spectrum EEG and the EEG gamma band for all patients. The root mean square error (standard deviation of the residuals) was used as an estimator of the error in our connectivity studies. In general, we noticed a lower error in functional connectivity analyses between experimental fNIRS and fNIRS reconstructions

derived from full spectrum EEG as compared with experimental fNIRS and fNIRS reconstructions derived from the gamma band. Our group results are shown in Figure 10 below.

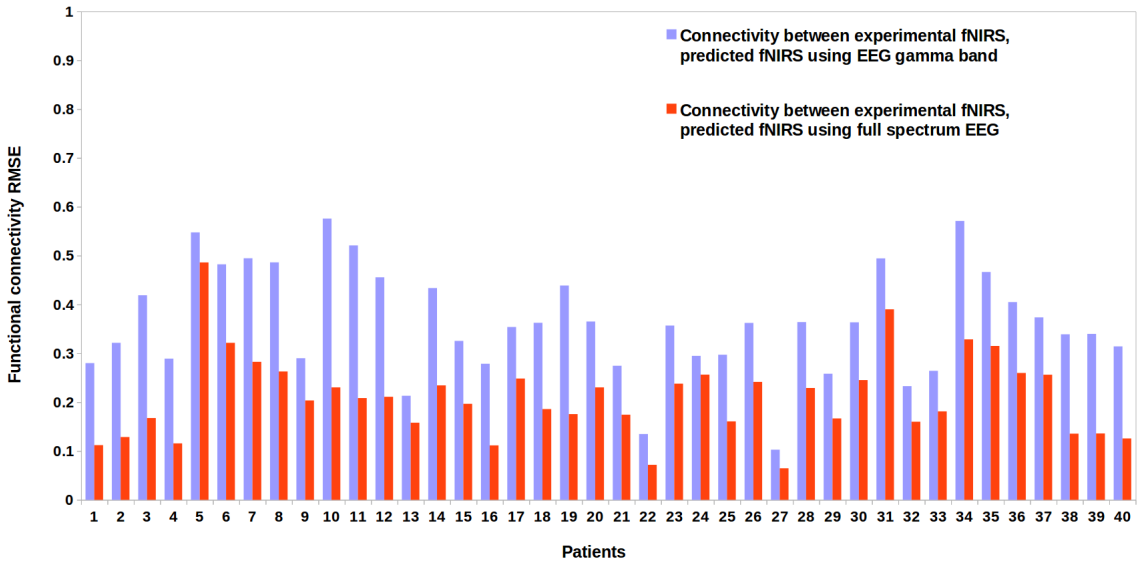

Figure 5.10: Functional connectivity results for all patients. Error for connectivity analyses between experimental fNIRS and predictions using full spectrum and gamma band EEG signal input. The connectivity derived from the full spectrum EEG time series consistently has lower error compared to the connectivity derived from the gamma band.

Figures 11,12 below show an example of the functional connectivity mapping results generated using the correlations of the timeseries from patient 22. The seed channel was chosen as channel 22. First, we used full spectrum EEG predictions as input for functional connectivity computations (Figure 11), followed by analysis using the EEG gamma frequency band as input (Figure 12).

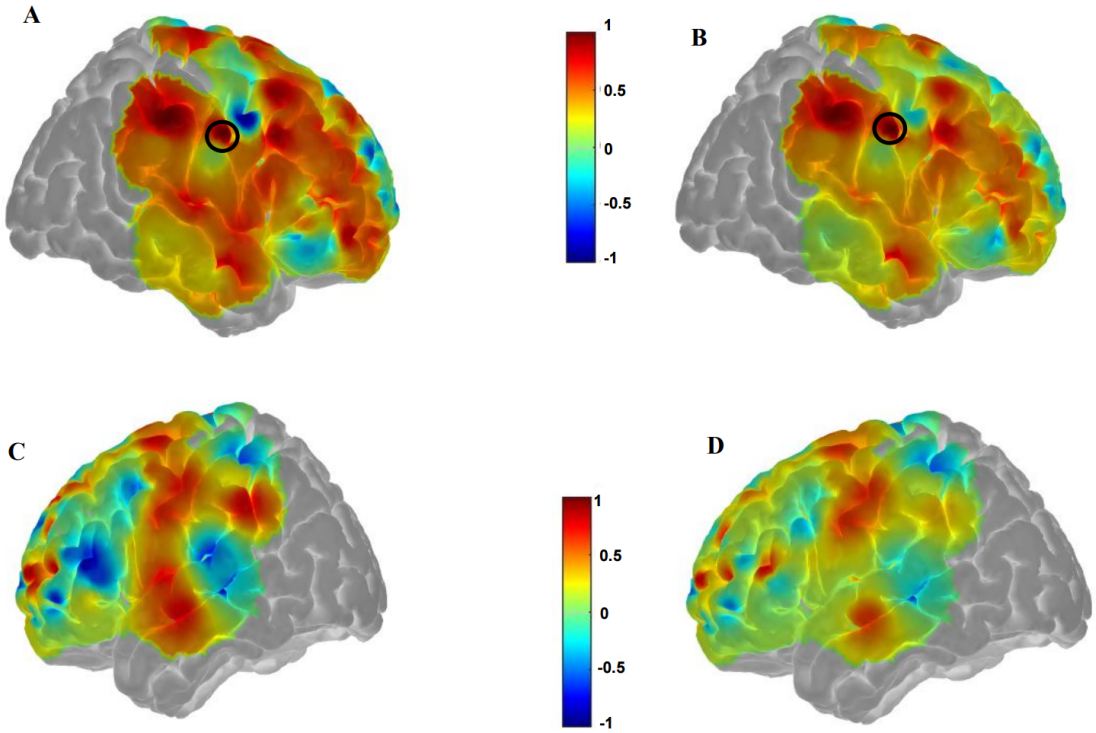

Figure 5.11*:* Functional connectivity results between experimental fNIRS and predicted resting state fNIRS using full spectrum EEG as input for patient 22. We employed seed based functional connectivity analysis to obtain a surface brain map that describes brain functional connectivity patterns. The seed region of interest (dark circle) is shown and full spectrum EEG was used as input into the model. Bilateral brain correlations using experimental fNIRS (A, C) and predicted resting state fNIRS (B, D) are shown. **A** and **B** display the right side of the brain, **C** and **D** display the left side of the brain. The connectivity profiles are seen to be similar between the maps generated using the experimental fNIRS results and the predictions of the model.

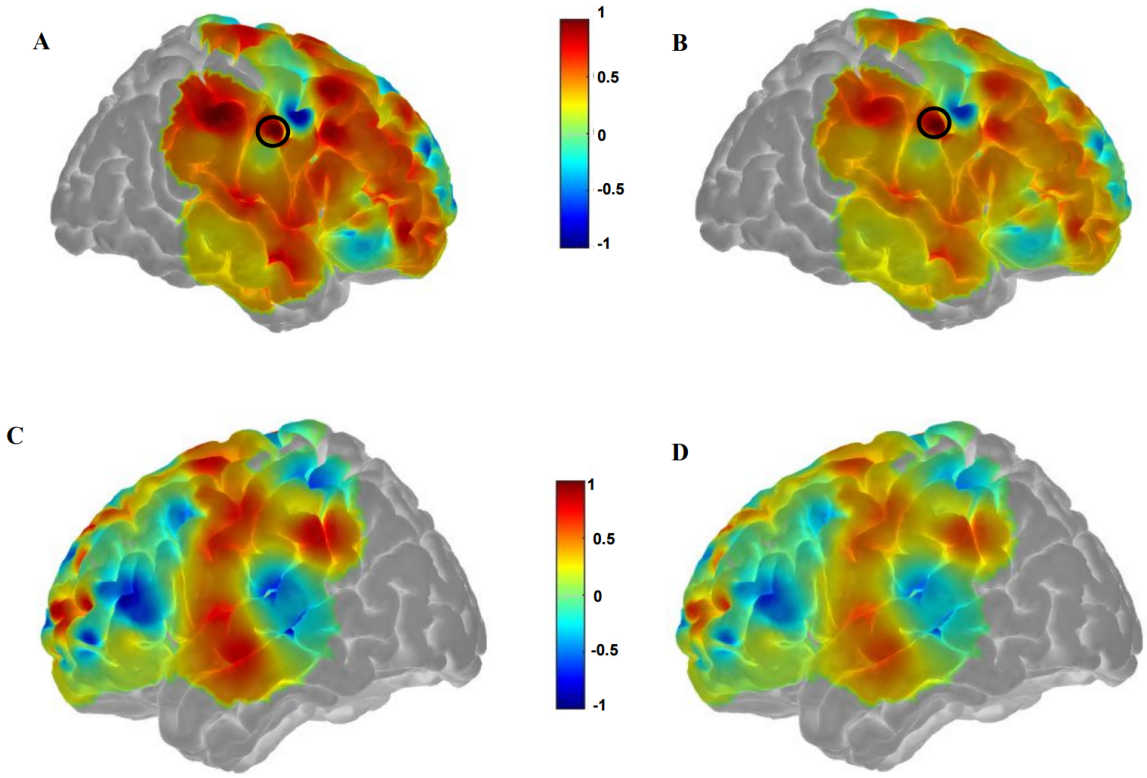

Figure 5.12: Functional connectivity results between experimental fNIRS and predicted fNIRS resting state using EEG gamma band as input for patient 22. Correlations from experimental fNIRS and predicted resting state fNIRS using EEG gamma band as input into our model are displayed. Bilateral brain correlations using experimental fNIRS (A, C) and predicted fNIRS (B, D) are shown.

5.5 Discussion

Deep learning models obviate cumbersome and brittle feature engineering processes replacing them with hierarchical feature learning. In this work, we developed a deep learning sequence-to-sequence autoencoder with long short-term units and convolutional modules to predict hemodynamic fNIRS waveforms from resting state EEG signals. Our model was trained using a 70/20/10 split for training, testing, and validation, respectively. As resting state EEG signals flow through the convolutional layers, the resulting vector is encoded and subsequently enters into LSTM layers.

Our results demonstrate that in the context of resting state recordings, fNIRS resting state intervals are able to be predicted using full spectrum as well as specific frequency range EEG signals to a certain extent. Our experimental findings can be related to known physiological phenomena being generated at the frequency of Mayer waves (~ 0.1 Hz), as these oscillations reflect fluctuation in cerebral arterial blood pressure. The presence of these oscillations persisting after data processing (filtering) can be partly due to

the fact that they share a common spectral range with typical hemodynamic responses including resting state fNIRS signals from the brain (Yücel et al., 2016). On the other hand, these oscillations might be of an extra neuronal origin corresponding to cerebral vasomotion—which as opposed to Mayer waves, is related to blood vessel tonal oscillation (Aalkjær et al., 2011; Julien, 2006; Quaresima & Ferrari, 2019; Sassaroli et al., 2012).

The exact mechanics of physiological signal presence within EEG waveforms has not been established with certainty. However, experimental results from this work suggest the following: our model is able to capture subtle hemodynamic dependencies within the EEG resting state signal and its fNIRS correlate via the neurovascular coupling phenomenon. These nuanced features are encoded and subsequently decoded by the architectural components of the model particularly the convolutional LSTM parameters (Greff et al., 2017; Sutskever et al., 2014b). The encoder and decoder components of the model and model parameters (e.g., the activation function utilized) may have enhanced feature extraction in resting state EEG data and its corresponding correlate in fNIRS waveforms. In addition, the features computed by using the outputs or hidden states of the recurrent units and the model may extract long-term dependencies (electrical and/or physiological) in resting state EEG sequence data from the LSTM modules via the gating mechanism (Sutskever et al., 2014a). Furthermore, when cerebral blood flow (CBF) varies, changes occur in both the metabolic and electrical activity of cortical neurons with corresponding EEG changes (Sassaroli et al., 2012).

Neuronal events responsible for evoking the fNIRS response can be divided into subthreshold synaptic and suprathreshold spiking activities (Curtin et al., 2019; Sharbrough et al., 1973). Furthermore, excitatory and inhibitory neurons, which are often located within close proximity in the brain are simultaneously active and may both contribute to the hemodynamic response (Franaszczuk et al., 2003). Slower EEG frequencies (primarily delta and theta) are generated by the thalamus and cortical cells in layers II-VI. Faster frequencies (gamma, typically 30-100 Hz) arise from cells in layers IV and V of the cortex (Foreman & Claassen, 2012; Merker, 2016). Changes in electrical potential as shown in EEG recordings are closely tied to cerebral blood flow (CBF) and when normal CBF declines to approximately 25– 35 ml/100 g/min, the EEG first loses faster frequencies, then as the CBF decreases to approximately 17– 18 ml/100 g/min, slower frequencies gradually increase. The interdependent relationship between CBF and cerebral electro-potential firing is theorized to be captured by the model used in this work. Exploring the spatial localization of low EEG frequency oscillations can help to determine if the presence of physiological signals is variable across patients and electrode (channel) sites, thereby possibly lending credence to the hypothesis that these oscillations are unlikely to be generated by one source.

We show spatial decoding is possible using our model. Examination of the LSTM memory units and the latent space architecture in autoencoders can demonstrate correlation between data that were previously unknown. A point for further investigation is to integrate an attention mechanism in our model. Since LSTM cells can lead to ambiguous memory activations, attention allows the model to encode input into a sequence of vectors and choose a subset of these vectors adaptively during decoding. Thus, the model no longer needs to utilize fixed length vectors which may lead to increased performance metrics at the cost of computational time. Attention implemented in our model would enable us to inspect the relationship between encoded and decoded sequences by model weight visualization.

In comparison with lower frequency range EEG signals, our work has established that higher frequency EEG signals (primarily the gamma and beta bands), reconstruct fNIRS waveforms with more fidelity as compared to lower frequency EEG signals. Results here corroborate that EEG gamma band based fNIRS reconstructions show a closer fit between the observed and predicted hemodynamic responses as opposed to other EEG frequency ranges (Ebisch et al., 2005). This is possibly due to the fact that higher frequencies engage an increased number of neurons, but it is less apparent if this is due to baseline network activity or part of a pivotal functional role. Gamma rhythms in the brain provide an indication of engaged networks and have been observed in a number of cortical and subcortical structures. These rhythms are typically stronger for some stimuli as compared to others, thereby displaying selectivity to that of nearby neuronal activity (Jia & Kohn, 2011; Whittingstall & Logothetis, 2009). However, to fully interpret the impact of this activity warrants an investigation of the cellular mechanisms responsible for their generation. GABA-ergic inhibitory interneuron activity is considered to be crucial to generate EEG gamma frequency activity and this may be increased via interactions with excitatory neurons (Jia & Kohn, 2011; Park et al., 2011; Ray & Maunsell, 2010).

In the second part of our work, we explored functional connectivity in the resting state. fMRI resting state data has shown distant correlations at low frequency organized as connected networks, and we hypothesized that our model's predictions would be able to reveal similar functional connections as compared with experimental fNIRS. On a group level, predicted fNIRS from full spectrum EEG had higher connectivity as compared to predictions derived from the EEG gamma band. Experimental resting state fNIRS data and predicted fNIRS data was correlated to reveal similarly near the set seed but metrics decreased generally as distance increased from the seed. This can be due to numerous factors: 1. noise causing a decrease in reconstruction quality, 2. a decrease in gamma activations at the region of interest, and 3. model parameters unable to completely learn the nuances present within the signal. Furthermore, systemic artifacts from the scalp and skull behave as dominant noise sources in resting state fNIRS signals, leading to inaccurate reconstruction. Utilizing an EEG-fNIRS experimental setup with short separation

channels, measuring approximately 1-2 centimeters in spatial separation between source and detector (Gagnon et al., 2012; Kohno et al., 2007), could lead to sufficient noise reduction and improved signal sensitivity. We hypothesize that reconstruction metrics as well as corresponding functional connectivity network measures stabilize with increased signal quality and increased resting state duration, thereby decreasing the disparities present between experimental and predicted time series. Our model reconstructed fNIRS signals for certain patients with decreased error across frequency ranges.

5.6 Conclusion

We designed and implemented a deep learning model to predict resting state hemodynamics given specific electro-potential frequencies using resting state scalp EEG signals from a cohort of epileptic patients. We performed a thorough analysis of each EEG frequency range and its complementary fNIRS prediction; further we analyzed functional connectivity between brain regions using frequency range predictions. Our model was specifically designed to predict fNIRS waveforms from full spectrum and frequency specific EEG input. The gamma and beta EEG frequency bands provided hemodynamic predictions of fNIRS resting state with the highest metrics.

Disclosures

The authors have no relevant financial interests in this article and no potential conflicts of interest to disclose.

Acknowledgments

This project was generously supported by The Natural Sciences and Engineering Research Council of Canada grant 239876-2011 and Canadian Institutes of Health Research grant 387183.

5.7 References

1. Aalkjær, C., Boedtkjer, D., & Matchkov, V. (2011). Vasomotion – what is currently thought? In Acta Physiologica. https://doi.org/10.1111/j.1748-1716.2011.02320.x

2. Aasted, C. M., Yücel, M. A., Cooper, R. J., Dubb, J., Tsuzuki, D., Becerra, L., Petkov, M. P., Borsook, D., Dan, I., & Boas, D. A. (2015). Anatomical guidance for functional near-infrared spectroscopy: AtlasViewer tutorial. Neurophotonics. https://doi.org/10.1117/1.nph.2.2.020801

3. Baytas, I. M., Xiao, C., Zhang, X., Wang, F., Jain, A. K., & Zhou, J. (2017). Patient subtyping via time-aware LSTM networks. Proceedings of the ACM SIGKDD International Conference on Knowledge Discovery and Data Mining. https://doi.org/10.1145/3097983.3097997

4. Biswal, B., Zerrin Yetkin, F., Haughton, V. M., & Hyde, J. S. (1995). Functional connectivity in the motor cortex of resting human brain using echo-planar mri. Magnetic Resonance in Medicine, 34(4), 537–541. https://doi.org/10.1002/mrm.1910340409

5. Brilla, R. (2019). Electroencephalography (EEG). In Pain (pp. 201–203). Springer.

6. Chiarelli, A. M., Zappasodi, F., Di Pompeo, F., & Merla, A. (2017). Simultaneous functional near-infrared spectroscopy and electroencephalography for monitoring of human brain activity and oxygenation: a review. Neurophotonics. https://doi.org/10.1117/1.nph.4.4.041411

7. Cho, K., Van Merriënboer, B., Gulcehre, C., Bahdanau, D., Bougares, F., Schwenk, H., & Bengio, Y. (2014). Learning phrase representations using RNN encoder-decoder for statistical machine translation. EMNLP 2014 - 2014 Conference on Empirical Methods in Natural Language Processing, Proceedings of the Conference. https://doi.org/10.3115/v1/d14-1179

8. Chung, Y. A., Wu, C. C., Shen, C. H., Lee, H. Y., & Lee, L. S. (2016). Audio Word2Vec: Unsupervised learning of audio segment representations using sequence-to-sequence autoencoder. Proceedings of the Annual Conference of the International Speech Communication Association, INTERSPEECH. https://doi.org/10.21437/Interspeech.2016-82

9. Curtin, A., Tong, S., Sun, J., Wang, J., Onaral, B., & Ayaz, H. (2019). A systematic review of integrated functional near-infrared spectroscopy (fNIRS) and transcranial magnetic stimulation (TMS) studies. In Frontiers in Neuroscience. https://doi.org/10.3389/fnins.2019.00084

10. Czisch, M., Wehrle, R., Kaufmann, C., Wetter, T. C., Holsboer, F., Pollmächer, T., & Auer, D. P. (2004). Functional MRI during sleep: BOLD signal decreases and their electrophysiological correlates. European Journal of Neuroscience. https://doi.org/10.1111/j.1460-9568.2004.03518.x

11. Dressler, O., Schneider, G., Stockmanns, G., & Kochs, E. F. (2004). Awareness and the EEG power spectrum: Analysis of frequencies. British Journal of Anaesthesia. https://doi.org/10.1093/bja/aeh270

12. Ebisch, B., Schmidt, K. E., Niessing, M., Singer, W., Galuske, R. A. W., & Niessing, J. (2005). Hemodynamic Signals Correlate Tightly with Synchronized Gamma Oscillations. Science.

13. F., P., et al. (2015). Detectability of fast ripples on the scalp EEG: A preliminary study with subdermal electrodes. Epilepsy Currents.

14. Foreman, B., & Claassen, J. (2012). Quantitative EEG for the detection of brain ischemia. In Critical Care. https://doi.org/10.1186/cc11230

15. Fox, M. D., & Greicius, M. (2010). Clinical applications of resting state functional connectivity. In Frontiers in Systems Neuroscience. https://doi.org/10.3389/fnsys.2010.00019

16. Franaszczuk, P. J., Kudela, P., & Bergey, G. K. (2003). External excitatory stimuli can terminate bursting in neural network models. Epilepsy Research, 53(1–2), 65–80. https://doi.org/10.1016/S0920-1211(02)00248-6

17. Freeman, W. J., Burke, B. C., & Holmes, M. D. (2003). Aperiodic phase re-setting in scalp EEG of beta-gamma oscillations by state transitions at alpha-theta rates. Human Brain Mapping. https://doi.org/10.1002/hbm.10120

18. Gagnon, L., Cooper, R. J., Yücel, M. A., Perdue, K. L., Greve, D. N., & Boas, D. A. (2012). Short separation channel location impacts the performance of short channel regression in NIRS. NeuroImage. https://doi.org/10.1016/j.neuroimage.2011.08.095

19. Goldman, R. I., Stern, J. M., Engel Jr, J., & Cohen, M. S. (2002). Simultaneous EEG and fMRI of the alpha rhythm. Neuroreport, 13(18), 2487.

20. Goodfellow, I., Bengio, Y., & Courville, A. (2016). Deep learning. MIT press.

21. Gramfort, A., Luessi, M., Larson, E., Engemann, D. A., Strohmeier, D., Brodbeck, C., Parkkonen, L., & Hämäläinen, M. S. (2014). MNE software for processing MEG and EEG data. NeuroImage. https://doi.org/10.1016/j.neuroimage.2013.10.027

22. Greff, K., Srivastava, R. K., Koutnik, J., Steunebrink, B. R., & Schmidhuber, J. (2017). LSTM: A Search Space Odyssey. IEEE Transactions on Neural Networks and Learning Systems. https://doi.org/10.1109/TNNLS.2016.2582924

23. Gregor, K., Danihelka, I., Graves, A., Rezende, D. J., & Wierstra, D. (2015). DRAW: A recurrent neural network for image generation. 32nd International Conference on Machine Learning, ICML 2015.

24. Greicius, M. D., Krasnow, B., Reiss, A. L., & Menon, V. (2003). Functional connectivity in the resting brain: A network analysis of the default mode hypothesis. Proceedings of the National Academy of Sciences of the United States of America. https://doi.org/10.1073/pnas.0135058100

25. Gross, D. W., & Gotman, J. (1999). Correlation of high-frequency oscillations with the sleep-wake cycle and cognitive activity in humans. Neuroscience. https://doi.org/10.1016/S0306-4522(99)00343-7

26. Jia, X., & Kohn, A. (2011). Gamma rhythms in the brain. PLoS Biology, 9(4), 2–5. https://doi.org/10.1371/journal.pbio.1001045

27. Julien, C. (2006). The enigma of Mayer waves: Facts and models. In Cardiovascular Research. https://doi.org/10.1016/j.cardiores.2005.11.008

28. Kocsis, L., Herman, P., & Eke, A. (2006). The modified Beer-Lambert law revisited. Physics in Medicine and Biology, 51(5). https://doi.org/10.1088/0031-9155/51/5/N02

29. Kohno, S., Miyai, I., Seiyama, A., Oda, I., Ishikawa, A., Tsuneishi, S., Amita, T., & Shimizu, K. (2007). Removal of the skin blood flow artifact in functional near-infrared spectroscopic imaging data through independent component analysis. Journal of Biomedical Optics. https://doi.org/10.1117/1.2814249

30. Laufs, H., Krakow, K., Sterzer, P., Eger, E., Beyerle, A., Salek-Haddadi, A., & Kleinschmidt, A. (2003). Electroencephalographic signatures of attentional and cognitive default modes in spontaneous brain activity fluctuations at rest. Proceedings of the National Academy of Sciences of the United States of America. https://doi.org/10.1073/pnas.1831638100

31. Lecun, Y., Bengio, Y., & Hinton, G. (2015). Deep learning. In Nature. https://doi.org/10.1038/nature14539

32. Lemieux, L., Krakow, K., & Fish, D. R. (2001). Comparison of spike-triggered functional MRI BOLD activation and EEG dipole model localization. NeuroImage. https://doi.org/10.1006/nimg.2001.0896

33. Lindauer, U., Dirnagl, U., Füchtemeier, M., Böttiger, C., Offenhauser, N., Leithner, C., & Royl, G. (2010). Pathophysiological interference with neurovascular coupling–when imaging based on hemoglobin might go blind. Frontiers in Neuroenergetics, 2, 25.

34. Lipton, Z. C., Kale, D. C., Elkan, C., & Wetzel, R. (2016). Learning to diagnose with LSTM recurrent neural networks. 4th International Conference on Learning Representations, ICLR 2016 - Conference Track Proceedings.

35. Logothetis, N. K., Pauls, J., Augath, M., Trinath, T., & Oeltermann, A. (2001). Neurophysiological investigation of the basis of the fMRI signal. Nature. https://doi.org/10.1038/35084005

36. Lövblad, K. O., Thomas, R., Jakob, P. M., Scammell, T., Bassetti, C., Griswold, M., Ives, J., Matheson, J., Edelman, R. R., & Warach, S. (1999). Silent functional magnetic resonance imaging demonstrates focal activation in rapid eye movement sleep. Neurology.

https://doi.org/10.1212/wnl.53.9.2193

37. Lu, C. M., Zhang, Y. J., Biswal, B. B., Zang, Y. F., Peng, D. L., & Zhu, C. Z. (2010). Use of fNIRS to assess resting state functional connectivity. Journal of Neuroscience Methods. https://doi.org/10.1016/j.jneumeth.2009.11.010

38. Luong, M. T., Le, Q. V., Sutskever, I., Vinyals, O., & Kaiser, L. (2016). Multi-task sequence to sequence learning. 4th International Conference on Learning Representations, ICLR 2016 - Conference Track Proceedings.

39. Mantini, D., Perrucci, M. G., Del Gratta, C., Romani, G. L., & Corbetta, M. (2007). Electrophysiological signatures of resting state networks in the human brain. Proceedings of the National Academy of Sciences of the United States of America. https://doi.org/10.1073/pnas.0700668104

40. Martinez-Montes, E., Valdes-Sosa, P. A., Miwakeichi, F., Goldman, R. I., & Cohen, M. S. (2004). Concurrent EEG/fMRI analysis by multiway Partial Least Squares. NeuroImage, 22(3), 1023–1034. https://doi.org/10.1016/j.neuroimage.2004.03.038

41. Merity, S., Keskar, N. S., & Socher, R. (2018). Regularizing and optimizing LSTM language models. 6th International Conference on Learning Representations, ICLR 2018 - Conference Track Proceedings.

42. Merker, B. H. (2016). Cortical gamma oscillations: Details of their genesis preclude a role in cognition. Frontiers in Computational Neuroscience. https://doi.org/10.3389/fncom.2016.00078

43. Mikolov, T., Karafiát, M., Burget, L., Jan, C., & Khudanpur, S. (2010). Recurrent neural network based language model. Proceedings of the 11th Annual Conference of the International Speech Communication Association, INTERSPEECH 2010.

44. Mukamel, R., Gelbard, H., Arieli, A., Hasson, U., Fried, I., & Malach, R. (2005). Neuroscience: Coupling between neuronal firing, field potentials, and fMRI in human auditory cortex. Science. https://doi.org/10.1126/science.1110913

45. Ogawa, S., Tank, D. W., Menon, R., Ellermann, J. M., Kim, S. G., Merkle, H., & Ugurbil, K. (1992). Intrinsic signal changes accompanying sensory stimulation: Functional brain mapping with magnetic resonance imaging. Proceedings of the National Academy of Sciences of the United States of America. https://doi.org/10.1073/pnas.89.13.5951

46. Park, Y., Luo, L., Parhi, K. K., & Netoff, T. (2011). Seizure prediction with spectral power of EEG

using cost-sensitive support vector machines. Epilepsia, 52(10), 1761–1770. https://doi.org/10.1111/j.1528-1167.2011.03138.x

47. Pedregosa, F., Varoquaux, G., Gramfort, A., Michel, V., Thirion, B., Grisel, O., Blondel, M., Prettenhofer, P., Weiss, R., Dubourg, V., Vanderplas, J., Passos, A., Cournapeau, D., Brucher, M., Perrot, M., & Duchesnay, É. (2011). Scikit-learn: Machine learning in Python. Journal of Machine Learning Research.

48. Peng, K., Nguyen, D. K., Tayah, T., Vannasing, P., Tremblay, J., Sawan, M., Lassonde, M., Lesage, F., & Pouliot, P. (2014). FNIRS-EEG study of focal interictal epileptiform discharges. Epilepsy Research. https://doi.org/10.1016/j.eplepsyres.2013.12.011

49. Quaresima, V., & Ferrari, M. (2019). A mini-review on functional near-infrared spectroscopy (fNIRS): Where do we stand, and where should we go? Photonics, 6(3), 87. https://doi.org/10.3390/photonics6030087

50. Ray, S., & Maunsell, J. H. R. (2010). Differences in Gamma Frequencies across Visual Cortex Restrict Their Possible Use in Computation. Neuron, 67(5), 885–896. https://doi.org/10.1016/j.neuron.2010.08.004

51. Salek-Haddadi, A., Friston, K. J., Lemieux, L., & Fish, D. R. (2003). Studying spontaneous EEG activity with fMRI. In Brain Research Reviews. https://doi.org/10.1016/S0165-0173(03)00193-0

52. Sassaroli, A., Pierro, M., Bergethon, P. R., & Fantini, S. (2012). Low-frequency spontaneous oscillations of cerebral hemodynamics investigated with near-infrared spectroscopy: A review. In IEEE Journal on Selected Topics in Quantum Electronics. https://doi.org/10.1109/JSTQE.2012.2183581

53. Sharbrough, F. W., Messick, J. M., & Sundt, T. M. (1973). Correlation of continuous electroencephalograms with cerebral blood flow measurements during carotid endarterectomy. Stroke. https://doi.org/10.1161/01.STR.4.4.674

54. Shulman, R. G., Rothman, D. L., Behar, K. L., & Hyder, F. (2004). Energetic basis of brain activity: Implications for neuroimaging. In Trends in Neurosciences. https://doi.org/10.1016/j.tins.2004.06.005

55. Singh, K. D. (2012). Which “neural activity” do you mean? fMRI, MEG, oscillations and neurotransmitters. In NeuroImage. https://doi.org/10.1016/j.neuroimage.2012.01.028

56. Sirpal, P., Kassab, A., Pouliot, P., & Nguyen, D. K. (2019). fNIRS improves seizure detection in

multimodal EEG-fNIRS recordings. Journal of Biomedical Optics, 24(05), 1. https://doi.org/10.1117/1.jbo.24.5.051408

57. Sitnikova, E., Hramov, A. E., Grubov, V., & Koronovsky, A. A. (2016). Rhythmic activity in EEG and sleep in rats with absence epilepsy. Brain Research Bulletin. https://doi.org/10.1016/j.brainresbull.2015.11.012

58. Socher, R., Pennington, J., Huang, E. H., Ng, A. Y., & Manning, C. D. (2011). Semi-supervised recursive autoencoders for predicting sentiment distributions. EMNLP 2011 - Conference on Empirical Methods in Natural Language Processing, Proceedings of the Conference.

59. Srivastava, N., Mansimov, E., & Salakhutdinov, R. (2015). Unsupervised learning of video representations using LSTMs. 32nd International Conference on Machine Learning, ICML 2015.

60. Steinbrink, J., Villringer, A., Kempf, F., Haux, D., Boden, S., & Obrig, H. (2006). Illuminating the BOLD signal: combined fMRI-fNIRS studies. In Magnetic Resonance Imaging. https://doi.org/10.1016/j.mri.2005.12.034

61. Steriade, M. (2001). Impact of network activities on neuronal properties in corticothalamic systems. Journal of Neurophysiology, 86(1), 1–39. https://doi.org/10.1152/jn.2001.86.1.1

62. Sutskever, I., Vinyals, O., & Le, Q. V. (2014a). Sequence to sequence learning with neural networks. Advances in Neural Information Processing Systems, 4(January), 3104–3112.

63. Sutskever, I., Vinyals, O., & Le, Q. V. (2014b). Sequence to sequence learning with neural networks. Advances in Neural Information Processing Systems.

64. Tong, Y., Hocke, L. M., Licata, S. C., & deB. Frederick, B. (2012). Low-frequency oscillations measured in the periphery with near-infrared spectroscopy are strongly correlated with blood oxygen level-dependent functional magnetic resonance imaging signals. Journal of Biomedical Optics, 17(10), 1060041. https://doi.org/10.1117/1.jbo.17.10.106004

65. Tracy, J. I., & Doucet, G. E. (2015). Resting-state functional connectivity in epilepsy: Growing relevance for clinical decision making. In Current Opinion in Neurology. https://doi.org/10.1097/WCO.0000000000000178

66. Truong, N. D., Kuhlmann, L., Bonyadi, M. R., & Kavehei, O. (2018). Semi-supervised Seizure Prediction with Generative Adversarial Networks. 1–6. http://arxiv.org/abs/1806.08235

67. Tyvaert, L., LeVan, P., Grova, C., Dubeau, F., & Gotman, J. (2008). Effects of fluctuating

physiological rhythms during prolonged EEG-fMRI studies. Clinical Neurophysiology. https://doi.org/10.1016/j.clinph.2008.07.284

68. Varela, F., Lachaux, J.-P., Rodriguez, E., & Martinerie, J. (2001). The brainweb: Phase synchronization and large-scale integration. Nature Reviews Neuroscience, 2(4), 229–239. https://doi.org/10.1038/35067550

69. Vincent, P., Larochelle, H., Bengio, Y., & Manzagol, P. A. (2008). Extracting and composing robust features with denoising autoencoders. Proceedings of the 25th International Conference on Machine Learning. https://doi.org/10.1145/1390156.1390294

70. Vincent, P., Larochelle, H., Lajoie, I., Bengio, Y., & Manzagol, P. A. (2010). Stacked denoising autoencoders: Learning Useful Representations in a Deep Network with a Local Denoising Criterion. Journal of Machine Learning Research.

71. Wang, Y., Huang, M., Zhao, L., & Zhu, X. (2016). Attention-based LSTM for aspect-level sentiment classification. EMNLP 2016 - Conference on Empirical Methods in Natural Language Processing, Proceedings. https://doi.org/10.18653/v1/d16-1058

72. Whittingstall, K., & Logothetis, N. K. (2009). Frequency-Band Coupling in Surface EEG Reflects Spiking Activity in Monkey Visual Cortex. Neuron. https://doi.org/10.1016/j.neuron.2009.08.016

73. Worrell, G. A., Parish, L., Cranstoun, S. D., Jonas, R., Baltuch, G., & Litt, B. (2004). High-frequency oscillations and seizure generation in neocortical epilepsy. Brain. https://doi.org/10.1093/brain/awh149

74. Yücel, M. A., Selb, J., Aasted, C. M., Lin, P.-Y., Borsook, D., Becerra, L., & Boas, D. A. (2016). Mayer waves reduce the accuracy of estimated hemodynamic response functions in functional near-infrared spectroscopy. Biomedical Optics Express. https://doi.org/10.1364/boe.7.003078

75. Zhang, W. (2018). Generative Adversarial Nets for Information Retrieval. The 41st International ACM SIGIR Conference on Research & Development in Information Retrieval - SIGIR '18, 1375–1378. https://doi.org/10.1145/3209978.3210184

76. Zhao, F., Feng, J., Zhao, J., Yang, W., & Yan, S. (2018). Robust LSTM-Autoencoders for Face De-Occlusion in the Wild. IEEE Transactions on Image Processing. https://doi.org/10.1109/TIP.2017.2771408

CHAPTER 6 GENERAL DISCUSSION

This thesis explored EEG-fNIRS brain signals using a multichannel EEG-fNIRS multimodal system in the context of epileptic recordings in critically ill intensive care unit patients. Two scientific papers were presented in Chapters 4 and 5, focusing on seizure detection using fNIRS signals and the prediction of fNIRS signals given specific EEG input, respectively. This chapter reviews the objectives that were proposed in Chapter 1, validates the corresponding hypotheses, and discusses the limitations of the proposed techniques.

6.1 Objective 1

The first objective of this thesis addresses the hypothesis that fNIRS offers improved metrics in a seizure detection task. The long short-term memory deep learning model developed for achieving this objective proved that utilizing fNIRS along with EEG offers increased sensitivity and specificity of seizure detection. The results presented in Chapter 4 show that the mean precision of seizure detection using EEG alone compared to multimodal (EEG-fNIRS) data was 82.8 and 87.3, respectively. Thus, incorporating fNIRS recordings in seizure monitoring might be able to improve patient-specific seizure detection. These metrics can be increased further if the seizure onset zone is taken into account.

The delineation of the seizure onset zone (SOZ) via presurgical evaluation of brain neural activity is commonly carried out in epilepsy patients. The interpretation of seizure on EEG recordings albeit by technical experts is difficult because of the highly stochastic behavior of epilepsy. In this work, seizure events labeled in the ground truth by domain experts and the corroboration of epileptic foci on the brain MRI allowed for the spatial localization of the SOZ. However, the developed algorithm has the potential to accurately localize the SOZ by using the high dimensional information available in the data set such as the temporal and spatial information (channel wise) of neural activity extracted from EEG as well as hemodynamic activity from fNIRS recordings. Model adaptation by signal encoding requiring additional signal processing steps particularly: inverse problem solution, and the estimation of the EEG and fNIRS time courses extracted from spatial regions of interest. Contextually, the inverse problem involves inferring the anatomical brain localization of a seizure from multimodal recordings and subsequently correlating

seizure origin and seizure semiology. Following encoding of temporal and spatial dynamics of the seizure-related neural network, a measure can be used quantify the accuracy of SOZ localization. The results obtained from this adapted model can be validated by the SOZ on the MRI.

The LSTM model presented in Objective 1 was designed to avoid the common limitations of vanilla recurrent neural networks, such as the so called “vanishing gradient problem” and the so called “exploding gradient problem”. Briefly, the vanishing gradient problem considers the activation of one neuron as input to subsequent neurons, thereby behaving as repetitive input. Thus, there are neurons with similar (or same) weights, but different inputs linked via activations. The LSTM network developed here was trained in a supervised fashion to compute the gradients needed during the optimization process consequently updating each proportionally to the derivative of the error with respect to corresponding weight. Although the model presented for seizure detection avoids such problems, training the model by neuroevolution can be advantageous [260] or via policy gradient methods [261], particularly in an unsupervised situation when there is no "teacher" (i.e., training labels).

6.1.1 Clinical application

The current clinical state for seizure detection is exclusively dependent on the use of the scalp EEG. While the fNIRS method is by no means a replacement for current standard of clinical care, it can serve as an important complement to typical neuromonitoring using scalp EEG methods for the management of epilepsy. The results from Objective 1 suggest that fNIRS signals add value in a seizure detection task when combined with conventional scalp EEG recordings. We note that by using EEG-fNIRS multimodal signals, the developed LSTM algorithm can be extended to a range of epilepsy types including absence seizures and asymptomatic seizures (“silent seizures”). Furthermore, given the fact that fNIRS sequences usually are shifted by a few seconds as compared to EEG signals, the developed model is robust enough to have a varying baseline difference and ensure seizure detection.

6.2 Objective 2

The second objective of this thesis addresses the hypothesis that fNIRS resting state periods obtained from epileptic recordings can be predicted from resting state EEG recordings. This hypothesis takes into consideration the neurovascular coupling phenomenon (Section 1.3) as a

contributing factor for this predictive ability. The article presented in Chapter 5 proposes a sequence-sequence autoencoder model that considers spatial and temporal properties of EEG and fNIRS sequences via convolutional neural networks and long short-term memory units respectively. Although, the predictions of the hemodynamic response (fNIRS) from cerebral-electro-potential sequences (EEG) are patient-specific, intra-patient recordings demonstrate similar predictive ability as compared to other patients. Furthermore, consistent low reconstruction error among intra patient recordings lends credence to model parameterization as the model's training and validation was noted to decrease steadily with minimal gap between loss values. We confirmed that our model is spatially sensitive in its reconstruction ability as channel locations with acceptable SNR have lower reconstruction error.

The resting state fNIRS predictions derived from specific EEG frequency bands suggested that the higher frequency bands, particularly gamma have increased predictive ability as compared to lower frequency ranges. This finding suggests that higher frequency bands, particularly the gamma band, offer more predictive capacity for cerebral hemodynamics possibly due to the fact that neuronal firing during gamma oscillations and high cellular oxygen consumption have strong correlation [262]. This observation helps to substantiate the hypothesis that predictive capacity is improved with bands with higher frequency and cerebral hemodynamics in the resting state [52], [65], [263]. Furthermore, in this work, fNIRS signals were reconstructed with purely data-driven methods. Utilizing nonlinear methods to examine EEG signal characteristics includes adopting useful nonlinear parameters such as the approximate entropy and sample entropy [264] since nonlinear features are able to provide information regarding complex physiological phenomena such as abrupt transitions and chaotic behavior within EEG signals. Thereby allowing a correlation computation between nonlinear resting state EEG dynamic complexity with neuronal activity obtained by fNIRS.

An explicit goal of the functional connectivity studies was determining correlation between neuronal activity obtained by EEG rhythms and hemodynamic activity obtained by fNIRS. We examined the relationships between EEG patterns and brain activation obtained by reconstructions from our sequence-to-sequence autoencoder model during the resting state condition in 40 epileptic patients. The results demonstrated a substantial correlation between experimental resting state EEG (full spectrum and gamma band) and reconstructed resting state fNIRS signals. In our analyses, connectivity results are dependent on seed location, the region of interest and model output. We

controlled for seed location and corresponding region of interest and in general, we found that lower EEG frequencies had no reliable effect on fNIRS signal reconstruction and therefore connectivity. However, incrementally increasing the range of the EEG bands by possibly processing the EEG signal to include combination of multiple bands (i.e., [delta, theta], [alpha, beta], etc..) could offer insight into the EEG dynamic complexity and its corresponding fNIRS (hemodynamic) correlate as well as the corresponding functional connectivity. Our results indicate that features of EEG frequency bands are strongly associated with fluctuations of the hemodynamic signal during the resting state condition. Results from functional connectivity analyses performed in the context of Hypothesis 2.3, suggested that while full spectrum EEG when input into our model offered the most functional connections, the gamma band had the most similar connections as compared to full spectrum EEG. Furthermore, the root mean squared error of functional connections was shown to be consistently lower in analyses derived from full spectrum EEG input.

Resting state signals have been shown to be able to characterize the brain's underlying resting-state networks present in epilepsy [30], [265], [266]. Thus, resting state fNIRS connectivity measures could identify clinically relevant information in individual patients suffering from epilepsy. Strengths of this study laid in part in its experimental design, as it involved a relatively large number of patients with multiple multimodal EEG-fNIRS recordings. Furthermore, a large number of resting state periods were partitioned from multiple full recordings to be used for each patient. The results of validating our model on intra-patient resting state records is shown in Figure 5.5 of Article 2. As instrumental and analytical improvements for fNIRS signal processing (i.e., artifact removal) occur, the models proposed in this study should be further validated on larger patient datasets. The reconstruction of fNIRS signals from EEG waveforms highlights an interesting ability of the developed seq2seq model. A valuable consideration is the fact that the fNIRS technique is not readily able to obtain subcortical signals, but such signals from subcortical structures might possibly influence the relationships between neural and hemodynamic signals. Neurovascular coupling studies in subcortical brain structures discovered strong correlation between low frequency oscillations (LFO) measured peripherally by the fNIRS technique with the BOLD signals from fMRI; suggesting a global circulatory origin of LFOs in the human brain [87]. It is purported that resting state networks may to some extent reflect vascular anatomy associated with systemic LFOs, rather than neuronal connectivity—at approximately 0.1 Hz in BOLD signals, time delays were found between the precentral gyrus (PCG) and insula. Interestingly, in resting

state periods, phase coupling between BOLD oscillations at 0.1 Hz and heart rate oscillations in the mid cingulum were found; one representative of neural and the other of vascular BOLD oscillations [87].

Changes in electrical potential as shown in EEG recordings are linked closely to cerebral blood flow (CBF). When CBF declines to approximately 25– 35 ml/100 g/min, the EEG first loses faster frequencies, then as the CBF decreases to approximately 17– 18 ml/100 g/min, slower frequencies gradually increase. The interdependent relationship between CBF and cerebral electro-potential firing is theorized to be captured by the model used in this work. Slower EEG frequencies are related to CBF with the EEG first losing faster frequencies when normal CBF declines to approximately 25– 35 ml/100 g/min, and slower frequencies gradually increase as the CBF decreases to approximately 17– 18 ml/100 g/min, slower frequencies gradually increase. Further research is needed in determining the possible role brain structures have in Mayer wave (MW) generation. It is generally accepted that the generation and propagation of the MW in the cardiovascular and neurovascular systems result from mechanisms of vascular and neural origin involving several mutually interacting variables and the interdependent relationship between CBF and cerebral electro-potential firing is theorized to be captured by the model used in this work.

6.2.1 Clinical application

Resting state data from epileptic patients in Objective 2 and the subsequent results derived from it can be extended to multiple neurovascular conditions (e.g., traumatic brain injury, subarachnoid hemorrhage, sleep investigations, neurocognitive disorders) in which scalp EEG is used for diagnosis or treatment paradigms. We will discuss the clinical applications of Objective 2 and its results as it relates to it being used as a tool for epileptic pre-surgical assessment, traumatic brain injury, and sleep investigations.

6.2.1.1 Epileptic pre-surgical assessment using EEG as a predictor of hemodynamics

Our results study showed cerebral hemodynamics can be predicted from higher EEG frequency bands in the resting epileptic brain with low reconstruction error. Furthermore, higher frequency EEG signals show similar resting-state functional connectivity patterns in epileptic brains. Of interest is the fact that EEG frequencies are generally correlated with cerebral metabolic processes and our work here suggests that the hemodynamic correlates of these frequencies can be

predicted to some extent. The network dynamics of the epileptic brain is still not fully understood as basic and clinical research is underway to comprehend the mechanics, the method presented here has potential to be developed into a helpful clinical tool.

The results from our functional connectivity studies could serve as a surrogate for cerebral hemodynamic monitoring in clinical settings in which only scalp EEG technology exists (which is the case for most clinical settings). Our functional connectivity results suggest that the resting epileptic brain's hemodynamics are predictable to a certain degree by higher range EEG frequency bands (e.g., gamma and theta bands) lending further credence to the hypothesis that cerebral metabolic factors mediate brain function in epilepsy [161], [215], [225]. Eventually, this could lead to adding this technique to be part of the clinical repertoire for presurgical assessment of drug-resistant epilepsies.

6.2.1.2 Clinical applications: traumatic brain injury

Traumatic brain injury (TBI) is sustained brain damage due to sudden trauma to the head—common causes may include car or motorcycle crashes, falls, sports injuries, and physical assaults. During a TBI event, self-propagating waves of neuronal depolarization are observed leading to a phenomenon of spreading depolarizations (SD) [267]. Typically, sudden and concomitant increase in cerebral blood flow is associated with neuronal depolarizations. TBI may result in stupor where an individual can be aroused briefly by a strong stimulus (e.g. sharp pain). TBI patients can possibly enter into damaging brain states as follows: 1) a comatose state, whereby an individual is totally unconscious, unresponsive, unaware, and un-arousable; 2) vegetative state, where an individual is unconscious and unaware of his or her surroundings, but continues to have a sleep-wake cycle with periods of alertness; and 3) a persistent vegetative state, where an individual remains unresponsive for more than one month. It has been shown that TBI can lead to inversion of neurovascular communication on both the local and global level and TBI induced SD leads to a decrease rather than an increase in CBF [268]. At the level of the neurovascular unit, TBI surprisingly leads to an inversion of NVC from vasodilation to vasoconstriction and global ischemia may be implicated in severe TBI.

TBI acutely reduces the peak amplitude of both the brain's electrical and blood flow (CBF) responses, although recovery to baseline within $30 - 60$ minutes typically occurs after insult

[268]. Interestingly, TBI induces low-frequency oscillatory behavior in CBF, histological analyses suggest that the alteration in blood flow is not associated with concomitant anatomical changes. Thus, TBI can be characterized as acute (and possibly chronic) changes in neural and hemodynamic responses. Clinically, the timely transport to a hospital following acute traumatic brain injury, can significantly improve the prognosis for recovery as there is a dearth of rapidly acquired and interpretable quantitative biomarkers for TBI in the field. Determining such a neurophysiological signature depends on understanding the neural and hemodynamic patterns evoked during and after TBI and its subsequent clinical sequalae.

The findings from experiments related to Objective 2, suggest that cerebral activity (EEG) albeit limited (i.e., data derived from specific frequency bands) can influence cerebral blood flow and thus cerebral hemodynamics. Since, neurovascular coupling is a spontaneous process (present during resting state or baseline activity of the brain), encompassing coordinated activity of neurons, astrocytes, and parenchymal arterioles, (i.e. the "neurovascular unit") and active during a TBI, a mechanistic understanding of these events should provide novel strategies as a first diagnostic step.

6.2.1.3 Clinical applications: sleep studies

Sleep can be investigated within the framework of the neurovascular coupling phenomenon, since this can be used as a foundation to map intrinsic brain activities or synchronizations commonly present in sleep and sleep related brain patterns [269]. During different stages of sleep, the human brain undergoes substantial changes in neural transmitters, cerebral electrical potential and cerebral hemodynamics [270] and NVC dynamically changes across sleep–wake states in normal and epileptic brains. EEG-fMRI studies have demonstrated that the relationship between the amplitude of band specific EEG activity and the fMRI based BOLD response exists [271], [272]. It has been shown recently that spontaneous changes in cerebral electrical (EEG) signals and the BOLD fMRI signals persist across sleep and wakeful conditions.

Predicting the hemodynamic correlate and effective changes in cerebral hemodynamics from the theta EEG frequency band (i.e., the active frequency band in the human brain during sleep) is helpful in understanding the fundamental metabolic and cellular relationships during sleep. Since sleep can be considered to be a resting brain state, the baseline neuronal activities

occurring in the brain (as dictated by neurovascular coupling) are related to vasoactive mediators, such as nitric oxide (NO) and adenosine [273]. It has been noted that there is an acute decrease in NO in rapid eye movement (REM) and non-REM sleep [274].

Utilizing the results from Objective 2, the relationships between the neural activities and brain hemodynamics of sleep can be explored since it has been established that the brain experiences substantial changes in neural transmitters, cerebral electrical potentials, CBF, and cerebral hemodynamics during the sleep state. On the basis of the aforementioned findings, we speculate that brain metabolic changes are dependent on electrical potentials as measured by EEG and the NVC phenomenon is dynamically changing across sleep and wake states in the human brain. The results from Objective 2 and sleep multimodal EEG-fNIRS data, if collected and marked can be the first step towards better understanding sleep pathologies as well as in the development of a neural signature related to sleep pathologies that have a vascular component, particularly sleep-related breathing disorders: sleep apnea, and hypersomnia of central origin (narcolepsy).

6.3 Practical limitations

This thesis has offered insight into the potential of fNIRS in seizure detection and prediction of the resting state. However, the methodology described here has practical limitations. Several limitations are intrinsic to fNIRS technology that hinders it from being readily used in clinical settings. From a practical standpoint, the fNIRS technique has limited cerebral penetration depth, as it can only measure HbO, HbR changes directly under the placed sources/detectors; albeit this can be mitigated by short channel separation (approximately $3\ to\ 5\ cm$). Furthermore, fNIRS infers neural activity via neurovascular coupling. Thus, the relationship between experimentally derived hemodynamic changes and the underlying neural activity is not always readily understood—leading to sometimes obscure interpretations of fNIRS waveforms. Furthermore, there are several factors to consider when utilizing the fNIRS technique in practical clinical experiments; such as: how do factors such as: 1) epilepsy type, 2) the duration of the resting state, and 3) patient demographics, impact seizure detection and fNIRS resting state prediction metrics?

CHAPTER 7 CONCLUSIONS AND RECOMMENDATIONS

7.1 Summary

Throughout this dissertation, we present results relevant to multimodal neuroimaging particularly with a focus on human epilepsy data and resting state periods. While the specific objectives and potential applications of these results are varied, each is centered on a common premise: the dual activity of multimodal cerebral signals representing neurons and vascular neural networks. The characteristics of the deep learning models employed here are patient specific and can be understood well in isolation. The analysis and eventual generalization of such systems is highly challenging and requires a wide array of techniques including classical signal processing, and applied machine learning. Generalization of these techniques is best done by collecting more data and subsequently iterating the developed models. Specifically, if the data corpus increases and subsequently, the number of recorded seizures increases, the LSTM model developed for seizure detection has more available training data. In theory, this can improve model performance metrics and thus lead to a more generalizable model. In this situation, in which more EEG-fNIRS data is available (i.e., seizure and resting state data) the concern for appropriate model fit is relevant. By avoiding model overfitting (i.e., essentially learning spurious correlations in the data) by increasing the size of the training set should reduce these spurious correlations and improve model performance [275]. However, it should be kept in mind that signal fidelity is paramount to improving model generalizability. One situation where more data does not categorically improve model generalizability and may even reduce performance metrics if additional training data is noisy or has missing values [276], [277]. In addition, splitting the increased data corpus into larger training, testing and validation sets can lead to counterintuitive results, a phenomenon referred to as “double-descent” [278]. In this context, the size of the training dataset is set close to the number of learnable model parameters [279], [280] and as the training set size increases, model performance worsens. Finally, progressive improvement occurs as the model learns on the available increased training dataset examples [278], [281]. This phenomenon is not yet totally understood and is largely of theoretical interest.

In this thesis, extensive processing of these high-dimensional datasets was limited, since a combination of analytical and deep learning approaches prove to be generally fruitful. Although

the development of new mathematical models for deep learning is necessary to increase our understanding of neural network dynamics, combined methods (analytical and deep learning methods) will continue to lead future advances. However, the results obtained by the LSTM and sequence-to-sequence autoencoder models used here are largely dependent on the non-linearities in the seizure and resting state input data, and these so called non-linearities (i.e., features) helped to determine relationships between EEG and fNIRS signals. In summary, our results suggest that signal dynamics are not necessarily a general feature of deep networks but are influenced to a certain degree by the nonlinearities in data used to drive these networks. Examination of the information bottleneck principle itself may offer important insights into deep networks [282].

This thesis showed that fNIRS adds significance to the task of seizure detection (Article 1) and surmise that seizure free periods in EEG signals can be encoded to predict corresponding fNIRS resting state signals (Article 2). This has potential application for an improved fundamental understanding of brain dynamics (i.e., electrical and hemodynamic). We demonstrated how artificially intelligent methods can be used to achieve these goals. The experimental part of this thesis was divided into the following categories: 1. seizure detection in a multimodal dataset (Article 1), and 2. the prediction of resting state in fNIRS signals provided resting state EEG signals (Article 2). The following highlights the main contributions made across these experiments.

7.2 Main contributions

This section presents a summary of the main contributions of this thesis and we offer directions for further research. In Chapter 1, we presented the thesis objectives and subsequently implemented a deep learning LSTM model to detect seizure events with high sensitivity and specificity metrics. We demonstrate that statistically validated performance can be achieved with an appropriate deep learning model and that combined EEG-fNIRS signals improve metrics as opposed to EEG signals alone. We utilized the well documented CHB-MIT scalp EEG dataset for model validation, and we showed that by using our LSTM architecture, we are able to obtain metrics for a seizure detection task using scalp EEG data that rivals other methods. The statistical significance of our findings was verified across all patients. Following this, we tested our model using in-house multimodal EEG-fNIRS data. We show that EEG signals combined with fNIRS

signals improve seizure detection metrics as opposed to scalp EEG signals alone. This was the first work to our knowledge that utilized multimodal EEG-fNIRS data for a task of seizure detection. Thereby, results from this work suggest that in the situation in which intensive care unit patients require long-term continuous brain monitoring, the use of EEG-fNIRS systems will offer increased benefit in a seizure detection task as compared to the current clinical gold standard (i.e., scalp EEG signals). Albeit, the improvement in seizure detection metrics (sensitivity, specificity) of seizure detection is minimal when fNIRS is added to continuous monitoring, fNIRS signals offers the clinician increased insight into brain functioning and could help in detecting seizures in vulnerable patients.

In our subsequent experiments we hypothesized that resting state EEG signals derived from epileptic patients contain relevant time and frequency domain information to drive prediction in corresponding fNIRS resting state data. The results from our work suggests that as with full spectrum EEG signals, specific EEG frequency bands, can drive prediction of patient specific resting state hemodynamic signals using sequence to sequence learning. Neuron synchrony and associated desynchrony in response to periodic changes in multimodal EEG-fNIRS signals occurs with respect to the resting state. In general, one might intuitively expect oscillatory data types such as EEG and fNIRS to entrain to a common input, supported in part by the neurovascular coupling phenomenon; thus, expecting certain physiological states to encode a common input. The work here suggests a specific range of EEG input frequencies generate hemodynamic reconstructions with more fidelity as compared to others. Specifically, higher EEG frequency envelopes overwhelm other frequencies and drives fNIRS reconstructions with more fidelity as compared to lower frequency EEG bands.

7.3 Recommendations for future work

Many experiments have been relegated to the future simply due to time constraints. Future work includes transfer learning for the models proposed and proposals to experiment with new methodologies (experimental and algorithmic). This thesis has been mainly focused on the use of either seizure data (Objective 1) or resting state periods obtained in the context of epileptic recordings (Objective 2). The deep learning algorithms implemented in this research were adapted from active research and/or literature, leaving fundamental investigations of the algorithmic

components outside the scope of the thesis. However, given the robust dataset available, several avenues for future studies come to mind.

7.3.1 Real time detection and prediction

Building on the work put forth in this thesis, exploring the capability of the developed models to allow for real-time detection and prediction of seizure events is possible. Within the context of seizure detection, this thesis lays the groundwork for establishing the fact that hemodynamic fNIRS correlates to EEG signals offer increased metrics for detection of seizure events. For seizure prediction, the signal processing techniques mentioned in Chapters 4 and 5 can be extended for epileptic spikes, pre and post ictal, and ictal events. This would require expert marking of every EEG recording for spikes; a painstaking and tedious process. After which, the model developed in Chapter 4 can be extended to these different events via transfer learning, wherein information stored after solving one problem (i.e., seizure detection in this case) is used for solving a different, but related problem.

The results from Objective 2 as presented in Chapter 5 suggest that prediction of hemodynamics is possible from EEG signals given the developed model. Advancing prediction of fNIRS seizure waveforms given EEG signals incrementally is of great interest. Fine tuning (reparameterization of the existing model's LSTM modules) and retraining the model given the new dataset (seizure events) would be subsequent steps. In addition to predicting fNIRS seizure events, the model can be used to determine variability patterns in the hemodynamic response related to seizure events. Furthermore, if the results of seizure prediction using the sequence to sequence model is successful, then extending the model to predicting the end of a seizure (i.e., seizure cessation) would be a future step.

The objective of predicting seizure cessation would be loosely defined as predicting the point at which seizure is expected to end, which is validated by the ground truth corresponding to each recording. This allows for the computation of seizure duration, and the length of the time interval between pre, post, and future ictal events. These quantities have clinical significance as it relates to status epilepticus, since ictal events that are longer than ten minutes in duration, or a seizure cluster, could possibly be indicative of a transition into status epilepticus [207].

This project would be formatted as a pilot study and would aim to explore the feasibility of the developed sequence-to-sequence autoencoder model to detect and predict seizures collected from continuous long-term recorded multimodal EEG-fNIRS signals of a 15 epileptic patient cohort (and a control group). The inclusion and exclusion criteria would be similar to the one listed in Section 4.4.3.1. The patients would be recorded with similar multimodal instrumentation as detailed in Sections 4.4.3.2 and 5.4.3.2, preferably in an intensive care setting. However, given the higher likelihood of recording seizures in non-acute settings, the epilepsy monitoring unit can be a viable alternative. Once data is collected, the data must be expertly marked and prepared for model input. A small set of variables (i.e., latent space variables from an autoencoder model) inferred from the data can be used to determine a unique signature and predict fNIRS seizures from their EEG correlate.

7.3.2 Beyond seizures

The research presented here can be tailored towards neuro-prosthetic development. For example, responsive neurostimulation devices (RNS), are invasive seizure prevention systems that monitor brain activity. If aberrant brain activity is detected, a RNS system delivers electrical pulses in an attempt to prevent seizures. RNS devices have delivered promising results in treating pharmacologically resistant partial onset seizures [283]. The models developed here can be adapted for practical applications in RNS like systems by integration into their hardware and could potentially lead to improved and more accurate seizure-prevention systems. Finally, validation of our results on increased data can help in developing a higher dimensional, biophysically generalizable and realistic model for real time analysis.

In addition to the real time analyses mentioned in Section 7.3.1, utilizing the techniques developed in this thesis to investigate other common acute neurological and neurosurgical conditions, such as subarachnoid hemorrhage, traumatic brain injury, and stroke to name a few is possible. Developing smart algorithms that take into account multiple acute and chronic conditions can help in elucidating relationships which can eventually lead to biomarker development.

BIBLIOGRAPHY

[1] A. L. Hodgkin and A. F. Huxley, “A quantitative description of membrane current and its application to conduction and excitation in nerve,” *Bull. Math. Biol.*, 1990, doi: 10.1007/BF02459568.

[2] A. Palmini *et al.*, “From theory to practice: Critical points in the 2017 ILAE classification of epileptic seizures and epilepsies,” *Epilepsia*. 2020, doi: 10.1111/epi.16426.

[3] H. M. de Boer, M. Mula, and J. W. Sander, “The global burden and stigma of epilepsy,” *Epilepsy and Behavior*. 2008, doi: 10.1016/j.yebeh.2007.12.019.

[4] R. Kennett, “Modern electroencephalography,” *J. Neurol.*, 2012, doi: 10.1007/s00415-012-6425-6.

[5] M. Strein, J. P. Holton-Burke, L. R. Smith, and G. M. Brophy, “Prevention, Treatment, and Monitoring of Seizures in the Intensive Care Unit,” *J. Clin. Med.*, vol. 8, no. 8, p. 1177, Aug. 2019, doi: 10.3390/jcm8081177.

[6] J. D. Pandian, G. D. Cascino, E. L. So, E. Manno, and J. R. Fulgham, “Digital video-electroencephalographic monitoring in the neurological-neurosurgical intensive care unit: clinical features and outcome,” *Arch. Neurol.*, vol. 61, no. 7, pp. 1090–1094, 2004.

[7] M. B. Westover *et al.*, “The probability of seizures during EEG monitoring in critically ill adults,” *Clin. Neurophysiol.*, vol. 126, no. 3, pp. 463–471, 2015, doi: 10.1016/j.clinph.2014.05.037.

[8] J. Claassen, S. A. Mayer, R. G. Kowalski, R. G. Emerson, and L. J. Hirsch, “Detection of electrographic seizures with continuous EEG monitoring in critically ill patients,” *Neurology*, vol. 62, no. 10, pp. 1743 LP – 1748, May 2004, doi: 10.1212/01.WNL.0000125184.88797.62.

[9] M. Boly and R. Maganti, “Monitoring epilepsy in the intensive care unit: Current state of facts and potential interest of high density EEG,” *Brain Inj.*, vol. 28, no. 9, pp. 1151–1155, Aug. 2014, doi: 10.3109/02699052.2014.920525.

[10] K. Hobbs *et al.*, “Rapid bedside evaluation of seizures in the ICU by listening to the sound of brainwaves: a prospective observational clinical trial of ceribell’s brain stethoscope

function," *Neurocrit. Care*, vol. 29, no. 2, pp. 302–312, 2018.

[11] F. W. Drislane, M. R. Lopez, A. S. Blum, and D. L. Schomer, "Detection and treatment of refractory status epilepticus in the intensive care unit," *J. Clin. Neurophysiol.*, vol. 25, no. 4, pp. 181–186, 2008, doi: 10.1097/WNP.0b013e31817be70e.

[12] Y. Kubota, H. Nakamoto, S. Egawa, and T. Kawamata, "Continuous EEG monitoring in ICU," *J. Intensive Care*, vol. 6, no. 1, pp. 1–8, 2018, doi: 10.1186/s40560-018-0310-z.

[13] H. Girouard and C. Iadecola, "Neurovascular coupling in the normal brain and in hypertension, stroke, and Alzheimer disease," *J. Appl. Physiol.*, vol. 100, no. 1, pp. 328–335, 2006.

[14] F. Herold, P. Wiegel, F. Scholkmann, and N. Müller, "Applications of Functional Near-Infrared Spectroscopy (fNIRS) Neuroimaging in Exercise–Cognition Science: A Systematic, Methodology-Focused Review," *J. Clin. Med.*, 2018, doi: 10.3390/jcm7120466.

[15] J. U. Blicher *et al.*, "Visualization of altered neurovascular coupling in chronic stroke patients using multimodal functional MRI," *J. Cereb. Blood Flow Metab.*, vol. 32, no. 11, pp. 2044–2054, 2012.

[16] A. Iraji *et al.*, "Resting state functional connectivity in mild traumatic brain injury at the acute stage: independent component and seed-based analyses," *J. Neurotrauma*, vol. 32, no. 14, pp. 1031–1045, 2015.

[17] A. R. Mayer, M. V Mannell, J. Ling, C. Gasparovic, and R. A. Yeo, "Functional connectivity in mild traumatic brain injury," *Hum. Brain Mapp.*, vol. 32, no. 11, pp. 1825–1835, 2011.

[18] C. Luo *et al.*, "Altered functional connectivity in default mode network in absence epilepsy: A resting-state fMRI study," *Hum. Brain Mapp.*, vol. 32, no. 3, pp. 438–449, 2011, doi: 10.1002/hbm.21034.

[19] Y. Zhou *et al.*, "Characterization of thalamo-cortical association using amplitude and connectivity of functional MRI in mild traumatic brain injury," *J. Magn. Reson. Imaging*, vol. 39, no. 6, pp. 1558–1568, 2014.

[20] C. T. Drake and C. Iadecola, "The role of neuronal signaling in controlling cerebral blood flow," *Brain Lang.*, 2007, doi: 10.1016/j.bandl.2006.08.002.

[21] D. Attwell, A. M. Buchan, S. Charpak, M. Lauritzen, B. A. MacVicar, and E. A. Newman, “Glial and neuronal control of brain blood flow,” *Nature*. 2010, doi: 10.1038/nature09613.

[22] K. Whittingstall and N. K. Logothetis, “Frequency-Band Coupling in Surface EEG Reflects Spiking Activity in Monkey Visual Cortex,” *Neuron*, 2009, doi: 10.1016/j.neuron.2009.08.016.

[23] N. K. Logothetis and B. A. Wandell, “Interpreting the BOLD Signal,” *Annu. Rev. Physiol.*, 2004, doi: 10.1146/annurev.physiol.66.082602.092845.

[24] P. Lachert *et al.*, “Causal Coupling between Electrophysiological Signals, Cerebral Hemodynamics and Systemic Blood Supply Oscillations in Mayer Wave Frequency Range,” *Int. J. Neural Syst.*, 2019, doi: 10.1142/S0129065718500338.

[25] T. H. Schwartz, “Neurovascular Coupling and Epilepsy: Hemodynamic Markers for Localizing and Predicting Seizure Onset,” *Epilepsy Curr.*, 2007, doi: 10.1111/j.1535-7511.2007.00183.x.

[26] M. O’Regan, “Adenosine and the regulation of cerebral blood flow,” *Neurological Research*. 2005, doi: 10.1179/016164105X21931.

[27] R. D. Freeman and B. Li, “Neural – Metabolic coupling in the central visual pathway,” *Philosophical Transactions of the Royal Society B: Biological Sciences*. 2016, doi: 10.1098/rstb.2015.0357.

[28] K. R. Ko, A. C. Ngai, and H. R. Winn, “Role of adenosine in regulation of regional cerebral blood flow in sensory cortex,” *Am. J. Physiol. - Hear. Circ. Physiol.*, 1990, doi: 10.1152/ajpheart.1990.259.6.h1703.

[29] D. Attwell and C. Iadecola, “The neural basis of functional brain imaging signals,” *Trends in Neurosciences*. 2002, doi: 10.1016/S0166-2236(02)02264-6.

[30] S. M. Smith *et al.*, “Correspondence of the brain’s functional architecture during activation and rest,” *Proc. Natl. Acad. Sci. U. S. A.*, 2009, doi: 10.1073/pnas.0905267106.

[31] M. E. Raichle and M. A. Mintun, “BRAIN WORK AND BRAIN IMAGING,” *Annu. Rev. Neurosci.*, 2006, doi: 10.1146/annurev.neuro.29.051605.112819.

[32] C. Iadecola, “The Neurovascular Unit Coming of Age: A Journey through Neurovascular

Coupling in Health and Disease," *Neuron*. 2017, doi: 10.1016/j.neuron.2017.07.030.

[33] T. I. Netoff and S. J. Schiff, "Decreased neuronal synchronization during experimental seizures," *J. Neurosci.*, 2002, doi: 10.1523/jneurosci.22-16-07297.2002.

[34] A. Cymerblit-Sabba and Y. Schiller, "Development of hypersynchrony in the cortical network during chemoconvulsant-induced epileptic seizures in vivo," *J. Neurophysiol.*, 2012, doi: 10.1152/jn.00327.2011.

[35] F. Wendling, F. Bartolomei, J. J. Bellanger, J. Bourien, and P. Chauvel, "Epileptic fast intracerebral EEG activity: evidence for spatial decorrelation at seizure onset.," *Brain*, vol. 126, no. Pt 6, pp. 1449–1459, Jun. 2003, doi: 10.1093/brain/awg144.

[36] M. de Curtis and V. Gnatkovsky, "Reevaluating the mechanisms of focal ictogenesis: The role of low-voltage fast activity.," *Epilepsia*. 2009, doi: 10.1111/j.1528-1167.2009.02249.x.

[37] F. Cendes, W. H. Theodore, B. H. Brinkmann, V. Sulc, and G. D. Cascino, "Neuroimaging of epilepsy," in *Handbook of Clinical Neurology*, 2016.

[38] N. K. Logothetis, J. Pauls, M. Augath, T. Trinath, and A. Oeltermann, "Neurophysiological investigation of the basis of the fMRI signal," *Nature*, 2001, doi: 10.1038/35084005.

[39] M. J. Khan, U. Ghafoor, and K. S. Hong, "Early detection of hemodynamic responses using EEG: A hybrid EEG-fNIRS study," *Front. Hum. Neurosci.*, 2018, doi: 10.3389/fnhum.2018.00479.

[40] C. M. Lu, Y. J. Zhang, B. B. Biswal, Y. F. Zang, D. L. Peng, and C. Z. Zhu, "Use of fNIRS to assess resting state functional connectivity," *J. Neurosci. Methods*, 2010, doi: 10.1016/j.jneumeth.2009.11.010.

[41] R. I. Goldman, J. M. Stern, J. Engel Jr, and M. S. Cohen, "Simultaneous EEG and fMRI of the alpha rhythm," *Neuroreport*, vol. 13, no. 18, p. 2487, 2002.

[42] J. C. de Munck *et al.*, "The hemodynamic response of the alpha rhythm: an EEG/fMRI study," *Neuroimage*, vol. 35, no. 3, pp. 1142–1151, 2007.

[43] S. P. Koch, P. Werner, J. Steinbrink, P. Fries, and H. Obrig, "Stimulus-induced and state-dependent sustained gamma activity is tightly coupled to the hemodynamic response in humans," *J. Neurosci.*, vol. 29, no. 44, pp. 13962–13970, 2009.

[44] S. P. Koch, J. Steinbrink, A. Villringer, and H. Obrig, “Synchronization between background activity and visually evoked potential is not mirrored by focal hyperoxygenation: implications for the interpretation of vascular brain imaging,” *J. Neurosci.*, vol. 26, no. 18, pp. 4940–4948, 2006.

[45] S. P. Koch, S. Koendgen, R. Bourayou, J. Steinbrink, and H. Obrig, “Individual alpha-frequency correlates with amplitude of visual evoked potential and hemodynamic response,” *Neuroimage*, vol. 41, no. 2, pp. 233–242, 2008.

[46] J. Safaie, R. Grebe, H. A. Moghaddam, and F. Wallois, “Toward a fully integrated wireless wearable EEG-NIRS bimodal acquisition system,” *J. Neural Eng.*, vol. 10, no. 5, p. 56001, 2013.

[47] N. Roche-Labarbe, B. Zaaimi, P. Berquin, A. Nehlig, R. Grebe, and F. Wallois, “NIRS-measured oxy-and deoxyhemoglobin changes associated with EEG spike-and-wave discharges in children,” *Epilepsia*, vol. 49, no. 11, pp. 1871–1880, 2008.

[48] P. Giacometti and S. G. Diamond, “Compliant head probe for positioning electroencephalography electrodes and near-infrared spectroscopy optodes,” *J. Biomed. Opt.*, vol. 18, no. 2, p. 27005, 2013.

[49] M. Moosmann *et al.*, “Correlates of alpha rhythm in functional magnetic resonance imaging and near infrared spectroscopy,” *Neuroimage*, vol. 20, no. 1, pp. 145–158, 2003.

[50] A. Ekstrom, N. Suthana, D. Millett, I. Fried, and S. Bookheimer, “Correlation between BOLD fMRI and theta-band local field potentials in the human hippocampal area,” *J. Neurophysiol.*, vol. 101, no. 5, pp. 2668–2678, 2009.

[51] C. Amo, L. de Santiago, R. Barea, A. López-Dorado, and L. Boquete, “Analysis of gamma-band activity from human EEG using empirical mode decomposition,” *Sensors (Switzerland)*, vol. 17, no. 5, 2017, doi: 10.3390/s17050989.

[52] A. Sumiyoshi, H. Suzuki, T. Ogawa, J. J. Riera, H. Shimokawa, and R. Kawashima, “Coupling between gamma oscillation and fMRI signal in the rat somatosensory cortex: Its dependence on systemic physiological parameters,” *Neuroimage*, 2012, doi: 10.1016/j.neuroimage.2011.12.082.

[53] E. Martinez-Montes, P. A. Valdes-Sosa, F. Miwakeichi, R. I. Goldman, and M. S. Cohen,

"Concurrent EEG/fMRI analysis by multiway Partial Least Squares.," *Neuroimage*, vol. 22, no. 3, pp. 1023–1034, Jul. 2004, doi: 10.1016/j.neuroimage.2004.03.038.

[54] M. A. Kramer, U. T. Eden, E. D. Kolaczyk, R. Zepeda, E. N. Eskandar, and S. S. Cash, "Coalescence and fragmentation of cortical networks during focal seizures," *J. Neurosci.*, 2010, doi: 10.1523/JNEUROSCI.6309-09.2010.

[55] F. Grenier, I. Timofeev, and M. Steriade, "Neocortical very fast oscillations (ripples, 80-200 Hz) during seizures: Intracellular correlates," *J. Neurophysiol.*, 2003, doi: 10.1152/jn.00420.2002.

[56] J. S. Farrell *et al.*, "Postictal hypoperfusion/hypoxia provides the foundation for a unified theory of seizure-induced brain abnormalities and behavioral dysfunction," *Epilepsia*. 2017, doi: 10.1111/epi.13827.

[57] H. Ma, M. Zhao, and T. H. Schwartz, "Dynamic neurovascular coupling and uncoupling during ictal onset, propagation, and termination revealed by simultaneous in vivo optical imaging of neural activity and local blood volume," *Cereb. Cortex*, 2013, doi: 10.1093/cercor/bhs079.

[58] Z. M., and S. T.H., "Local neurometabolic coupling surrounding a seizure focus in rat neocortex," *Epilepsy Curr.*, 2011.

[59] M. Zhao, J. Nguyen, H. Ma, N. Nishimura, C. B. Schaffer, and T. H. Schwartz, "Preictal and ictal neurovascular and metabolic coupling surrounding a seizure focus," *J. Neurosci.*, 2011, doi: 10.1523/JNEUROSCI.2597-11.2011.

[60] Y. Song *et al.*, "Dysfunction of neurovascular/metabolic coupling in chronic focal epilepsy," *IEEE Trans. Biomed. Eng.*, 2016, doi: 10.1109/TBME.2015.2461496.

[61] M. Wenzel, J. P. Hamm, D. S. Peterka, and R. Yuste, "Acute Focal Seizures Start As Local Synchronizations of Neuronal Ensembles," *J. Neurosci.*, 2019, doi: 10.1523/JNEUROSCI.3176-18.2019.

[62] M. Wenzel, J. Hamm, D. Peterka, and R. M. Yuste, "Seizures start as silent microseizures by neuronal ensembles," *bioRxiv*, 2018, doi: 10.1101/358903.

[63] H. E. Scharfman, "The neurobiology of epilepsy," *Current Neurology and Neuroscience*

Reports. 2007, doi: 10.1007/s11910-007-0053-z.

[64] D. A. McCormick and D. Contreras, “On The Cellular and Network Bases of Epileptic Seizures,” *Annu. Rev. Physiol.*, 2001, doi: 10.1146/annurev.physiol.63.1.815.

[65] P. S. Hosford and A. V. Gourine, “What is the key mediator of the neurovascular coupling response?,” *Neuroscience and Biobehavioral Reviews*. 2019, doi: 10.1016/j.neubiorev.2018.11.011.

[66] D. J. Pinto, S. L. Patrick, W. C. Huang, and B. W. Connors, “Initiation, propagation, and termination of epileptiform activity in rodent neocortex in vitro involve distinct mechanisms,” *J. Neurosci.*, 2005, doi: 10.1523/JNEUROSCI.2278-05.2005.

[67] M. R. Nuwer *et al.*, “IFCN standards for digital recording of clinical EEG,” *Electroencephalogr. Clin. Neurophysiol.*, 1998, doi: 10.1016/S0013-4694(97)00106-5.

[68] G. A. Worrell, L. Parish, S. D. Cranstoun, R. Jonas, G. Baltuch, and B. Litt, “High-frequency oscillations and seizure generation in neocortical epilepsy,” *Brain*, vol. 127, no. 7, pp. 1496–1506, 2004, doi: 10.1093/brain/awh149.

[69] M. Iwasaki, E. Pestana, R. C. Burgess, H. O. Lüders, H. Shamoto, and N. Nakasato, “Detection of epileptiform activity by human interpreters: Blinded comparison between electroencephalography and magnetoencephalography,” *Epilepsia*. 2005, doi: 10.1111/j.0013-9580.2005.21104.x.

[70] D. L. Schomer and F. H. L. da Silva, *Niedermeyer’s electroencephalography: Basic principles, clinical applications, and related fields: Sixth edition*. 2012.

[71] N. E. Crone, A. Korzeniewska, and P. J. Franaszczuk, “Cortical gamma responses: Searching high and low,” *Int. J. Psychophysiol.*, vol. 79, no. 1, pp. 9–15, 2011, doi: 10.1016/j.ijpsycho.2010.10.013.

[72] X. Jia and A. Kohn, “Gamma rhythms in the brain,” *PLoS Biol.*, vol. 9, no. 4, pp. 2–5, 2011, doi: 10.1371/journal.pbio.1001045.

[73] D. A. Pizzagalli, “Electroencephalography and high-density electrophysiological source localization,” *Handb. Psychophysiol.*, vol. 3, pp. 56–84, 2007.

[74] D. L. Schomer and F. L. Da Silva, *Niedermeyer’s electroencephalography: basic principles,*

clinical applications, and related fields. Lippincott Williams & Wilkins, 2012.

[75] F. Lopes da Silva, "Neural mechanisms underlying brain waves: from neural membranes to networks," *Electroencephalography and Clinical Neurophysiology*. 1991, doi: 10.1016/0013-4694(91)90044-5.

[76] L. J. Greenfield, J. D. Geyer, and P. R. Carney, *Reading EEGs: A practical approach*. Lippincott Williams & Wilkins, 2012.

[77] S. Standring, *Gray's Anatomy E-Book: The Anatomical Basis of Clinical Practice*. 2016.

[78] D. P. Subha, P. K. Joseph, R. Acharya U, and C. M. Lim, "EEG signal analysis: a survey.," *J. Med. Syst.*, 2010, doi: 10.1007/s10916-008-9231-z.

[79] G. G. Knyazev, "EEG delta oscillations as a correlate of basic homeostatic and motivational processes," *Neurosci. Biobehav. Rev.*, vol. 36, no. 1, pp. 677–695, 2012.

[80] A. Gramfort *et al.*, "MNE software for processing MEG and EEG data," *Neuroimage*, 2014, doi: 10.1016/j.neuroimage.2013.10.027.

[81] Y. Roy, H. Banville, I. Albuquerque, A. Gramfort, T. H. Falk, and J. Faubert, "Deep learning-based electroencephalography analysis: A systematic review," *J. Neural Eng.*, vol. 16, no. 5, 2019, doi: 10.1088/1741-2552/ab260c.

[82] F. Amzica and M. Steriade, "Electrophysiological correlates of sleep delta waves," *Electroencephalogr. Clin. Neurophysiol.*, vol. 107, no. 2, pp. 69–83, 1998, doi: 10.1016/S0013-4694(98)00051-0.

[83] G. G. Knyazev, "EEG delta oscillations as a correlate of basic homeostatic and motivational processes," *Neurosci. Biobehav. Rev.*, vol. 36, no. 1, pp. 677–695, 2012, doi: 10.1016/j.neubiorev.2011.10.002.

[84] J. L. Cantero *et al.*, "Sleep-dependent theta oscillations in the human hippocampus and neocortex," *J. Neurosci.*, 2003, doi: 23/34/10897 [pii] ET - 2003/12/03.

[85] W. Klimesch, B. Schack, and P. Sauseng, "The Functional Significance of Theta and Upper Alpha Oscillations," *Exp. Psychol.*, vol. 52, no. 2, pp. 99–108, Jan. 2005, doi: 10.1027/1618-3169.52.2.99.

[86] G. Pfurtscheller, "Induced Oscillations in the Alpha Band: Functional Meaning," *Epilepsia*,

vol. 44, no. s12, pp. 2–8, 2003, doi: 10.1111/j.0013-9580.2003.12001.x.

[87] G. Pfurtscheller *et al.*, “Distinction between neural and vascular BOLD oscillations and intertwined heart rate oscillations at 0.1 Hz in the resting state and during movement,” *PLoS One*, vol. 12, no. 1, Jan. 2017, doi: 10.1371/journal.pone.0168097.

[88] T. A. Rihs, C. M. Michel, and G. Thut, “Mechanisms of selective inhibition in visual spatial attention are indexed by α-band EEG synchronization,” *Eur. J. Neurosci.*, vol. 25, no. 2, pp. 603–610, 2007, doi: 10.1111/j.1460-9568.2007.05278.x.

[89] R. Sigala, S. Haufe, D. Roy, H. R. Dinse, and P. Ritter, “The role of alpha-rhythm states in perceptual learning: Insights from experiments and computational models,” *Front. Comput. Neurosci.*, vol. 8, no. 1 APR, pp. 1–19, 2014, doi: 10.3389/fncom.2014.00036.

[90] Freeman WJ, “Origin, structure, and role of background EEG activity. Part 1. Analytic amplitude.,” *Clin. Neurophysiol.*, vol. 115, no. 9, p. :2077-2088., 2004.

[91] G. Buzsáki and X.-J. Wang, “Mechanisms of gamma oscillations,” *Annu. Rev. Neurosci.*, vol. 35, pp. 203–225, 2012.

[92] A. Kleinschmidt *et al.*, “Simultaneous recording of cerebral blood oxygenation changes during human brain activation by magnetic resonance imaging and near-infrared spectroscopy,” *J. Cereb. blood flow Metab.*, vol. 16, no. 5, pp. 817–826, 1996.

[93] G. R. Müller-Putz, “Electroencephalography,” in *Handbook of Clinical Neurology*, 2020.

[94] J. D. Kropotov, “Quantitative EEG, Event-Related Potentials And Neurotherapy. 525 B Street, Suite 1900, San Diego, CA 92101-4495.” USA: Elsevier Inc, 2009.

[95] R. W. Whitehouse, “Computed Tomography,” in *Medical Radiology*, 2020.

[96] J. E. Adams, “Quantitative computed tomography,” *Eur. J. Radiol.*, 2009, doi: 10.1016/j.ejrad.2009.04.074.

[97] D. J. Brenner and E. J. Hall, “Computed tomography - An increasing source of radiation exposure,” *New England Journal of Medicine*. 2007, doi: 10.1056/NEJMra072149.

[98] J. Hsieh, *Computed Tomography: Principles, Design, Artifacts, and Recent Advances*. 2015.

[99] B. F. Hutton, “The origins of SPECT and SPECT/CT,” *European Journal of Nuclear*

Medicine and Molecular Imaging. 2014, doi: 10.1007/s00259-013-2606-5.

[100] M. Wintermark *et al.*, "Comparative Overview of Brain Perfusion Imaging Techniques," *Stroke*, 2005, doi: 10.1161/01.str.0000177884.72657.8b.

[101] C. la Fougère, A. Rominger, S. Förster, J. Geisler, and P. Bartenstein, "PET and SPECT in epilepsy: A critical review," *Epilepsy and Behavior*. 2009, doi: 10.1016/j.yebeh.2009.02.025.

[102] K. Goffin, S. Dedeurwaerdere, K. Van Laere, and W. Van Paesschen, "Neuronuclear Assessment of Patients With Epilepsy," *Seminars in Nuclear Medicine*. 2008, doi: 10.1053/j.semnuclmed.2008.02.004.

[103] W. Van Paesschen, P. Dupont, S. Sunaert, K. Goffin, and K. Van Laere, "The use of SPECT and PET in routine clinical practice in epilepsy," *Current Opinion in Neurology*. 2007, doi: 10.1097/WCO.0b013e328042baf6.

[104] R. Deichmann, "Principles of MRI and functional MRI," in *Neuromethods*, 2016.

[105] M. William Herring, "Learning radiology: recognizing the basics," in *Recognizing Some Common Causes of Intracranial Pathology*, 2017.

[106] M. Symms, H. R. Jäger, K. Schmierer, and T. A. Yousry, "A review of structural magnetic resonance neuroimaging," *Journal of Neurology, Neurosurgery and Psychiatry*. 2004, doi: 10.1136/jnnp.2003.032714.

[107] A. De Ciantis and L. Lemieux, "Localisation of epileptic foci using novel imaging modalities," *Current Opinion in Neurology*. 2013, doi: 10.1097/WCO.0b013e328363372c.

[108] M. K. Sidhu, J. S. Duncan, and J. W. Sander, "Neuroimaging in epilepsy," *Current Opinion in Neurology*. 2018, doi: 10.1097/WCO.0000000000000568.

[109] W. D. Gaillard, J. H. Cross, J. S. Duncan, H. Stefan, and W. H. Theodore, "Epilepsy imaging study guideline criteria: Commentary on diagnostic testing study guidelines and practice parameters," *Epilepsia*, 2011, doi: 10.1111/j.1528-1167.2011.03155.x.

[110] J. Von Oertzen *et al.*, "Standard magnetic resonance imaging is inadequate for patients with refractory focal epilepsy," *J. Neurol. Neurosurg. Psychiatry*, 2002, doi: 10.1136/jnnp.73.6.643.

[111] T. W. Wilson, E. Heinrichs-Graham, A. L. Proskovec, and T. J. McDermott, "Neuroimaging with magnetoencephalography: A dynamic view of brain pathophysiology," *Translational Research*. 2016, doi: 10.1016/j.trsl.2016.01.007.

[112] T. H. Sander, J. Preusser, R. Mhaskar, J. Kitching, L. Trahms, and S. Knappe, "Magnetoencephalography with a chip-scale atomic magnetometer," *Biomed. Opt. Express*, 2012, doi: 10.1364/boe.3.000981.

[113] H. Okamoto, "Clinical applications," in *Clinical Applications of Magnetoencephalography*, 2016.

[114] S. Kharkar and R. Knowlton, "Magnetoencephalography in the presurgical evaluation of epilepsy," *Epilepsy and Behavior*. 2015, doi: 10.1016/j.yebeh.2014.11.029.

[115] C. C. Gallen *et al.*, "Neuromagnetic mapping of brain function," *Radiology*, 1993, doi: 10.1148/radiology.187.3.8497647.

[116] W. W. Sutherling *et al.*, "Dipole localization of human induced focal afterdischarge seizure in simultaneous magnetoencephalography and electrocorticography," *Brain Topogr.*, 2001, doi: 10.1023/A:1012940812742.

[117] S. J. Williamson, Z. L. Lü, D. Karron, and L. Kaufman, "Advantages and limitations of magnetic source imaging," *Brain Topogr.*, 1991, doi: 10.1007/BF01132773.

[118] R. Srinivasan, W. R. Winter, and P. L. Nunez, "Source analysis of EEG oscillations using high-resolution EEG and MEG.," *Prog. Brain Res.*, vol. 159, pp. 29–42, 2006, doi: 10.1016/S0079-6123(06)59003-X.

[119] Z. S. Tovar-Spinoza, A. Ochi, J. T. Rutka, C. Go, and H. Otsubo, "The role of magnetoencephalography in epilepsy surgery," *Neurosurgical Focus*. 2008, doi: 10.3171/FOC/2008/25/9/E16.

[120] M. Oishi *et al.*, "Epileptic spikes: Magnetoencephalography versus simultaneous electrocorticography," *Epilepsia*, 2002, doi: 10.1046/j.1528-1157.2002.10702.x.

[121] G. Pellegrino *et al.*, "Clinical yield of magnetoencephalography distributed source imaging in epilepsy: A comparison with equivalent current dipole method," *Hum. Brain Mapp.*, 2018, doi: 10.1002/hbm.23837.

[122] C. Grova, M. Aiguabella, R. Zelmann, J. M. Lina, J. A. Hall, and E. Kobayashi, “Intracranial EEG potentials estimated from MEG sources: A new approach to correlate MEG and iEEG data in epilepsy,” *Hum. Brain Mapp.*, 2016, doi: 10.1002/hbm.23127.

[123] K. D. Singh, “Which ‘neural activity’ do you mean? fMRI, MEG, oscillations and neurotransmitters,” *NeuroImage*. 2012, doi: 10.1016/j.neuroimage.2012.01.028.

[124] G. Muehllehner and J. S. Karp, “Positron emission tomography,” *Physics in Medicine and Biology*. 2006, doi: 10.1088/0031-9155/51/13/R08.

[125] R. Turner and T. Jones, “Techniques for imaging neuroscience,” *British Medical Bulletin*. 2003, doi: 10.1093/bmb/65.1.3.

[126] M. Richardson, “Current themes in neuroimaging of epilepsy: Brain networks, dynamic phenomena, and clinical relevance,” *Clinical Neurophysiology*. 2010, doi: 10.1016/j.clinph.2010.01.004.

[127] A. Otte and U. Halsband, “Brain imaging tools in neurosciences,” *J. Physiol. Paris*, 2006, doi: 10.1016/j.jphysparis.2006.03.011.

[128] M. D. Fox and M. E. Raichle, “Spontaneous fluctuations in brain activity observed with functional magnetic resonance imaging,” *Nature Reviews Neuroscience*. 2007, doi: 10.1038/nrn2201.

[129] B. Biswal, F. Zerrin Yetkin, V. M. Haughton, and J. S. Hyde, “Functional connectivity in the motor cortex of resting human brain using echo-planar mri,” *Magn. Reson. Med.*, 1995, doi: 10.1002/mrm.1910340409.

[130] V. Scarapicchia, C. Brown, C. Mayo, and J. R. Gawryluk, “Functional magnetic resonance imaging and functional near-infrared spectroscopy: Insights from combined recording studies,” *Frontiers in Human Neuroscience*. 2017, doi: 10.3389/fnhum.2017.00419.

[131] J. Wirsich, A.-L. Giraud, and S. Sadaghiani, “Concurrent EEG- and fMRI-derived functional connectomes exhibit linked dynamics,” *bioRxiv*, no. 12, p. 464438, 2018, doi: 10.1101/464438.

[132] F. Scholkmann *et al.*, “A review on continuous wave functional near-infrared spectroscopy and imaging instrumentation and methodology,” *Neuroimage*, vol. 85, pp. 6–27, 2014.

[133] F. F. Jobsis, “Noninvasive, infrared monitoring of cerebral and myocardial oxygen sufficiency and circulatory parameters,” *Science (80-.).*, vol. 198, no. 4323, pp. 1264–1267, 1977.

[134] B. Chance, Z. Zhuang, C. UnAh, C. Alter, and L. Lipton, “Cognition-activated low-frequency modulation of light absorption in human brain.,” *Proc. Natl. Acad. Sci.*, vol. 90, no. 8, pp. 3770–3774, 1993.

[135] Y. Hoshi and M. Tamura, “Dynamic multichannel near-infrared optical imaging of human brain activity,” *J. Appl. Physiol.*, vol. 75, no. 4, pp. 1842–1846, 1993.

[136] T. Kato, A. Kamei, S. Takashima, and T. Ozaki, “Human visual cortical function during photic stimulation monitoring by means of near-infrared spectroscopy,” *J. Cereb. Blood Flow Metab.*, vol. 13, no. 3, pp. 516–520, 1993.

[137] A. Villringer, J. Planck, C. Hock, L. Schleinkofer, and U. Dirnagl, “Near infrared spectroscopy (NIRS): a new tool to study hemodynamic changes during activation of brain function in human adults,” *Neurosci. Lett.*, vol. 154, no. 1–2, pp. 101–104, 1993.

[138] W. G. Zijlstra, A. Buursma, and O. W. van Assendelft, *Visible and near infrared absorption spectra of human and animal haemoglobin: determination and application*. VSP, 2000.

[139] T. J. Huppert, S. G. Diamond, M. A. Franceschini, and D. A. Boas, “HomER: a review of time-series analysis methods for near-infrared spectroscopy of the brain,” *Appl. Opt.*, vol. 48, no. 10, pp. D280–D298, 2009.

[140] S. L. Jacques and L. Wang, “Monte Carlo Modeling of Light Transport in Tissues,” in *Optical-Thermal Response of Laser-Irradiated Tissue*, 1995.

[141] C. Zhu and Q. Liu, “Review of Monte Carlo modeling of light transport in tissues,” *J. Biomed. Opt.*, 2013, doi: 10.1117/1.jbo.18.5.050902.

[142] L. Wang, S. L. Jacques, and L. Zheng, “MCML-Monte Carlo modeling of light transport in multi-layered tissues,” *Comput. Methods Programs Biomed.*, 1995, doi: 10.1016/0169-2607(95)01640-F.

[143] J. R. Lorenzo, *Principles of diffuse light propagation: light propagation in tissues with applications in biology and medicine*. World Scientific, 2012.

[144] J. Gervain *et al.*, “Near-infrared spectroscopy: a report from the McDonnell infant methodology consortium,” *Dev. Cogn. Neurosci.*, vol. 1, no. 1, pp. 22–46, 2011.

[145] X. Cui, S. Bray, and A. L. Reiss, “Functional near infrared spectroscopy (NIRS) signal improvement based on negative correlation between oxygenated and deoxygenated hemoglobin dynamics,” *Neuroimage*, 2010, doi: 10.1016/j.neuroimage.2009.11.050.

[146] D. A. Boas, C. E. Elwell, M. Ferrari, and G. Taga, “Twenty years of functional near-infrared spectroscopy: Introduction for the special issue,” *NeuroImage*. 2014, doi: 10.1016/j.neuroimage.2013.11.033.

[147] J. León-Carrión and U. León-Domínguez, “Functional near-infrared spectroscopy (fNIRS): principles and neuroscientific applications,” *Neuroimaging methods. Rijeka, Croat. InTech*, pp. 47–74, 2012.

[148] Y. Zhang *et al.*, “Signal extraction of brain activity response by near infrared spectroscopy based on recursive least squares adaptive filtering,” in *IFMBE Proceedings*, 2013, doi: 10.1007/978-3-642-29305-4_99.

[149] A. Torricelli *et al.*, “Time domain functional NIRS imaging for human brain mapping,” *NeuroImage*. 2014, doi: 10.1016/j.neuroimage.2013.05.106.

[150] P. Rolfe, “In Vivo Near-Infrared Spectroscopy,” *Annu. Rev. Biomed. Eng.*, 2000, doi: 10.1146/annurev.bioeng.2.1.715.

[151] S. M. Coyle, T. E. Ward, and C. M. Markham, “Brain-computer interface using a simplified functional near-infrared spectroscopy system.,” *J. Neural Eng.*, 2007, doi: 10.1088/1741-2560/4/3/007.

[152] M. L. Meade, “Advances in lock-in amplifiers,” *J. Phys. E.*, 1982, doi: 10.1088/0022-3735/15/4/001.

[153] D. T. Delpy, M. Cope, P. van der Zee, S. R. Arridge, S. Wray, and J. S. Wyatt, “Estimation of optical pathlength through tissue from direct time of flight measurement,” *Phys. Med. Biol.*, vol. 33, no. 12, p. 1433, 1988.

[154] L. Kocsis, P. Herman, and A. Eke, “The modified Beer-Lambert law revisited,” *Phys. Med. Biol.*, vol. 51, no. 5, 2006, doi: 10.1088/0031-9155/51/5/N02.

[155] J. S. Ultman and C. A. Piantadosi, “Differential pathlength factor for diffuse photon scattering through tissue by a pulse-response method,” *Math. Biosci.*, 1991, doi: 10.1016/0025-5564(91)90072-Q.

[156] M. Kohl *et al.*, “Physical model for the spectroscopic analysis of cortical intrinsic optical signals,” *Phys. Med. Biol.*, 2000, doi: 10.1088/0031-9155/45/12/317.

[157] S. Lloyd-Fox, A. Blasi, and C. E. Elwell, “Illuminating the developing brain: the past, present and future of functional near infrared spectroscopy,” *Neurosci. Biobehav. Rev.*, vol. 34, no. 3, pp. 269–284, 2010.

[158] K. Uludağ and A. Roebroeck, “General overview on the merits of multimodal neuroimaging data fusion,” *Neuroimage*, vol. 102, pp. 3–10, 2014.

[159] H. Niu and Y. He, “Resting-State Functional Brain Connectivity,” *Neurosci.*, vol. 20, no. 2, pp. 173–188, 2014, doi: 10.1177/1073858413502707.

[160] S. Sasai, F. Homae, H. Watanabe, and G. Taga, “Frequency-specific functional connectivity in the brain during resting state revealed by NIRS,” *Neuroimage*, 2011, doi: 10.1016/j.neuroimage.2010.12.075.

[161] J. I. Tracy and G. E. Doucet, “Resting-state functional connectivity in epilepsy: Growing relevance for clinical decision making,” *Current Opinion in Neurology*. 2015, doi: 10.1097/WCO.0000000000000178.

[162] K. Gopinath *et al.*, “Striatal functional connectivity networks are modulated by fMRI resting state conditions,” *Neuroimage*, 2011, doi: 10.1016/j.neuroimage.2010.07.021.

[163] B. Park, J. Il Kim, D. Lee, S. O. Jeong, J. D. Lee, and H. J. Park, “Are brain networks stable during a 24-hour period?,” *Neuroimage*, 2012, doi: 10.1016/j.neuroimage.2011.07.049.

[164] M. J. Donahue *et al.*, “Spontaneous blood oxygenation level-dependent fMRI signal is modulated by behavioral state and correlates with evoked response in sensorimotor cortex: A 7.0-T fMRI study,” *Hum. Brain Mapp.*, 2012, doi: 10.1002/hbm.21228.

[165] C. I. Petkov, C. Kayser, M. Augath, and N. K. Logothetis, “Optimizing the imaging of the monkey auditory cortex: sparse vs. continuous fMRI,” *Magn. Reson. Imaging*, 2009, doi: 10.1016/j.mri.2009.01.018.

[166] C. F. Schmidt, T. Zaehle, M. Meyer, E. Geiser, P. Boesiger, and L. Jancke, “Silent and continuous fMRI scanning differentially modulate activation in an auditory language comprehension task,” *Hum. Brain Mapp.*, 2008, doi: 10.1002/hbm.20372.

[167] S. Haller, A. J. Bartsch, E. W. Radue, M. Klarhöfer, E. Seifritz, and K. Scheffler, “Effect of fMRI acoustic noise on non-auditory working memory task: Comparison between continuous and pulsed sound emitting EPI,” *Magn. Reson. Mater. Physics, Biol. Med.*, 2005, doi: 10.1007/s10334-005-0010-2.

[168] N. Novitski, I. Anourova, S. Martinkauppi, H. J. Aronen, R. Näätänen, and S. Carlson, “Effects of noise from functional magnetic resonance imaging on auditory event-related potentials in working memory task,” *Neuroimage*, 2003, doi: 10.1016/S1053-8119(03)00390-2.

[169] F. Esposito *et al.*, “Independent component model of the default-mode brain function: Assessing the impact of active thinking,” *Brain Res. Bull.*, 2006, doi: 10.1016/j.brainresbull.2006.06.012.

[170] A. M. Fjell and K. B. Walhovd, “Structural brain changes in aging: Courses, causes and cognitive consequences,” *Reviews in the Neurosciences*. 2010, doi: 10.1515/REVNEURO.2010.21.3.187.

[171] R. S. Mohtasib, G. Lumley, J. A. Goodwin, H. C. A. Emsley, V. Sluming, and L. M. Parkes, “Calibrated fMRI during a cognitive Stroop task reveals reduced metabolic response with increasing age,” *Neuroimage*, 2012, doi: 10.1016/j.neuroimage.2011.07.092.

[172] C. Benninger, P. Matthis, and D. Scheffner, “EEG development of healthy boys and girls. Results of a longitudinal study,” *Electroencephalogr. Clin. Neurophysiol.*, 1984, doi: 10.1016/0013-4694(84)90002-6.

[173] M. Filippi, P. Valsasina, P. Misci, A. Falini, G. Comi, and M. A. Rocca, “The organization of intrinsic brain activity differs between genders: A resting-state fMRI study in a large cohort of young healthy subjects,” *Hum. Brain Mapp.*, 2013, doi: 10.1002/hbm.21514.

[174] G. Gong, P. Rosa-Neto, F. Carbonell, Z. J. Chen, Y. He, and A. C. Evans, “Age- and gender-related differences in the cortical anatomical network,” *J. Neurosci.*, 2009, doi: 10.1523/JNEUROSCI.2308-09.2009.

[175] N. Jaušovec and K. Jaušovec, “Resting brain activity: Differences between genders,” *Neuropsychologia*, 2010, doi: 10.1016/j.neuropsychologia.2010.09.020.

[176] V. V. Nikulin and T. Brismar, “Long-range temporal correlations in electroencephalographic oscillations: Relation to topography, frequency band, age and gender,” *Neuroscience*, 2005, doi: 10.1016/j.neuroscience.2004.10.007.

[177] S. M. Pincus, “Approximate entropy as a measure of system complexity,” *Proc. Natl. Acad. Sci. U. S. A.*, 1991, doi: 10.1073/pnas.88.6.2297.

[178] K. R. A. van Dijk, M. R. Sabuncu, and R. L. Buckner, “The influence of head motion on intrinsic functional connectivity MRI,” *Neuroimage*, 2012, doi: 10.1016/j.neuroimage.2011.07.044.

[179] J. D. Power, K. A. Barnes, A. Z. Snyder, B. L. Schlaggar, and S. E. Petersen, “Spurious but systematic correlations in functional connectivity MRI networks arise from subject motion,” *Neuroimage*, 2012, doi: 10.1016/j.neuroimage.2011.10.018.

[180] M. Jansen *et al.*, “Motion-related artefacts in EEG predict neuronally plausible patterns of activation in fMRI data,” *Neuroimage*, 2012, doi: 10.1016/j.neuroimage.2011.06.094.

[181] P. G. Sämann *et al.*, “Development of the brain’s default mode network from wakefulness to slow wave sleep,” *Cereb. Cortex*, 2011, doi: 10.1093/cercor/bhq295.

[182] E. Charniak, *Introduction to deep learning*. The MIT Press, 2019.

[183] I. Goodfellow, Y. Bengio, and A. Courville, *Deep learning*. MIT press, 2016.

[184] R. Brilla, “Electroencephalography (EEG),” in *Pain*, Springer, 2019, pp. 201–203.

[185] C. Baumgartner *et al.*, “Preictal SPECT in temporal lobe epilepsy: Regional cerebral blood flow is increased prior to electroencephalography-seizure onset,” *J. Nucl. Med.*, vol. 39, no. 6, pp. 978–982, 1998.

[186] P. D. Adelson, E. Nemoto, M. Scheuer, M. Painter, J. Morgan, and H. Yonas, “Noninvasive continuous monitoring of cerebral oxygenation periictally using near-infrared spectroscopy: a preliminary report.,” *Epilepsia*, vol. 40, no. 11, pp. 1484–1489, Nov. 1999, doi: 10.1111/j.1528-1157.1999.tb02030.x.

[187] P. Federico, D. F. Abbott, R. S. Briellmann, A. S. Harvey, and G. D. Jackson, “Functional

MRI of the pre-ictal state.," *Brain*, vol. 128, no. Pt 8, pp. 1811–1817, Aug. 2005, doi: 10.1093/brain/awh533.

[188] D. H. Kerem and A. B. Geva, "Forecasting epilepsy from the heart rate signal.," *Med. Biol. Eng. Comput.*, vol. 43, no. 2, pp. 230–239, Mar. 2005, doi: 10.1007/bf02345960.

[189] F. Mormann *et al.*, "On the predictability of epileptic seizures," *Clin. Neurophysiol.*, vol. 116, no. 3, pp. 569–587, 2005, doi: 10.1016/j.clinph.2004.08.025.

[190] F. Mormann, R. G. Andrzejak, C. E. Elger, and K. Lehnertz, "Seizure prediction: The long and winding road," *Brain*, vol. 130, no. 2, pp. 314–333, 2007, doi: 10.1093/brain/awl241.

[191] S. S. Viglione and G. O. Walsh, "Proceedings: Epileptic seizure prediction.," *Electroencephalogr. Clin. Neurophysiol.*, vol. 39, no. 4, pp. 435–436, Oct. 1975.

[192] Y. Salant, I. Gath, and O. Henriksen, "Prediction of epileptic seizures from two-channel EEG.," *Med. Biol. Eng. Comput.*, vol. 36, no. 5, pp. 549–556, Sep. 1998, doi: 10.1007/bf02524422.

[193] Z. Rogowski, I. Gath, and E. Bental, "On the prediction of epileptic seizures.," *Biol. Cybern.*, vol. 42, no. 1, pp. 9–15, 1981, doi: 10.1007/bf00335153.

[194] A. Siegel, C. L. Grady, and A. F. Mirsky, "Prediction of spike-wave bursts in absence epilepsy by EEG power-spectrum signals.," *Epilepsia*, vol. 23, no. 1, pp. 47–60, Feb. 1982, doi: 10.1111/j.1528-1157.1982.tb05052.x.

[195] M. Le Van Quyen, J. Martinerie, M. Baulac, and F. Varela, "Anticipating epileptic seizures in real time by a non-linear analysis of similarity between EEG recordings.," *Neuroreport*, vol. 10, no. 10, pp. 2149–2155, Jul. 1999, doi: 10.1097/00001756-199907130-00028.

[196] B. Litt *et al.*, "Epileptic seizures may begin hours in advance of clinical onset: a report of five patients.," *Neuron*, vol. 30, no. 1, pp. 51–64, Apr. 2001, doi: 10.1016/s0896-6273(01)00262-8.

[197] L. D. Iasemidis, J. C. Sackellares, H. P. Zaveri, and W. J. Williams, "Phase space topography and the Lyapunov exponent of electrocorticograms in partial seizures.," *Brain Topogr.*, vol. 2, no. 3, pp. 187–201, 1990, doi: 10.1007/bf01140588.

[198] W. Chaovalitwongse, L. D. Iasemidis, P. M. Pardalos, P. R. Carney, D.-S. Shiau, and J. C.

Sackellares, “Performance of a seizure warning algorithm based on the dynamics of intracranial EEG.,” *Epilepsy Res.*, vol. 64, no. 3, pp. 93–113, May 2005, doi: 10.1016/j.eplepsyres.2005.03.009.

[199] S. Faul, G. Boylan, S. Connolly, L. Marnane, and G. Lightbody, “An evaluation of automated neonatal seizure detection methods.,” *Clin. Neurophysiol.*, vol. 116, no. 7, pp. 1533–1541, Jul. 2005, doi: 10.1016/j.clinph.2005.03.006.

[200] J. Gotman, D. Flanagan, B. Rosenblatt, A. Bye, and E. M. Mizrahi, “Evaluation of an automatic seizure detection method for the newborn EEG.,” *Electroencephalogr. Clin. Neurophysiol.*, vol. 103, no. 3, pp. 363–369, Sep. 1997, doi: 10.1016/s0013-4694(97)00005-2.

[201] A. Liu, J. S. Hahn, G. P. Heldt, and R. W. Coen, “Detection of neonatal seizures through computerized EEG analysis.,” *Electroencephalogr. Clin. Neurophysiol.*, vol. 82, no. 1, pp. 30–37, Jan. 1992, doi: 10.1016/0013-4694(92)90179-l.

[202] P. Celka and P. Colditz, “A computer-aided detection of EEG seizures in infants: a singular-spectrum approach and performance comparison.,” *IEEE Trans. Biomed. Eng.*, vol. 49, no. 5, pp. 455–462, May 2002, doi: 10.1109/10.995684.

[203] Y. U. Khan and J. Gotman, “Wavelet based automatic seizure detection in intracerebral electroencephalogram.,” *Clin. Neurophysiol.*, vol. 114, no. 5, pp. 898–908, May 2003, doi: 10.1016/s1388-2457(03)00035-x.

[204] M. Oddo, F. Villa, and G. Citerio, “Brain multimodality monitoring: An update,” *Current Opinion in Critical Care*. 2012, doi: 10.1097/MCC.0b013e32835132a5.

[205] C. M. Miller, “Update on multimodality monitoring,” *Curr. Neurol. Neurosci. Rep.*, 2012, doi: 10.1007/s11910-012-0274-7.

[206] G. M. Brophy *et al.*, “Guidelines for the evaluation and management of status epilepticus,” *Neurocritical Care*. 2012, doi: 10.1007/s12028-012-9695-z.

[207] R. Sutter and P. W. Kaplan, “Electroencephalographic criteria for nonconvulsive status epilepticus: Synopsis and comprehensive survey,” *Epilepsia*, 2012, doi: 10.1111/j.1528-1167.2012.03593.x.

[208] J. A. Wahr, K. K. Tremper, S. Samra, and D. T. Delpy, “Near-infrared spectroscopy: Theory and applications,” *J. Cardiothorac. Vasc. Anesth.*, 1996, doi: 10.1016/S1053-0770(96)80107-8.

[209] T. W. L. Scheeren, P. Schober, and L. A. Schwarte, “Monitoring tissue oxygenation by near infrared spectroscopy (NIRS): Background and current applications,” in *Journal of Clinical Monitoring and Computing*, 2012, doi: 10.1007/s10877-012-9348-y.

[210] A. L. Cole, R. A. Herman, J. B. Heimlich, S. Ahsan, B. A. Freedman, and M. S. Shuler, “Ability of near infrared spectroscopy to measure oxygenation in isolated upper extremity muscle compartments,” *J. Hand Surg. Am.*, 2012, doi: 10.1016/j.jhsa.2011.10.037.

[211] H. Obrig, “NIRS in clinical neurology—a 'promising'tool?,” *Neuroimage*, 2014.

[212] C. W. A. Pennekamp, M. L. Bots, L. J. Kappelle, F. L. Moll, and G. J. de Borst, “The Value of Near-Infrared Spectroscopy Measured Cerebral Oximetry During Carotid Endarterectomy in Perioperative Stroke Prevention. A Review,” *European Journal of Vascular and Endovascular Surgery*. 2009, doi: 10.1016/j.ejvs.2009.07.008.

[213] C. Storm *et al.*, “Regional cerebral oxygen saturation after cardiac arrest in 60 patients-A prospective outcome study,” *Resuscitation*, 2014, doi: 10.1016/j.resuscitation.2014.04.021.

[214] A. M. Naidech, B. R. Bendok, M. L. Ault, and T. P. Bleck, “Monitoring with the somanetics INVOS 5100C after aneurysmal subarachnoid hemorrhage,” *Neurocrit. Care*, 2008, doi: 10.1007/s12028-008-9077-8.

[215] A. Dagal and A. M. Lam, “Cerebral blood flow and the injured brain: How should we monitor and manipulate it?,” *Curr. Opin. Anaesthesiol.*, 2011, doi: 10.1097/ACO.0b013e3283445898.

[216] J. Simons, E. D. Sood, C. D. Derby, and C. Pizarro, “Predictive value of near-infrared spectroscopy on neurodevelopmental outcome after surgery for congenital heart disease in infancy,” *J. Thorac. Cardiovasc. Surg.*, 2012, doi: 10.1016/j.jtcvs.2011.09.007.

[217] J. M. Murkin, “NIRS: A standard of care for CPB vs. an evolving standard for selective cerebral perfusion?,” in *Journal of Extra-Corporeal Technology*, 2009.

[218] M. Qaraqe, M. Ismail, E. Serpedin, and H. Zulfi, “Epileptic seizure onset detection based on EEG and ECG data fusion,” *Epilepsy Behav.*, 2016, doi: 10.1016/j.yebeh.2016.02.039.

[219] D. K. Nguyen *et al.*, “Non-invasive continuous EEG-fNIRS recording of temporal lobe seizures,” *Epilepsy Res.*, 2012, doi: 10.1016/j.eplepsyres.2011.10.035.

[220] M. Leming, L. Su, S. Chattopadhyay, and J. Suckling, “Normative pathways in the functional connectome,” *Neuroimage*, vol. 184, pp. 317–334, Jan. 2019, doi: 10.1016/j.neuroimage.2018.09.028.

[221] B. Biswal, F. Zerrin Yetkin, V. M. Haughton, and J. S. Hyde, “Functional connectivity in the motor cortex of resting human brain using echo-planar mri,” *Magn. Reson. Med.*, vol. 34, no. 4, pp. 537–541, 1995, doi: 10.1002/mrm.1910340409.

[222] R. L. Buckner, J. R. Andrews-Hanna, and D. L. Schacter, “The brain’s default network: Anatomy, function, and relevance to disease,” *Annals of the New York Academy of Sciences*. 2008, doi: 10.1196/annals.1440.011.

[223] M. D. Greicius, G. Srivastava, A. L. Reiss, and V. Menon, “Default-mode network activity distinguishes Alzheimer’s disease from healthy aging: Evidence from functional MRI,” *Proc. Natl. Acad. Sci. U. S. A.*, 2004, doi: 10.1073/pnas.0308627101.

[224] J. Gotman, C. Grova, A. Bagshaw, E. Kobayashi, Y. Aghakhani, and F. Dubeau, “Generalized epileptic discharges show thalamocortical activation and suspension of the default state of the brain,” *Proc. Natl. Acad. Sci. U. S. A.*, 2005, doi: 10.1073/pnas.0504935102.

[225] J. Folbergrová, M. Ingvar, and B. K. Siesjö, “Metabolic Changes in Cerebral Cortex, Hippocampus, and Cerebellum During Sustained Bicuculline-Induced Seizures,” *J. Neurochem.*, 1981, doi: 10.1111/j.1471-4159.1981.tb04673.x.

[226] S. Shariff, M. Suh, M. Zhao, H. Ma, and T. H. Schwartz, “Recent developments in oximetry and perfusion-based mapping techniques and their role in the surgical treatment of neocortical epilepsy,” *Epilepsy and Behavior*. 2006, doi: 10.1016/j.yebeh.2005.11.006.

[227] A. Custo, D. Van De Ville, W. M. Wells, M. I. Tomescu, D. Brunet, and C. M. Michel, “Electroencephalographic Resting-State Networks: Source Localization of Microstates,” *Brain Connect.*, 2017, doi: 10.1089/brain.2016.0476.

[228] C. P. Pawela *et al.*, “Resting-state functional connectivity of the rat brain,” *Magn. Reson. Med.*, vol. 59, no. 5, pp. 1021–1029, 2008, doi: 10.1002/mrm.21524.

[229] M. W. Cole, T. Yarkoni, G. Repovš, A. Anticevic, and T. S. Braver, “Global connectivity of prefrontal cortex predicts cognitive control and intelligence,” *J. Neurosci.*, 2012, doi: 10.1523/JNEUROSCI.0536-12.2012.

[230] Y. Hoshi, “Functional Near-Infrared Spectroscopy: Potential and Limitations in Neuroimaging Studies,” *International Review of Neurobiology*. 2005, doi: 10.1016/S0074-7742(05)66008-4.

[231] H. Obrig *et al.*, “Spontaneous low frequency oscillations of cerebral hemodynamics and metabolism in human adults,” *Neuroimage*, 2000, doi: 10.1006/nimg.2000.0657.

[232] M. S. Green, S. Sehgal, and R. Tariq, “Near-infrared spectroscopy: The new must have tool in the intensive care unit?,” *Seminars in Cardiothoracic and Vascular Anesthesia*. 2016, doi: 10.1177/1089253216644346.

[233] D. Bahdanau, K. Cho, and Y. Bengio, “Neural Machine Translation by Jointly Learning to Align and Translate,” pp. 1–15, 2014.

[234] A. Zhang, Z. C. Lipton, M. Li, and A. J. Smola, “Dive into Deep Learning,” p. 639, 2018.

[235] C. Szegedy *et al.*, “Intriguing properties of neural networks,” in *2nd International Conference on Learning Representations, ICLR 2014 - Conference Track Proceedings*, 2014.

[236] S. Hochreiter and J. Schmidhuber, “Long Short-Term Memory,” *Neural Comput.*, 1997, doi: 10.1162/neco.1997.9.8.1735.

[237] K. Greff, R. K. Srivastava, J. Koutnik, B. R. Steunebrink, and J. Schmidhuber, “LSTM: A Search Space Odyssey,” *IEEE Trans. Neural Networks Learn. Syst.*, 2017, doi: 10.1109/TNNLS.2016.2582924.

[238] Z. C. Lipton, D. C. Kale, C. Elkan, and R. Wetzel, “Learning to diagnose with LSTM recurrent neural networks,” in *4th International Conference on Learning Representations, ICLR 2016 - Conference Track Proceedings*, 2016.

[239] J. F. Kolen and S. C. Kremer, “Gradient Flow in Recurrent Nets: The Difficulty of Learning

LongTerm Dependencies," in *A Field Guide to Dynamical Recurrent Networks*, 2010.

[240] S. Merity, N. S. Keskar, and R. Socher, "Regularizing and optimizing LSTM language models," in *6th International Conference on Learning Representations, ICLR 2018 - Conference Track Proceedings*, 2018.

[241] D. T. A. Luong and V. Chandola, "Learning Deep Representations from Clinical Data for Chronic Kidney Disease," no. 1, 2018.

[242] F. A. Gers, J. Schmidhuber, and F. Cummins, "Learning to forget: Continual prediction with LSTM," *Neural Comput.*, 2000, doi: 10.1162/089976600300015015.

[243] B. Mitra and N. Craswell, "Neural Models for Information Retrieval," 2017.

[244] J. Pennington, R. Socher, and C. D. Manning, "GloVe : Global Vectors for Word Representation," pp. 1532–1543, 2014.

[245] T. Mikolov, K. Chen, G. Corrado, and J. Dean, "Distributed Representations of Words and Phrases and their Compositionality," pp. 1–9.

[246] Z. S. Harris, "Distributional Structure," vol. 7956, no. 1954, pp. 146–162, 2015, doi: 10.1080/00437956.1954.11659520.

[247] I. Sutskever, O. Vinyals, and Q. V. Le, "Sequence to sequence learning with neural networks," in *Advances in Neural Information Processing Systems*, 2014.

[248] U. R. Acharya, S. L. Oh, Y. Hagiwara, J. H. Tan, and H. Adeli, "Deep convolutional neural network for the automated detection and diagnosis of seizure using EEG signals," *Comput. Biol. Med.*, vol. 100, no. July 2017, pp. 270–278, 2018, doi: 10.1016/j.compbiomed.2017.09.017.

[249] A. H. Ansari, P. J. Cherian, and H. H. Sciences, "Neonatal Seizure Detection Using Deep Convolutional Neural Networks," no. October, 2018, doi: 10.1142/S0129065718500119.

[250] A. Supratak, L. Li, and Y. Guo, "Feature Extraction with Stacked Autoencoders for Epileptic Seizure Detection," *2014 36th Annu. Int. Conf. IEEE Eng. Med. Biol. Soc.*, pp. 4184–4187, 2014, doi: 10.1109/EMBC.2014.6944546.

[251] K. Tsiouris, V. C. Pezoulas, M. Zervakis, S. Konitsiotis, D. D. Koutsouris, and D. I. Fotiadis, "A Long Short-Term Memory deep learning network for the prediction of epileptic seizures

using EEG signals," *Comput. Biol. Med.*, 2018, doi: 10.1016/j.compbiomed.2018.05.019.

[252] C. M. Lu, Y. J. Zhang, B. B. Biswal, Y. F. Zang, D. L. Peng, and C. Z. Zhu, "Use of fNIRS to assess resting state functional connectivity," *J. Neurosci. Methods*, vol. 186, no. 2, pp. 242–249, 2010, doi: 10.1016/j.jneumeth.2009.11.010.

[253] F. A. Fishburn, M. E. Norr, A. V. Medvedev, and C. J. Vaidya, "Sensitivity of fNIRS to cognitive state and load," *Front. Hum. Neurosci.*, 2014, doi: 10.3389/fnhum.2014.00076.

[254] H. Niu and Y. He, "Resting-State Functional Brain Connectivity," *Neurosci.*, vol. 20, no. 2, pp. 173–188, Apr. 2014, doi: 10.1177/1073858413502707.

[255] C. Zhang *et al.*, "Characteristics of resting-state functional connectivity in intractable unilateral temporal lobe epilepsy patients with impaired executive control function," *Front. Hum. Neurosci.*, 2017, doi: 10.3389/fnhum.2017.00609.

[256] E. Sitnikova, A. E. Hramov, V. Grubov, and A. A. Koronovsky, "Rhythmic activity in EEG and sleep in rats with absence epilepsy," *Brain Res. Bull.*, 2016, doi: 10.1016/j.brainresbull.2015.11.012.

[257] D. W. Gross and J. Gotman, "Correlation of high-frequency oscillations with the sleep-wake cycle and cognitive activity in humans," *Neuroscience*, 1999, doi: 10.1016/S0306-4522(99)00343-7.

[258] G. A. Worrell, L. Parish, S. D. Cranstoun, R. Jonas, G. Baltuch, and B. Litt, "High-frequency oscillations and seizure generation in neocortical epilepsy," *Brain*, 2004, doi: 10.1093/brain/awh149.

[259] D. Mantini, M. G. Perrucci, C. Del Gratta, G. L. Romani, and M. Corbetta, "Electrophysiological signatures of resting state networks in the human brain," *Proc. Natl. Acad. Sci. U. S. A.*, 2007, doi: 10.1073/pnas.0700668104.

[260] D. Wierstra, F. J. Gomez, and J. Schmidhuber, "Evolino: Hybrid neuroevolution/optimal linear search for sequence learning," in *Proceedings of the 19th International Joint Conference on Artificial Intelligence (IJCAI), Edinburgh*, 2005, pp. 853–858.

[261] A. Fallah, A. Mokhtari, and A. Ozdaglar, "Provably Convergent Policy Gradient Methods for Model-Agnostic Meta-Reinforcement Learning," *arXiv Prepr. arXiv2002.05135*, 2020.

[262] S. Harris *et al.*, “Coupling between gamma-band power and cerebral blood volume during recurrent acute neocortical seizures,” *Neuroimage*, 2014, doi: 10.1016/j.neuroimage.2014.04.014.

[263] J. Goense, H. Merkle, and N. K. Logothetis, “High-Resolution fMRI Reveals Laminar Differences in Neurovascular Coupling between Positive and Negative BOLD Responses,” *Neuron*, 2012, doi: 10.1016/j.neuron.2012.09.019.

[264] U. R. Acharya, S. Vinitha Sree, G. Swapna, R. J. Martis, and J. S. Suri, “Automated EEG analysis of epilepsy: A review,” *Knowledge-Based Syst.*, 2013, doi: 10.1016/j.knosys.2013.02.014.

[265] S. M. Stufflebeam, H. Liu, J. Sepulcre, N. Tanaka, R. L. Buckner, and J. R. Madsen, “Localization of focal epileptic discharges using functional connectivity magnetic resonance imaging: Clinical article,” *J. Neurosurg.*, 2011, doi: 10.3171/2011.1.JNS10482.

[266] Z. Shehzad *et al.*, “The resting brain: Unconstrained yet reliable,” *Cereb. Cortex*, 2009, doi: 10.1093/cercor/bhn256.

[267] A. C. Mckee and D. H. Daneshvar, “The neuropathology of traumatic brain injury,” in *Handbook of Clinical Neurology*, 2015.

[268] K. Blennow, J. Hardy, and H. Zetterberg, “The Neuropathology and Neurobiology of Traumatic Brain Injury,” *Neuron*. 2012, doi: 10.1016/j.neuron.2012.11.021.

[269] S. G. Horovitz *et al.*, “Low frequency BOLD fluctuations during resting wakefulness and light sleep: A simultaneous EEG-fMRI study,” *Hum. Brain Mapp.*, 2008, doi: 10.1002/hbm.20428.

[270] M. G. Frank, “Astroglial regulation of sleep homeostasis,” *Current Opinion in Neurobiology*. 2013, doi: 10.1016/j.conb.2013.02.009.

[271] E. Tagliazucchi, F. von Wegner, A. Morzelewski, V. Brodbeck, and H. Laufs, “Dynamic BOLD functional connectivity in humans and its electrophysiological correlates,” *Front. Hum. Neurosci.*, 2012, doi: 10.3389/fnhum.2012.00339.

[272] R. Scheeringa, K. M. Petersson, A. Kleinschmidt, O. Jensen, and M. C. m. Bastiaansen, “EEG Alpha Power Modulation of fMRI Resting-State Connectivity,” *Brain Connect.*,

2012, doi: 10.1089/brain.2012.0088.

[273] M. E. Raichle, “The restless brain: How intrinsic activity organizes brain function,” *Philosophical Transactions of the Royal Society B: Biological Sciences*. 2015, doi: 10.1098/rstb.2014.0172.

[274] A. Kostin, D. McGinty, R. Szymusiak, and M. N. Alam, “Sleep-wake and diurnal modulation of nitric oxide in the perifornical-lateral hypothalamic area: Real-time detection in freely behaving rats,” *Neuroscience*, 2013, doi: 10.1016/j.neuroscience.2013.09.022.

[275] M. Lin, Q. Chen, and S. Yan, “Network in network,” in *2nd International Conference on Learning Representations, ICLR 2014 - Conference Track Proceedings*, 2014.

[276] P. Royston, “Multiple imputation of missing values: Update,” *Stata J.*, 2005, doi: 10.1177/1536867x0500500204.

[277] Z. Che, S. Purushotham, K. Cho, D. Sontag, and Y. Liu, “Recurrent Neural Networks for Multivariate Time Series with Missing Values,” *Sci. Rep.*, 2018, doi: 10.1038/s41598-018-24271-9.

[278] A. M. Saxe *et al.*, “On the information bottleneck theory of deep learning,” *J. Stat. Mech. Theory Exp.*, 2019, doi: 10.1088/1742-5468/ab3985.

[279] Hawkin, “Intriguing properties of neural networks, Christian Szegedy, Wojciech Zaremba, Ilya Sutskever, Joan Bruna, Dumitru Erhan, Ian Goodfellow, Rob Fergus,” *arXiv Prepr.*, 2014, doi: 978-0131471399.

[280] I. Sutskever, J. Martens, G. Dahl, and G. Hinton, “On the importance of initialization and momentum in deep learning,” in *30th International Conference on Machine Learning, ICML 2013*, 2013.

[281] M. Opper, “Expectation propagation,” in *Statistical Physics, Optimization, Inference, and Message-Passing Algorithms*, 2016.

[282] Deye, N., Vincent, F., Michel, P., Ehrmann, S., Da Silva, D., Piagnerelli, M.,Laterre, P.-F. (2016). “Healthcare databases for paediatric studies: A report from the grip network global survey,” *Pharmacoepidemiol. Drug Saf.*, 2014, doi: 10.1002/pds.3701.

[283] M. Morrell, “Brain stimulation for epilepsy: Can scheduled or responsive neurostimulation

stop seizures?," *Current Opinion in Neurology*. 2006, doi: 10.1097/01.wco.0000218233.60217.84.